



جامعة الملك عبد الله
للعلوم والتقنية

King Abdullah University of
Science and Technology

Synthesis Strategies of Porous Carbon for Supercapacitor Applications

Item Type	Article
Authors	Yin, Jian; Zhang, Wenli; Alhebshi, Nuha; Salah, Numan; Alshareef, Husam N.
Citation	Yin, J., Zhang, W., Alhebshi, N. A., Salah, N., & Alshareef, H. N. (2020). Synthesis Strategies of Porous Carbon for Supercapacitor Applications. <i>Small Methods</i> , 1900853. doi:10.1002/smtd.201900853
Eprint version	Post-print
DOI	10.1002/smtd.201900853
Publisher	Wiley
Journal	Small Methods
Rights	Archived with thanks to Small Methods
Download date	09/08/2022 05:45:48
Link to Item	http://hdl.handle.net/10754/661533

Dear Author,

Please correct your galley proofs carefully and return them no more than four days after the page proofs have been received.

Please limit corrections to errors already in the text; cost incurred for any further changes or additions will be charged to the author, unless such changes have been agreed upon by the editor.

The editors reserve the right to publish your article without your corrections if the proofs do not arrive in time.

Note that the author is liable for damages arising from incorrect statements, including misprints.

Please note any queries that require your attention. These are indicated with a Q in the PDF and a question at the end of the document.

Reprints may be ordered by filling out the accompanying form.

Return the reprint order form by fax or by e-mail with the corrected proofs, to Wiley-VCH : small-methods@wiley.com

Corrections should be made directly in the PDF file using the PDF annotation tools. If you have questions about this, please contact the editorial office. The corrected PDF and any accompanying files should be uploaded to the journal's Editorial Manager site.

To avoid commonly occurring errors, **please ensure that the following important items are correct** in your proofs (please note that once your article is published online, no further corrections can be made):

Names of all authors present and spelled correctly

Titles of authors correct (Prof. or Dr. only: please note, Prof. Dr. is not used in the journals)

Addresses and **postcodes** correct

E-mail address of corresponding author correct (current email address)

Funding bodies included and grant numbers accurate

Title of article OK

All **figures** included

Equations correct (symbols and sub/superscripts)

Author Query Form

WILEY

Journal SMTD
Article smtd201900853

Dear Author,

During the copyediting of your manuscript the following queries arose.

Please refer to the query reference callout numbers in the page proofs and respond to each by marking the necessary comments using the PDF annotation tools.

Please remember illegible or unclear comments and corrections may delay publication.

Many thanks for your assistance.

Query No.	Description	Remarks
Q-OO	<p>Open access publication of this work is possible via Wiley OnlineOpen. Information about this is available at: https://authorservices.wiley.com/author-resources/Journal-Authors/licensing-open-access/open-access/onlineopen.html.</p> <p>The cost of publishing your manuscript OnlineOpen may be covered by one of Wiley's national agreements. To find out more, visit https://authorservices.wiley.com/author-resources/Journal-Authors/open-access/affiliation-policies-payments/index.html.</p> <p>Note that eligibility for fee coverage is determined by the affiliation of the primary corresponding author designated at submission. Please log in to your Wiley Author Services account at https://authorservices.wiley.com/ and confirm your affiliation to see if you are eligible.</p> <p>Instructions for placing an OnlineOpen order can be found at: https://authorservices.wiley.com/author-resources/Journal-Authors/open-access/how-to-order-onlineopen.html.</p> <p>To publish your article open access, please complete the order process before completing your proof corrections.</p>	<p>please publish this paper in subscription way</p>
Q1	Please confirm that forenames/given names (blue) and surnames/family names (vermilion) have been identified correctly.	They are right
Q2	Please note that it is not as per journal style to feature or to provide information regarding numbers of articles published, awards, or patents, as well as information on external editorial work, in author biographies. This text has therefore been deleted.	Ok
Q3	Please check that all author names and affiliations are presented correctly.	they are right
Q4	Please confirm that all elements of the TOC image are original. If they are not, a new TOC image is required, even if you have permission to use it, it nevertheless has to be 100% original.	it is original
Q5	Please check all equations have been correctly typeset.	Some equations have been changed
Q6	Please confirm that figure 1 is original, i.e., has not been published before.	it is original
Q7	Please obtain permission for figure reproduction for all figure elements that are not original and cite them in the following way: Reproduced with permission.[Ref.] Copyright Year, Publisher.	we have requested all the copyright

Please confirm that Funding Information has been identified correctly.

Please confirm that the funding sponsor list below was correctly extracted from your article: that it includes all funders and that the text has been matched to the correct FundRef Registry organization names. If a name was not found in the FundRef registry, it may not be the canonical name form, it may be a program name rather than an organization name, or it may be an organization not yet included in FundRef Registry. If you know of another name form or a parent organization name for a "not found" item on this list below, please share that information.

FundRef Name	FundRef Organization Name
King Abdullah University of Science and Technology	King Abdullah University of Science and Technology

J. Yin, W. Zhang, N. A. Alhebshi,
N. Salah, H. N. Alshareef* 1900853

Synthesis Strategies of Porous Carbon for Supercapacitor Applications



The synthesis strategies of porous carbon for supercapacitor (SC) applications, including traditional methods and novel emerging methods developed in recent years, are reviewed in this article. This review proposes promising future directions and synthesis strategies for porous carbons used in SC applications.

Q4

1
2
3
4
5
6
7
8
9
10
11
12
13
14
15
16
17
18
19
20
21
22
23
24
25
26
27
28
29
30
31
32
33
34
35
36
37
38
39
40
41
42
43
44
45
46
47
48
49
50
51
52
53
54
55
56
57
58
59

1
2
3
4
5
6
7
8
9
10
11
12
13
14
15
16
17
18
19
20
21
22
23
24
25
26
27
28
29
30
31
32
33
34
35
36
37
38
39
40
41
42
43
44
45
46
47
48
49
50
51
52
53
54
55
56
57
58
59

UNCORRECTED PROOF

Synthesis Strategies of Porous Carbon for Supercapacitor Applications

Jian Yin, Wenli Zhang, Nuha A. Alhebshi, Numan Salah, and Husam N. Alshareef*

Supercapacitors (SCs) have experienced a significant increase in research activity and commercialization during the past few decades. As the primary and most important electrode active material for commercial SCs, porous carbon is produced at an industrial-scale through traditional carbonization-activation strategies. Nevertheless, commercial porous carbon materials have some disadvantages, such as high production cost, corrosion of equipment, and emission of toxic gases, and byproduct pollutants during production. In recent years, huge efforts have been made to develop novel synthesis strategies for porous carbon materials. This review focuses on the pore formation mechanisms in traditional carbonization-activation methods, emerging activation methods, template methods, self-template methods, and novel emerging methods for the synthesis of porous carbons for SCs. Strategies developed so far for the synthesis of porous carbon materials are summarized. The mechanisms and recent advances for each strategy are reviewed. Furthermore, proposed are future directions and synthesis strategies for porous carbons used in SC applications.

of most transition-metal compounds (represented by manganese oxide) in aqueous electrolytes.^[1] As a result, most commercially available SCs are EDLCs assembled using porous carbon electrodes and organic electrolytes composed of tetraethylammonium tetrafluoroborate solute and acetonitrile or propylene carbonate solvents.^[2] Nowadays, commercial SCs are starting to supplement lithium-ion batteries (LIBs) in some pivotal but small number of applications. These applications include regenerative braking systems in hybrid electric vehicles, frequency regulation in smart grid, energy storage modules in electronics, and uninterruptable power supply.^[3]

There are two reasons for the limited commercial deployment of SCs. On the one hand, the energy densities of SCs are limited to as low as 5–8 Wh kg⁻¹ (≈250 Wh kg⁻¹ for LIB, and ≈40 Wh kg⁻¹ for lead-acid battery).^[4] On the other hand, the capital cost per watt-hour of SC is much higher than LIB and lead-acid battery.^[5] The energy storage cost of SCs is ≈20 000 \$ kWh⁻¹ which is 20 times that of LIB (1000 \$ kWh⁻¹) and more than 100 times that of lead-acid battery (150 \$ kWh⁻¹).^[6] The high capital cost of SC is mainly ascribed to the high cost of porous carbon electrode active materials. Porous carbons used for SC applications have high prices ranging from 30 to 50 \$ kg⁻¹ depending on their specific surface areas (SSAs) and pore volumes which are determining factors for the capacitances of SCs.^[7] As an example, the YP-80F (SSA 2100 m² g⁻¹) from Kuraray chemical costs more than YP-50F (SSA 1660 m² g⁻¹). The high cost of porous carbon increases the cost of SC devices and the levelized cost of energy storage devices (LCES). LCES, to some extent, limits the widespread of SCs. LCES determines how much we spend on energy storage devices per watt-hour energy output during its entire lifetime (Equation (1))

$$\text{LCES} = \frac{C_c + C_m}{n \times E \times \text{EE}} \quad (1)$$

here C_c is the capital cost, C_m is the maintenance cost, n is the lifetime cycling number, E is the energy stored in the round-trip energy storage process (depending on voltage, capacity, and its depth of discharge), EE is the energy efficiency. To lower LCES, we can either decrease the numerator or increase the denominator. Given the advantages of ultralong cycling life, low maintenance, and high EE for SCs, if we can lower the C_c of SCs to the level of LIB, we can significantly expand their market

1. Introduction

Supercapacitors (SCs) are high-power energy storage devices based on the fast accumulation/release of charges at the electrode/electrolyte interface through electrostatic or electrochemical ion adsorptions. SCs have two subcategories, including electric double-layer capacitors (EDLCs) and pseudocapacitors.^[1] The application of pseudocapacitors in commercial devices has been hampered by the intrinsic high cost of RuO₂ and the electrochemical instabilities

Dr. J. Yin, Dr. W. Zhang, Prof. H. N. Alshareef
Materials Science and Engineering
Physical Science and Engineering Division
King Abdullah University of Science and Technology (KAUST)
Thuwal 23955-6900, Saudi Arabia
E-mail: husam.alshareef@kaust.edu.sa

Prof. N. A. Alhebshi
Physics Department
Faculty of Science
King Abdulaziz University
Jeddah 21589, Saudi Arabia

Prof. N. Salah
Center of Nanotechnology
King Abdulaziz University
Jeddah 21589, Saudi Arabia

The ORCID identification number(s) for the author(s) of this article can be found under <https://doi.org/10.1002/smt.201900853>.

DOI: 10.1002/smt.201900853

1 penetration. Hence, the development of low-cost porous carbon
2 using simple and scalable preparation methods has significant
3 practical implications.

4 The capacitance and energy of an EDLC-type SC greatly
5 depend on the porous architecture of porous carbon electrodes
6 which store energy through the electrostatic charge accumula-
7 tion at the electrode/electrolyte interface. The capacitance of a
8 porous carbon electrode can be calculated based on the model
9 proposed by Helmholtz, as indicated by Equation (2)

$$10 \quad C = \frac{\epsilon_r \epsilon_0 A}{d} \quad (2)$$

14 where ϵ_r is the electrolyte dielectric constant, A is the active sur-
15 face area of the porous carbon electrode, ϵ_0 is the permittivity of
16 vacuum, and d is the distance of the electric double layer. The
17 capacitance of EDLC is proportional to the active surface area of
18 porous carbon. Although the pore size and surface chemistry of
19 porous carbons influence the construction of the electric double
20 layer, the development of high surface area porous carbon is
21 the main strategy to enhance the capacitance of EDLC-type
22 SC. According to the classification of the International Union
23 of Pure and Applied Chemistry (IUPAC), the pores in porous
24 materials are classified into macropore (>50 nm), mesopore
25 (2–50 nm), and micropore (<2 nm).^[8] In the case of electrode
26 materials used for SC, macropores of porous carbons serve
27 as reservoirs of electrolyte ions. Mesopores serve as the dif-
28 fusion channels for electrolyte ions. Micropores of porous
29 carbon materials play the dominant roles for ion storage since
30 micropores contribute more to high SSA and capacitance com-
31 pared with mesopores and macropores. From the synthetic
32 perspective, any carbon sources can be transformed into porous
33 carbonaceous materials. Besides, structural parameters, such as
34 SSA, pore-size distribution, surface functionalities, and tap den-
35 sity can be engineered by controlling the synthetic parameters.
36 Nevertheless, the preparation of porous carbon relies on empir-
37 ical protocols using different carbon sources, such as resins,
38 petrochemicals, coal, transition-metal carbide, lignin, cellulose,
39 and polymers. So, it is imperative to summarize the synthesis
40 methodologies of porous carbons into different groups based
41 on their pore formation mechanisms (as shown in Figure 1).

42 Traditionally, porous carbons are prepared by a combined
43 carbonization–activation strategy. Generally, carbonization is
44 realized by carbonizing organic precursors at temperatures
45 ranging from 400 to 1000 °C in an inert atmosphere. Through
46 carbonization, we can get nonporous solid carbons known as
47 coal char or biochar. Pore-forming agents (porogens) are used to
48 create pores in the activation process. The obtained coal char or
49 biochar then undergo oxidation reactions with activation agents
50 (CO₂, O₂, air, or H₂O in physical activation; KOH, Na₂CO₃,
51 ZnCl₂, or H₃PO₄ in chemical activation).^[9,10] Most commer-
52 cially available porous carbons are produced from coconut
53 shells by physical activation using steam as an activation agent,
54 which yields porous carbons with high purity and SSA of
55 ≈1500 m² g⁻¹. Chemical activation strategy is usually applied to
56 produce porous carbons with high SSAs ranging from 1000 to
57 3000 m² g⁻¹ using KOH or NaOH as the activation agents.^[11–13]
58 The production of chemically activated porous carbons is
59 limited to lab-scale due to their high production cost owing to



mainly focuses on carbon materials for supercapacitors,
lithium-ion batteries, and lead-acid batteries.



University, China, in 2017. Currently, his research interests
focus on carbonaceous materials for rechargeable batteries
and supercapacitors.



industry, he joined KAUST in 2009, where he has
been running a research group focused on developing
inorganic nanomaterials for energy and electronics. He is
a Fellow of the Royal Society of Chemistry, Fellow of the
American Physical Society, IEEE Distinguished Speaker
in Nanotechnology, and Senior Member of IEEE. He was
chair of the 2014 Materials Research Society (MRS) Fall
Meeting in Boston, USA, and has served on various MRS
committees.

the high activation agent/char ratios (normally ranging from
1 to 5, sometimes up to 10),^[14,15] and the high cost of activation
agent (especially KOH). The SSAs and pore-size distributions







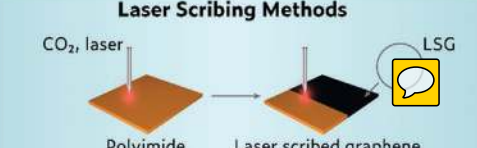
Methodology	Porogen	Pore-forming mechanism	Structure
Carbonization-Activation Methods 	$\text{CO}_2, \text{H}_2\text{O}$ NaOH, KOH $\text{H}_3\text{PO}_4, \text{ZnCl}_2$	$\text{H}_2\text{O} + \text{C} \rightarrow \text{H}_2 + \text{CO}$, $\text{CO}_2 + \text{C} \rightarrow 2\text{CO}$ $2\text{KOH} \rightarrow \text{K}_2\text{O} + \text{H}_2\text{O}$, $\text{K}_2\text{O} + \text{CO}_2 \rightarrow \text{K}_2\text{CO}_3$ $\text{K}_2\text{O} + \text{C} \rightarrow 2\text{K} + \text{CO}$, $\text{K}_2\text{CO}_3 + 2\text{C} \rightarrow 2\text{K} + 3\text{CO}$	S_{BET} up to $3000 \text{ m}^2\text{g}^{-1}$ Micro/mesopores Smooth surface
New Activation Methods 	HNO_3 KMnO_4 KNO_3 $(\text{NH}_4)_2\text{S}_2\text{O}_8$	Oxidative reactions towards carbon precursors. Decomposition of activation agents results in the formation of inorganic templates	S_{BET} up to $2500 \text{ m}^2\text{g}^{-1}$ Micro/mesopores Hierarchical pore
Template Methods 	$\text{SiO}_2, \text{TiO}_2$ Soft templates	Carbon skeleton forms around (inside) template. Upon removal of template, porous carbon obtained	S_{BET} around $1000 \text{ m}^2\text{g}^{-1}$ Mesopores 3D morphology
Self-Template Methods 	Self-generated carbonates and oxides	Organic salts decompose. Template and activation agent remains inside	S_{BET} 500 to $2200 \text{ m}^2\text{g}^{-1}$ Micro/mesopores 3D sheet morphology
Direct Pyrolysis Methods 	Organic chains (molecules) with low thermostability	Phase separation during carbonization. Template role of polymer monomers. Decomposition of polymer or functional groups	S_{BET} 300 to $3022 \text{ m}^2\text{g}^{-1}$ Micro/mesopores Tunable morphology
Self-Activation Methods 	$\text{CO}_2, \text{H}_2\text{O}$	Decomposition gases ($\text{CO}_2, \text{H}_2\text{O}$) $\text{CO}_2 + \text{C} \rightarrow 2\text{CO}$ $\text{H}_2\text{O} + \text{C} \rightarrow \text{CO} + \text{H}_2$	S_{BET} up to $2600 \text{ m}^2\text{g}^{-1}$ Amorphous Micro/mesopores
Laser Scribing Methods 	Heat-expansion Stacking of graphene dots	CO_2 laser adsorbed by sp^3 C-C bonds. Carbon dots are generated and assembled. Pores from heat-expansion, stacking of carbon dots	S_{BET} 80 to $1000 \text{ m}^2\text{g}^{-1}$ 3D graphene Mesopores

Figure 1. Synthesis methodologies used to produce porous carbons for SC applications. The porogens, pore-forming mechanisms, and structural characteristics of the resultant porous carbons are summarized.

of porous carbons obtained by carbonization-activation strategy vary with preparation parameters and activation agents, as will be discussed later.

Recently, there has been a fast development using novel emerging activation agents such as copper chloride (CuCl_2) and potassium permanganate (KMnO_4) for the preparation of porous carbons.^[16,17] These novel activation agents produce porous carbons with high SSA and unique morphologies but may generate toxic gases that need further decontamination. As the synthesis of chemically activated porous carbons using

these novel activation agents is not environmentally friendly, the search for environmentally benign chemical activation agents and green chemical activation processes is critical for the sustainable development of porous carbons.

Various template methods have been applied as versatile strategies for the preparation and assembly of mesoporous carbons.^[18] The advantage of template methods is that they can finely tune the pore-size distribution by tuning the template size, enabling extremely narrow pore-size distribution. However, the synthesis and removal of templates are

1 tedious procedures that increase production complexity and
2 cost. Besides, the pore sizes of porous carbons prepared from
3 template methods are usually dominated by mesopores, which
4 are largely restricted by the template sizes.

5 Carbide-derived carbons (CDCs) are microporous carbon
6 materials produced from a high-temperature etching of metal
7 carbides (TiC, SiC, VC₂) under chlorine gas atmosphere. CDC
8 is the earliest example that uses the self-generated template as
9 a porogen.^[19] Recently, researchers have become more inclined
10 to use abundant alkaline metal-organic salts as the carbon
11 precursors by applying self-template strategies. In these strat-
12 egies, the pyrolysis-generated metal oxides or metal carbon-
13 ates act as templates and activation agents. To obtain porous
14 carbons, these templates are further removed by water or acid
15 washing.^[20,21] Metal-organic framework (MOF)-derived porous
16 carbons can also be grouped into the self-templated carbons,
17 as the porogens of these obtained carbons are also generated
18 during carbonization.^[22] With the fast development of MOFs
19 for energy storage applications, more and more elaborately
20 designed MOF-derived porous carbons are being produced
21 based on the self-template role of MOFs.

22 Direct pyrolysis of various organic precursors, such as
23 co-polymers, chemically treated biomasses, and polyionic
24 liquids, has been developed fast since this strategy does not
25 need specially added porogens and post-treatments.^[23] Direct
26 pyrolysis method holds great promise to be exploited as the
27 second-generation preparation technology for porous carbon
28 electrodes in SCs. In recent years, there has been a fast develop-
29 ment in using CO₂ laser scribing technique to prepare porous
30 laser-scribed graphene (LSG) electrodes for SC applications.^[24]
31 Laser scribing is usually carried out in an ambient environ-
32 ment without the protection of inert gases. The vast biomass
33 precursors that can be used in laser scribing make this tech-
34 nique attractive to realize renewable graphitic porous carbons
35 with different pore architectures. Besides the laser scribing
36 technique, there are several emerging carbonization methods
37 such as microwave carbonization,^[25,26] dehydrogenation/deoxy-
38 genation,^[27,28] and dehalogenation.^[29] Some of these methods
39 produce porous carbons with high SSAs, which makes these
40 techniques promising for the fabrication of SC electrodes.
41 Nevertheless, some of these techniques need to be carefully
42 designed to obtain effective porogens during carbonization.

43 There exist many reviews discussing porous carbon materi-
44 als for SCs, such as 2D porous carbons,^[30] porous carbons
45 for flexible and wearable SCs,^[31] porous carbons derived
46 from copolymers,^[23] porous carbons derived from renewable
47 biomasses,^[32] graphene-based materials,^[3] and nanoporous
48 carbons from molecular design.^[18] These reviews mainly focus
49 on the textural properties, surface chemistries, and capacitive
50 performances of porous carbons. However, it is important to
51 know how these porous carbons are generated through cer-
52 tain porogens, and the different mechanisms that these poro-
53 gens undergo for the preparation of porous carbons. Although
54 carbon nanotubes and carbon aerogels are commonly used
55 as electrode active materials in SCs,^[33] they possess relatively
56 low SSA and specific capacitance compared with commercial
57 porous carbons. Given the above considerations, this review
58 focuses on the fundamental mechanism aspects of both tra-
59 ditional and emerging synthesis strategies of porous carbon

for SC applications. Additionally, we discuss the remaining
challenges and suggest new synthesis strategies of porous car-
bons for commercial SC applications.

2. Carbonization–Activation Methods

Porous carbons prepared from combined carbonization–
activation strategies are usually called activated carbons.
Activated carbons were initially used to describe the activated
coal chars or biochars with high SSAs that could be used as
adsorbents for purification or carriers of catalysts. With the
invention of SC by General Electric's H.I. Becker in 1957, acti-
vated carbon became the primary and most important electrode
active material in SC applications. Generally, activated carbons
are produced by two separate steps, i.e., carbonization and
activation.^[9] Carbonization is usually carried out by pyrolysis
in an inert atmosphere. Carbonization enables the formation
of nonporous solid carbonaceous materials with high carbon
content and low oxygen or hydrogen contents. The obtained
carbonaceous materials are then activated chemically or physi-
cally to obtain activated carbon.

2.1. Carbonization

Carbonization is a complex physicochemical process in which
many reactions take place concurrently, such as dehydrogena-
tion, deoxygenation, condensation, crosslinking, hydrogen
transfer, and isomerization.^[34] During the carbonization
process, dehydrogenation, deoxygenation, and crosslinking
reactions proceed with the release of volatile compounds,
finally resulting in carbonaceous residue.^[35] Usually, the
pyrolysis processes are carried out under an inert atmosphere.
As replacements of pyrolysis, some novel techniques like
hydrothermal carbonization,^[36] microwave-assisted carboniza-
tion,^[34] dehydrogenation/deoxygenation enabled by high con-
centrated sulfuric acid,^[28] and dehalogenation of halogenated
organic polymers^[37] have also been applied to perform the
carbonization process. These novel carbonization techniques
enable the formation of carbonaceous materials with novel
structures and different chemical compositions compared
with traditional carbonization methods. Chaiwat et al. reported
a pressurized hot water treatment of cellulose, which sup-
presses the tar formation by producing a random and highly
cross-linked carbonaceous structure.^[36] Furthermore, Zhao
et al. investigated the relationship between the torrefaction
temperature, residence time, and the char yield of torrefied
corncoals (Figure 2a).^[38] Results show that by increasing torre-
faction temperature and residence time, a higher char yield can
be achieved because the crosslinking and charring of cellulose
mainly occurred at relatively high temperatures around 300 °C.
Microwave radiation can penetrate the organic solutions and
solid organics like lignocellulose, thereby achieving rapid and
volumetric heating, which enables effective carbonization.^[39]
The advantages of microwave-assisted carbonization include:
1) reducing heating time; 2) providing volumetric heating;
3) instantaneous start and stop of heating; and 4) reducing the
reactor size. Chen et al. employed the microwaves to torrefy

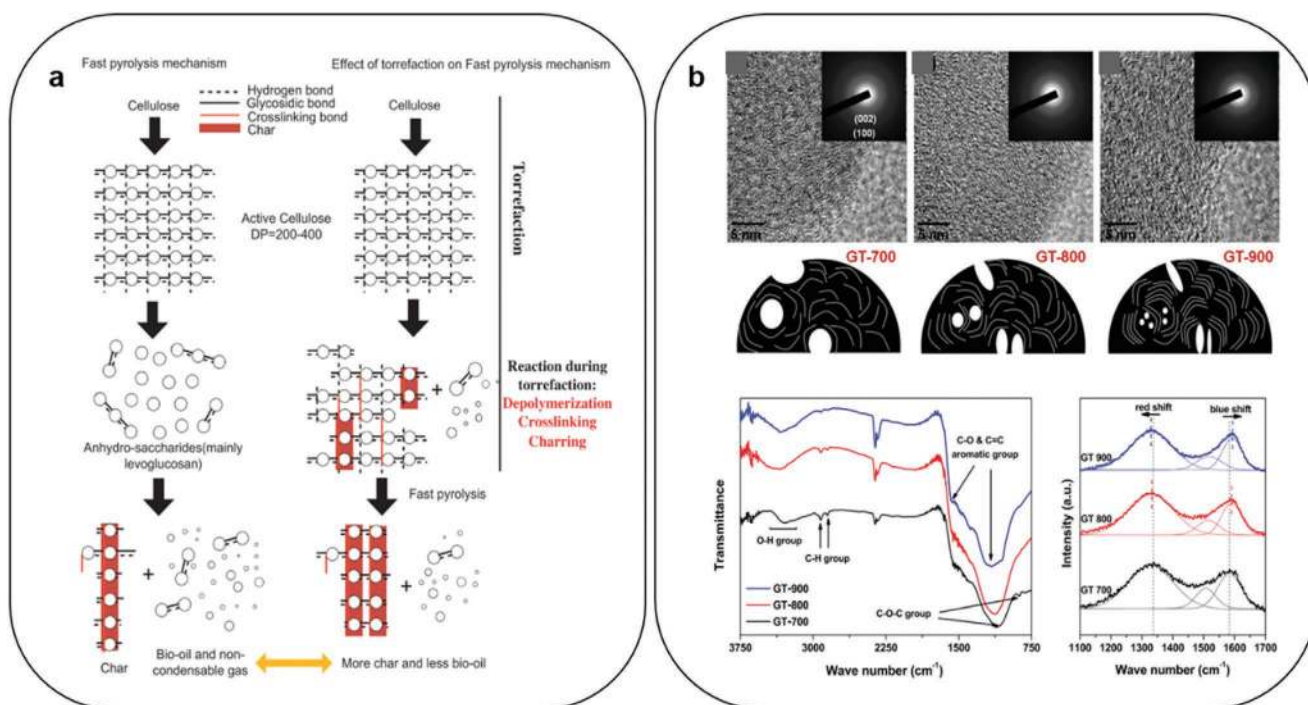


Figure 2. a) Effects of torrefaction on fast pyrolysis of cellulose. Reproduced with permission.^[38] Copyright 2012, Elsevier. b) TEM images and schematic illustrations of the physical characterization, Fourier-transform infrared spectroscopy (FT-IR), and Raman spectra obtained for green tea-derived carbon under temperatures of 700, 800, and 900 °C (GT-700, 800, and 900). Reproduced with permission.^[41] Copyright 2014, Elsevier.

the biomass in solutions of water or diluted sulfuric acid at 180 °C.^[40] The calorific value of bagasse increased up to 20.3% from wet torrefaction, which indicates the partial carbonization achieved by microwave carbonization.

Despite these numerous reports on various novel carbonization methods, pyrolysis is still the most common and most widely used carbonization technique to prepare carbonaceous materials. During pyrolysis, disordered carbons containing a relatively large amount of defects form at low temperature, while high-temperature results in partially ordered carbons were composed of defective graphene layers (Figure 2b).^[41] The pyrolysis process is so complex that it is hard to be elaborated in detail. Generally, in low-temperature pyrolysis, the organics experience the following reactions: losing adsorbed water (temperature <150 °C), dehydration from the carbohydrate unit, (<250 °C), scission of C–O and C–C bonds by free radical reactions (<400 °C), and aromatization.^[42] Because the deoxygenation reactions begin at temperatures around 400–600 °C, the low-temperature carbonized carbon is of high oxygen content, while the high-temperature carbonized carbon is of low oxygen content. During pyrolysis, the sp² hybridized graphene nanodomains also increase with the decrease of turbostratic sp³ hybridized carbons. Even though the carbonaceous structures highly rely on different carbon precursors, Kercher and Nagle proposed a general quasi-percolation model to describe the structural evolution of carbon during pyrolysis.^[43] In the quasi-percolation model, when the carbonization temperature is increased above 600 °C, the large turbostratic crystallites grew very little, but the graphene sheets grew substantially. Meanwhile, volumetric shrinkage occurs due to

the condensation of turbostratic structures. At ≈900 °C, graphene layers significantly impinge on each other. This general carbonization scenario of various carbon sources can help us understand the physical or chemical activation processes since oxygen content (depends on the pyrolysis temperature), crystal structure (graphitic degree), and pristine pore (original pores in coal char) may influence the pore-forming process in the activation process.

2.2. Physical Activation

Physical activation of char usually proceeds with an oxidizing atmosphere in a temperature-controlled tube furnace filled with inert gases operated at high temperatures ranging from 600 to 1200 °C. Normally, steam or CO₂ is used as activation agents in physical activation.^[9] Compared with solid chemical activation agents (NaOH, KOH), steam and CO₂ show low corrosive effects with the production facilities, which is more suitable for practical application.^[44] Researches have shown that the physical activation temperatures have nearly linear effects on micropore volumes.^[45–47] Few pores are developed by gas generation, and evolution, the pores in porous carbon mainly form through oxidative reactions (Equations (3) and (4)) in oxidizing atmospheres (e.g., H₂O and CO₂) during the physical activation process^[48]



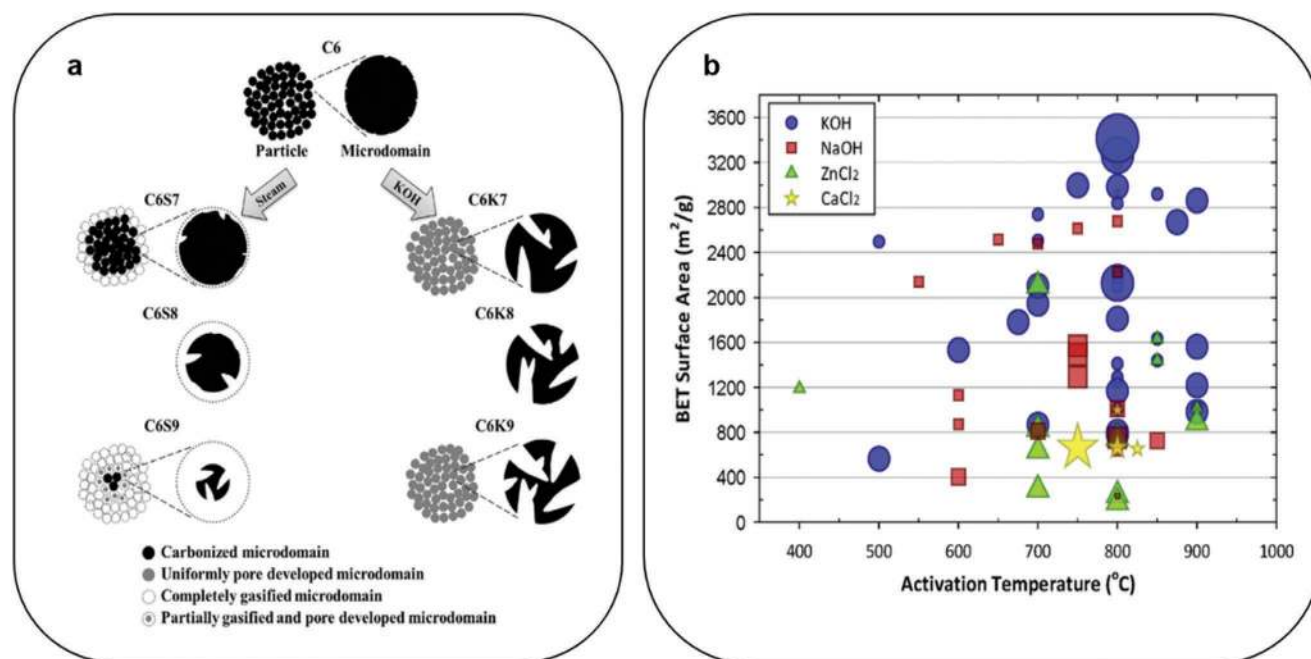


Figure 3. a) Structural mechanism model of pore formation in the carbon material using steam and KOH as activation agents. Reproduced with permission.^[46] Copyright 2016, Elsevier. b) SSAs of porous carbons as a function of the chemical activation agents (KOH, NaOH, ZnCl₂, and CaCl₂) and activation temperatures. Reproduced with permission.^[59] Copyright 2017, Elsevier.

Physical activation permits tailoring of the pore-size distribution more accurately and narrowly, which results in more micropores than the chemical activation. Besides, physical activation reduces both the particle and microdomain sizes in the resultant activated carbons.^[46] Srinivasakannan et al. investigated the effects of physical activation using CO₂ and chemical activation using H₃PO₄ and ZnCl₂ on the porous structures of activated carbon.^[49] Their results show that chemical activations using H₃PO₄ or ZnCl₂ as activation agents result in the formation of porous carbons with relatively higher tap densities, a higher proportion of mesopores, accompanied by lower weight losses during the activation processes. Compared with chemical activation, physical activation usually has the characteristics of high activation temperatures, long activation time, relatively low yields, low tap density, small pore sizes, and low SSA (Figure 3a).^[46] However, from a production point of view, physical activation shows low corrosion toward the reactor compared with chemical activation. So physical activation is more feasible and widely used for industrial production. To improve the SSA of porous carbons produced by physical activation, Şahin and Saka produced activated carbons from corn shells by physical activation method using CO₂ and H₂O as activation agents and a two-step pretreatment using the activated agents of ZnCl₂ and HCl. With the increase of impregnation concentration of agents, Brunauer–Emmett–Teller (BET) SSA and pore volume of the produced activated carbon reached to 1779 m² g⁻¹ and 0.927 cm³ g⁻¹, respectively.^[50]

2.3. Traditional Chemical Activation

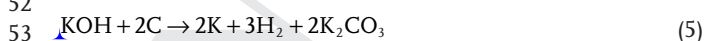
Compared with physical activation, chemical activation offers several advantages: high carbon yields, relatively

low-temperature processes, and high mesopore ratios in the resultant porous carbon.^[45,47] A large number of studies have demonstrated the synthesis of porous carbon by chemical activation with the abundant choices of carbon sources and activation agents such as alkaline metal hydroxides, alkaline metal carbonates, and phosphoric acids. Besides, researchers could exert the unique chemical or structural characteristics of carbon sources to synthesize various porous carbons with different pore structures.^[43–45] Traditionally, potassium hydroxide (KOH),^[51,52] sodium hydroxide (NaOH),^[53,54] zinc chloride (ZnCl₂),^[55] phosphoric acid (H₃PO₄),^[49,56] sodium carbonate (Na₂CO₃),^[57] and potassium carbonate (K₂CO₃)^[57,58] have been used as activation agents. For a high-level summary of the effect of traditional chemical activation agents on porous carbon, the relationships between the SSA and activation temperature of the activated carbon are shown in Figure 3b for a few chemical activation agents.^[59] The data indicate that KOH is the most powerful activation agent, while NaOH takes the second place. Salt activation agents, such as ZnCl₂, produce porous carbons with lower SSAs. Normally, chemical activation can produce porous carbons with high SSAs ranging from 500 to 3600 m² g⁻¹.^[60,61] Lin et al. compared the effects of hydroxide activation agents, such as NaOH, KOH and a specific mixture of them on the chemical activation of biochar from rice husk.^[62] The derived activated carbon using NaOH, KOH, and the mixture of them were termed as NC, KC, and NKC, respectively. NC, KC, and NKC exhibited SSAs of 2260, 1702, and 2747 m² g⁻¹, and pore volumes of 1.31, 0.74, and 1.40 cm³ g⁻¹, respectively. Interestingly, NKC possessed the most developed pore structure and widest pore-size distribution among three porous carbon materials. Their results indicate that the pore size of all three samples is centered at 1.0 nm with a

1 wide range of 0.5–3.0 nm, while NaOH assists the formation
2 of mesoporous structure compared with KOH. When used
3 as electrodes of SC, NKC displayed a specific capacitance of
4 194.6 F g⁻¹ at 0.5 A g⁻¹ tested by galvanostatic charge–discharge
5 (GCD) in H₂SO₄ electrolyte.

6 Carbonization and activation can be combined in one step.
7 The combination of activation and carbonization can result
8 in highly macroporous carbons, which is due to the fact that
9 organics can be easily decomposed in alkaline media at high
10 temperatures. In this regard, the ratio of activation agent/
11 organic precursor should be controlled below one. Zhang et al.
12 synthesized a 3D porous carbon foam (PCF) with one-step car-
13 bonization of K₂CO₃ containing chitosan.^[63] PCF shows a high
14 SSA about 1030 m² g⁻¹ and micropores centered at 0.66 nm.
15 The specific capacitance of PCF was 246.5 F g⁻¹ at 0.5 A g⁻¹,
16 while 67.5% of its capacitance was maintained at 100 A g⁻¹.
17 Fuertes et al. mixed polypyrrole (PPy) and KOH, and did car-
18 bonization and activation in one step.^[64] The as-prepared
19 porous carbon showed an ultrahigh SSA of 3000–3500 m² g⁻¹
20 and a pore volume up to 2.6 cm³ g⁻¹. They further investi-
21 gated the pore size development along with the activation
22 temperature.^[65] In the case of PPy used as carbon precursor,
23 narrow micropores of 1 nm were formed at 600 °C, and a
24 large fraction of mesopores centering at 2.7 nm was formed at
25 800 °C. Similarly, Zhang et al. synthesized a hierarchical porous
26 carbon by carbonizing lignin and KOH directly.^[66] The obtained
27 hierarchical porous carbon exhibited an SSA of 907 m² g⁻¹ with
28 a wide pore-size distribution ranging from 0.6 to 40 nm and a
29 high specific capacitance of 165.0 F g⁻¹ at 0.05 A g⁻¹ in H₂SO₄
30 electrolyte. Although with the same KOH activation agent, the
31 obtained porous carbon materials showed different porous
32 architecture, SSA, and specific capacitance, which is resulted
33 from the different activation activities of KOH toward different
34 organic precursors.

35 The activation mechanism of the normally used chemical
36 activation agents is still not well understood due to the various
37 variables and different carbon precursors used in the activation
38 process. In the case of KOH, pores formed below 500 °C are
39 caused by the evaporation of volatiles from dehydrating reac-
40 tions or radical reactions.^[10] In the chemical activation stage, the
41 pores are further developed with the consumption of carbon, as
42 shown in Equation (5). Equation (5) normally occurs at temper-
43 atures lower than 570 °C. Although this reaction occurs at low
44 temperature, the produced K further reacts with KOH forming
45 K₂O. K₂CO₃ begins to form at around 400 °C due to the reac-
46 tion between K₂O and CO₂ pyrolysis gases (Equation (6)).^[10]
47 KOH is completely consumed at 600 °C. So the main etching
48 agents of KOH activation are K₂CO₃ and K₂O (reactions are
49 shown in Equations (7) and (8)) around 700 °C. Meanwhile, the
50 activation products of CO₂ may also take some part in the pore-
51 forming process due to their physical activation effects



From the structural consideration, the influences of car-
bonization and activation temperatures on the crystal struc-
ture of porous carbon are still needed to be explored, as
the graphitic carbon and amorphous carbon show different
electrochemical behaviors as electrodes of SC. The oxygen-
containing functional groups also need to be investigated,
as the defective oxygen-containing sites are highly active
toward chemical activation. Although papers are reporting
the influence of carbonization temperatures toward chemical
activation,^[67] the influence of carbonization temperatures
on the crystalline structures and surface functional groups
of porous carbons need to be studied in detail since the
oxygen functional groups sometimes limit the cycling life of
an SC.^[68]

Chemical activation is the most widespread method for the
preparation of porous carbons in lab-scale research. Due to the
high consumption of the KOH activation agent and the highly
corrosive environment of KOH at high temperatures toward
reactors, KOH activation is unlikely to be used in industrial
production. Besides, chemical activation generates a lot of
contaminants that are generally high alkaline and polluting.
Toward future industrial productions, green synthesis methods
need to be developed, and the quantities of chemical activation
agents should be reduced.

3. New Chemical Activation Methods

Porous carbon materials with high SSA up to thousands of
square meters per gram can be easily achieved by chemical
activation. However, the traditional chemical–activation syn-
thesis strategies suffer from the drawbacks of severe corrosion
of reactor, small pore size, and pore structure collapse due to
the high temperatures. Another consideration of chemical
activation is its environmental impact. Since chemical activation
produces highly concentrated alkaline pollutants, which need
to be further treated to minimize the emission of pollutants,
this inevitably increases the production cost of porous carbon.
In recent years, there has been a huge effort to search for
efficient chemical activation agents. Even though these chem-
ical activation agents may not be considered as green agents,
they provide opportunities to develop new activation strategies
for the synthesis of porous carbons. These new chemical agents
can be classified according to their different activation mecha-
nisms into three groups: molten salt, decomposable salt, and
oxidative salt.

3.1. Molten Salt Etching

Molten salt etching methods are used to describe methodolo-
gies which use corrosive molten chemical agents that react with
carbon to generate porous structures under high temperatures.
In recent years, CuCl₂,^[17,69] NiCl₂,^[70,71] NaCl,^[72–74] KCl,^[74]
and FeCl₃^[75–77] have been used as molten salts in chemical
activation. For example, CuCl₂ was proved to show less destruc-
tive effect on the natural structure of the biomass precursor,
while traditional activation agents like KOH and ZnCl₂ crushed
the carbon precursors into carbon fragments in the activation

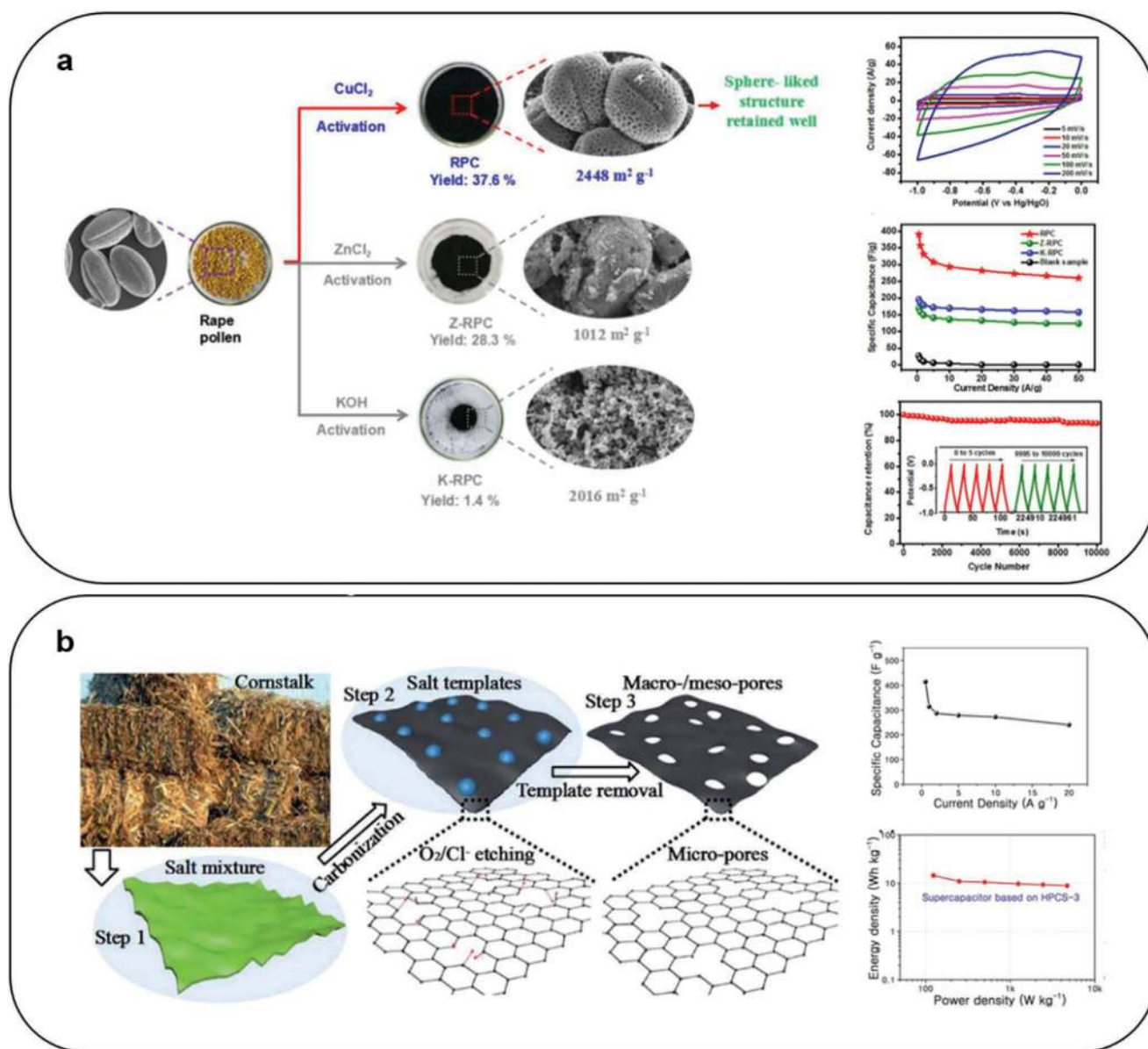
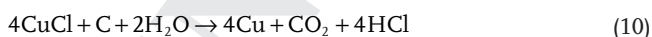


Figure 4. a) The preparation schematic diagram of RPC, Z-RPC, and K-RPC as activation agents (left); CV curves of RPC at different scan rates, specific capacitances of RPC, Z-RPC, K-RPC, and the blank sample at different current densities and the long-term cycling test measured at 20 A g^{-1} (inset graph is the GCD curves of RPC). Reproduced with permission.^[17] Copyright 2018, The Royal Society of Chemistry. b) The preparation schematic diagram of HPCS from cornstalk under an air atmosphere (left), electrochemical performances of the symmetric SC in a two-electrode system in $1.0 \text{ M H}_2\text{SO}_4$ aqueous electrolyte, specific capacitances of HPCS-3//HPCS-3 at different current densities, and Ragone plot (right). Reproduced with permission.^[72] Copyright 2018, The Royal Society of Chemistry.

process (Figure 4a).^[17] The mechanisms of CuCl_2 porogen are described as follows^[69]



The sphere-like porous carbon prepared from CuCl_2 activation (RPC) exhibited a high SSA up to $2488 \text{ m}^2 \text{ g}^{-1}$, with the pore size distributed below 2 nm and pore-size distribution centered at 1.2 nm . With the same activation temperature,

porous carbon derived from ZnCl_2 activation (Z-RPC) shows a wide pore-size distribution ranging from 1 to 60 nm while the pore size of KOH activation porous carbon (K-RPC) is distributed below 3 nm . Moreover, RPC exhibits a high yield up to 37.6% based on the raw materials, which is much higher than that of Z-RPC (28.3%) and K-RPC (1.4%). When used as electrodes of SC, the porous carbon prepared from CuCl_2 activation presents a high gravimetric capacitance of 390 F g^{-1} at 0.5 A g^{-1} in 6.0 mol L^{-1} KOH aqueous electrolyte. The mechanism of CuCl_2 activation is demonstrated by the formation of Cu and CuCl intermediate species. Namely, carbon is oxidized by Cu^{2+}

ions. Since there is no mechanism study in this report, the role of Cl^- ion needs to be confirmed. From a practical production view, the outlet gases from CuCl_2 activation need to be determined and purified for green synthesis. The mixture salt of KCl and NaCl has also been developed as the molten salt agent. Wang et al. investigated the pore-forming mechanism of the cornstarch in KCl/NaCl mixture molten salt using thermogravimetric techniques.^[72] They found that oxygen molecules act as an etching agent at lower temperatures, while at temperatures of above 800°C , Cl^- ions diffuse into the carbon skeleton and etch it, which assists the formation of micro- and mesopores (Figure 4b). By employing this strategy, the as-prepared hierarchical porous carbon with SSA of $1588\text{ m}^2\text{ g}^{-1}$ exhibited a high specific capacitance of 407 F g^{-1} at 1 A g^{-1} . Chen et al. reported that the SSAs of porous carbons prepared with the mixture molten salt of KCl and NaCl are higher than porous carbons prepared with mere KCl or NaCl .^[74] With the help of KCl and NaCl mixture, porous carbons generate micropores and mesopores centered at ≈ 1.4 , 2.7 , and 3.8 nm , respectively. This research also proved that KCl agent creates more micropores and NaCl creates more mesopores from the same carbon precursor, which is similar to the conclusion of Lin et al.^[62] So it can be concluded that cations such as K^+ and Na^+ take part in the activation process, which affects the micropore or mesopore formation. FeCl_3 is another molten salt that can be used as an activation agent. Combined with ZnCl_2 and KCl , the molten salt mixture can produce hierarchical porous carbon with SSAs up to $3155\text{ m}^2\text{ g}^{-1}$.^[76] The role of FeCl_3 during activation has been investigated.^[75] FeCl_3 breaks hydrogen bonds below 100°C and depolymerizes organic material at 135°C . When the temperature increased to $200\text{--}330^\circ\text{C}$, dehydroxylation reactions take place as shown by Equation (11). At $330\text{--}700^\circ\text{C}$, the generation of Fe_2O_3 and CO_2 promotes the development of micropores, as described in Equations (12) and (13). During this process, the microporous structure of porous carbon is further developed by the formation of Lewis acid with the synergistic effect of Fe^{3+} and Cl^- . Moreover, the reaction products of iron oxides also show a positive influence on the formation of micropores. Porous carbon exhibited a relatively stable structure at temperatures ranging from 700 to 800°C . The reduction reactions of iron oxides further modified the microporous structure of amorphous carbon (Equations (14)–(16))



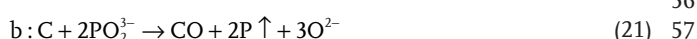
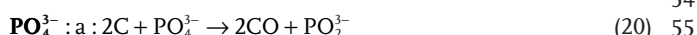
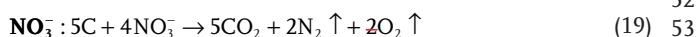
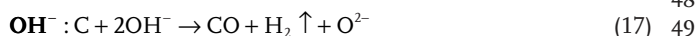
The role of Cl^- ion in chlorides still needs to be confirmed using in situ techniques. Additionally, other porogens, such as KOH and NaOH , can be added into the molten salts to contribute to the porous structure of carbon products.

Undoubtedly, the molten salt strategy is milder compared with chemical activation methods. However, the high cost of molten salt used for preparation is an obstacle for practical production.

3.2. Decomposable Salts Etching

Various salts are decomposable and thus, the decomposition gases can etch carbons to form pores. The decomposable salt is a huge family with numerous members such as zinc acetate,^[78] $\text{Zn}(\text{NO}_3)_2$,^[79] NaNO_3 ,^[80] calcium acetate,^[81] sodium acetate,^[82] MgCO_3 ,^[83] sodium chloroacetate,^[84] K_3PO_4 ,^[85] NaH_2PO_4 ,^[86] tetraethylorthosilicate, and potassium acid phthalate. Generally, Zn salts are regarded as a dehydration agent.^[87] The mechanism of Zn salts is supposed to promote the formation of double bonds between the carbon atoms by capturing H_2O molecules from organic carbon sources.^[88,89] Moreover, it is well-known that the condensation reactions of aromatic hydrocarbons, such as alkylation and acylation reactions, are more likely to take place in the presence of Zn components.^[90,91] Thus, Zn components can be used as a cyclo-addition porogen. As an example, a kind of polyacrylonitrile (PAN)/pitch/lignin-based carbon nanofibers (CNFs) with ZnO (PPL-Zn) was fabricated by one-step electrospinning the mixture of PAN, pitch, lignin, and zinc acetate. The decomposition product, Zn, was removed during the high-temperature annealing process. CNF exhibited an SSA of $1194\text{ m}^2\text{ g}^{-1}$ and a specific capacitance of 165 F g^{-1} (Figure 5a).^[78] The porous carbon that prepared with decomposable zinc acetate presented an SSA almost two times that of the CNF fabricated without zinc acetate. Especially as a porogen, zinc acetate shows the ability to increase the SSA and mesopore volume.

Li et al. fabricated a cross-coupled macro- and mesoporous carbon material by using the decomposable and water-removable NaNO_3 as porogen in the gelatin biopolymer aerogel (Figure 5b).^[78] This porous carbon exhibited small-sized mesopores ($2\text{--}4\text{ nm}$) and macropores ($50\text{--}150\text{ nm}$) which gave a high SSA of $2872.2\text{ cm}^2\text{ g}^{-1}$. NaNO_3 begins to decompose above 600°C , generating pyrolysis gases of N_2 , O_2 , and NO , which assists in creating mesoporous structure in the final porous carbon product. Antonietti et al. studied a series of salts with oxygen-containing anions on their abilities to create pores in the molten LiCl/KCl system (melting point of 353°C).^[92] In the liquid flux media of LiCl/KCl , a series of oxysalts were used to prepare porous carbons with the SSA up to $3200\text{ m}^2\text{ g}^{-1}$.^[93,94] Meanwhile, the pore-forming mechanisms of oxysalt anions have been described as follows



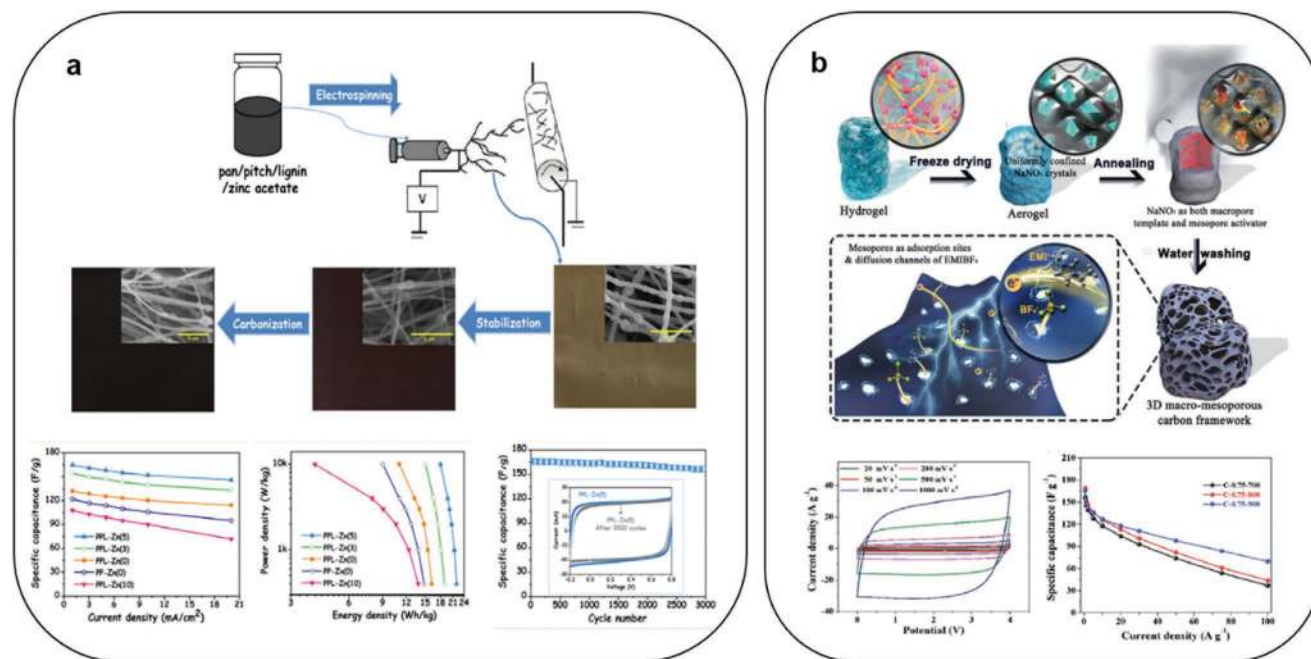
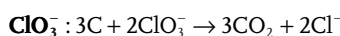
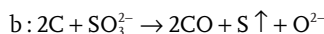


Figure 5. a) The preparation schematic diagram of PPL-Zn composite (above). Electrochemical tests of the two electrodes in 6 mol L⁻¹ KOH aqueous electrolyte: specific capacitances as a function of current densities, Ragone plots, and the cycling performance over 3000 cycles of PPL-Zn at 1 mA cm⁻² (below). Reproduced with permission.^[78] Copyright 2019, Elsevier. b) The synthesis schematic diagram of 3D cross-coupled macro- and mesoporous carbon electrode via NaNO₃ as porogen strategy and its application in ion liquid-based capacitor at 4 V (above), CV plot, and rate capability of porous carbon prepared with NaNO₃ porogen (below). Reproduced with permission.^[80] Copyright 2018, Wiley-VCH.

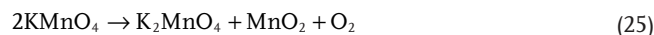


Generally, the cations of these salts, such as K⁺, are believed to take part in chemical activation, as described in Equations (5)–(8). However, Liu and Antonietti argued that in the case of potassium oxysalts, like KH₂PO₄, it is the anion groups of H₂PO₄⁻ rather than K⁺ that manage the carbothermal reduction under the temperature below 1000 °C based on thermodynamic considerations.^[95] The precise mechanism still needs to be further analyzed using various physicochemical methods and in situ techniques. Based on the above mechanisms, many oxygen-containing salts based on these anions have the potential to be used as activation agents.

3.3. Oxidative Salt Etching

The pore engineering of carbon materials can also be achieved with oxidative activation agents. Oxidative activation agents such as HNO₃,^[96–98] KMnO₄,^[25,99,100] KNO₃,^[101,102] and Mn(NO₃)₂^[103] were used to create porous carbons by oxidizing carbon at room temperature or high annealing temperatures. Wang et al. treated carbon cloth with KMnO₄, HNO₃, and H₂O₂, respectively, at room temperature. After treatment, the SSA of carbon cloth increased from 5.3 to 61.2 m² g⁻¹.^[99] Yang et al. fabricated single-wall carbon nanohorns (SWNHs) with high SSA up to 1464 m² g⁻¹ and high pore volume about 1.05 cm³ g⁻¹ by merely soaking SWNHs with 69% HNO₃.^[96] The treatment of

HNO₃ can efficiently produce microporosity in the range of 0.4–1.9 nm. On the other hand, KMnO₄ turned out to be an effective porogen for hierarchical porous carbon. When KMnO₄ was applied as an activation agent, the derived carbon exhibited more macropores and mesopores compared with the carbon materials activated by KOH.^[100] A large number of macropores and mesopores were generated due to the reactions described in Equations (25)–(27). KMnO₄ is decomposed into K₂MnO₄, MnO₂, and O₂. These products play crucial roles in etching carbon skeleton and creating mesoporous structure. When the temperature increases to 700 °C, the decomposed K₂CO₃ shows apparent influence on the creation of the microporous structure of carbon material, which has been discussed in Section 2.3. The KMnO₄-activated carbon exhibited an SSA up to 1199 m² g⁻¹ and a pore volume of 11.7 cm³ g⁻¹. The capacitances of KMnO₄-activated carbon are 242 F g⁻¹ at 1 A g⁻¹ and 145 F g⁻¹ at 10 A g⁻¹



The KNO₃ generates huge expansion when carbon is heated under an inert atmosphere due to the strong explosive characteristic of KNO₃. Wang et al. used KNO₃ to put substantial inner stress to explode the carbon into slices, as shown in Figure 6a.^[102] After KOH activation, the obtained porous carbon nanosheets (PCNSs) exhibited an SSA up to 2788 m² g⁻¹, and

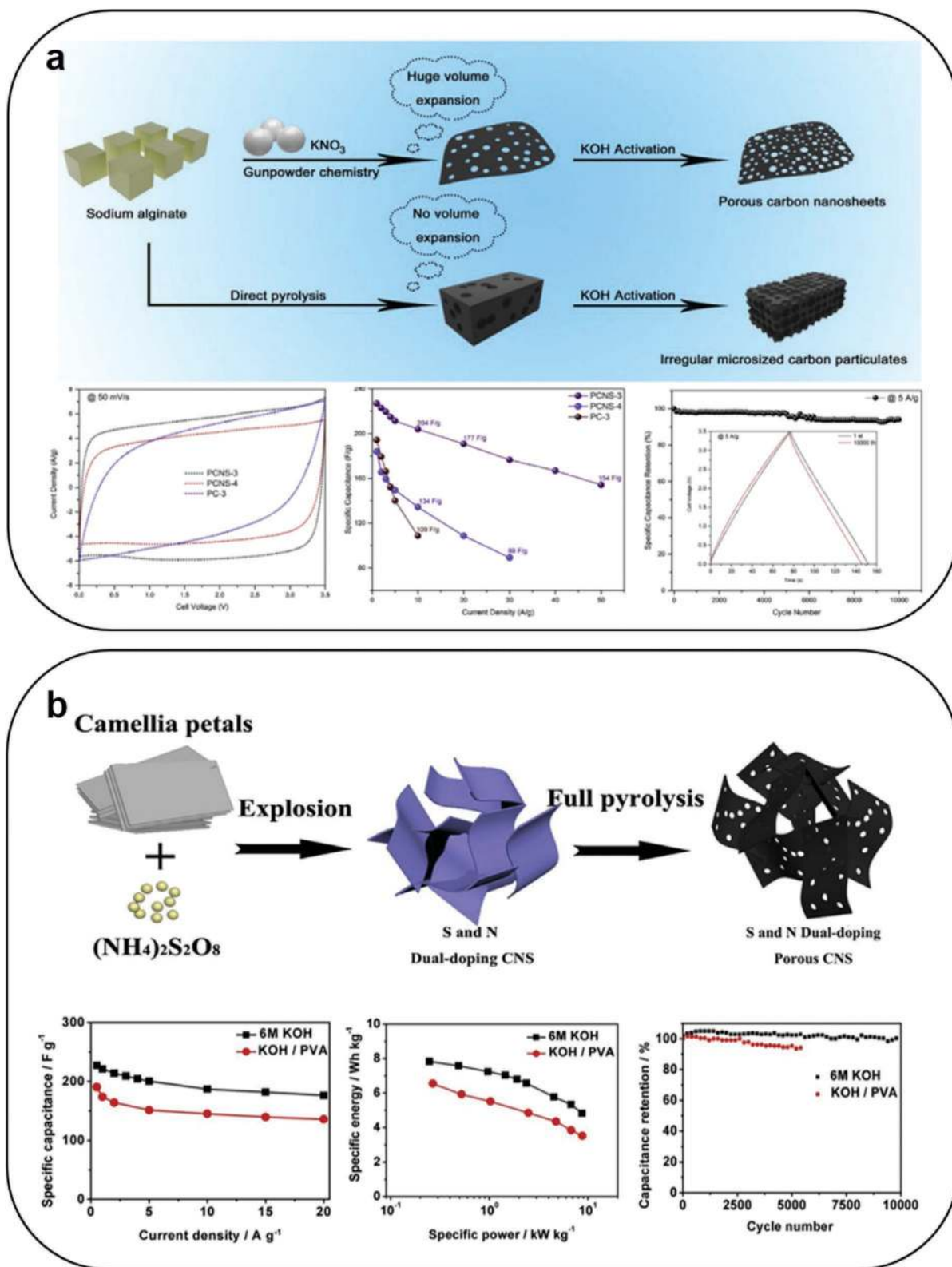
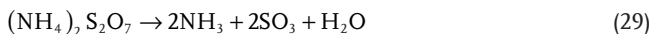
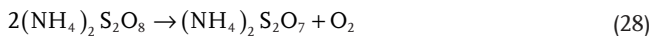


Figure 6. a) The preparation schematic of porous carbons with KNO_3 exploding carbon into slices (above). CV curves at a scan rate of 50 mV s^{-1} , rate capability as a function of current densities, and cycling stability test of the PCNS-based SC at 5 A g^{-1} for 10 000 cycles (the inset is the GCD profiles of the initial and 10 000th cycles). Reproduced with permission.^[102] Copyright 2019, Elsevier. b) The preparation schematic of CNSs (above), the correlation of specific capacitances with current densities, Ragone plot, and the GCD cycling performance of CNS (below). Reproduced with permission.^[104] Copyright 2016, Elsevier.

1 high mesopore volume. Because of the high mesopore volume
2 of PCNS, PCNS showed a superior rate performance. PCNS
3 exhibited a high specific capacitance of 226.9 F g⁻¹ at 1 A g⁻¹,
4 while a specific capacitance of 154.3 F g⁻¹ still maintained at
5 50 A g⁻¹



11 Another typical oxidative chemical activation agent is ammo-
12 nium persulfate ((NH₄)₂S₂O₈). (NH₄)₂S₂O₈ decomposes first
13 at temperatures higher than 180 °C (Equation (28)), and finally
14 decomposes completely into NH₃, SO₃, and H₂O at tempera-
15 tures higher than 400 °C (Equation (29)).^[104,105] In a one-step
16 experiment fabricating PCNSs, camellia petals were mixed with
17 (NH₄)₂S₂O₈ and carbonized at high temperature (Figure 6b).^[104]
18 The obtained CNS exhibited a high SSA of 1122 m² g⁻¹, specific
19 capacitances of 227.0 F g⁻¹ at 0.5 A g⁻¹ and 176.2 F g⁻¹ at 20 A g⁻¹.

4. Template Methods

4.1. Hard Templates

25 Template synthesis is one of the most mature methods to
26 fabricated carbon materials with well-defined pore structures
27 and narrow pore-size distributions. Hard templates such as

SiO₂,^[106–108] MgO,^[109–111] ZnO,^[112–114] Al₂O₃,^[115,116] TiO₂,^[117] as
2 well as zeolite^[118,119] are usually used as templates which can be
3 easily synthesized into uniform and regular porous structure.
4 The key steps in the hard template methodology include:^[120]
5 1) fabrication of the desirable hard template, 2) impregnation
6 of hard template with carbon sources, 3) pyrolysis under high
7 temperature, and 4) etching templates by acid or alkali solution
8 etching. Among these oxide templates, silica is one of the most
9 mature templates used for mesoporous carbon synthesis, and
10 some silica templates have been commercially produced.^[107,108]
11 Liang et al. fabricated three kinds of mesoporous carbon cata-
12 lysts using 12 nm SiO₂ nanoparticles (silica colloid), ordered
13 mesoporous silica (SBA-15), and montmorillonite (MMT) as
14 templates.^[106] By employing vitamin B12 (VB12) as a carbon
15 precursor, the carbon catalyst fabricated with silica nanopar-
16 ticles exhibited a higher SSA (572 m² g⁻¹) than that of the other
17 samples (Figure 7a).^[106] The carbon catalysts fabricated with
18 SBA-15 and MMT as templates presented SSAs about 387 and
19 134 m² g⁻¹ with the pore-size distribution centered at 3.5 and
20 4.5 nm. Porous anodic aluminum oxide (AAO) is a porous
21 hard template that has been widely used for preparing porous
22 carbons for nano-functional devices.^[121] The porous carbons pre-
23 pared using AAO templates have evenly distributed pores sizes
24 in the range of 50–200 nm, which is too large for SC electrode
25 application. Zhao et al. prepared ordered mesoporous carbon
26 nanosheets using AAO membrane as template.^[116] The
27 resultant mesoporous carbon nanosheets had pore sizes of

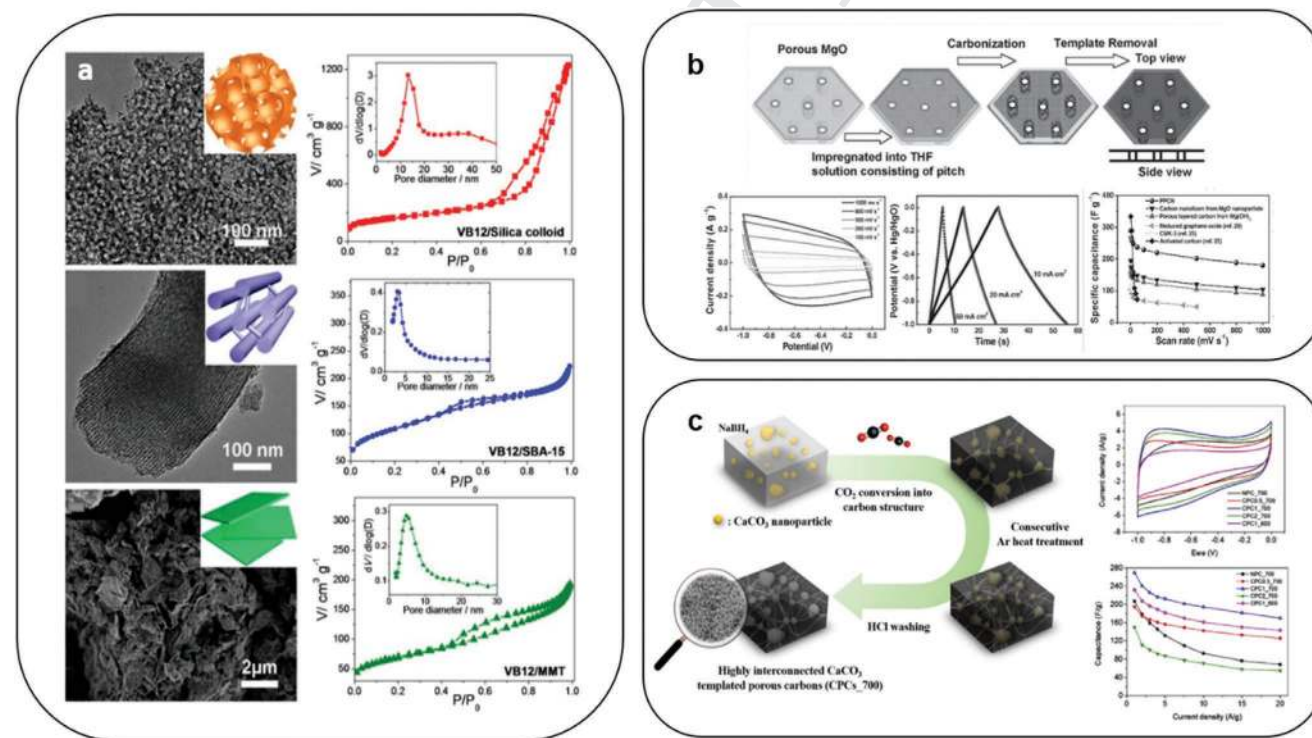


Figure 7. a) TEM, SEM images, and N₂ adsorption isotherms of as-prepared porous carbon electrocatalysts: VB12/silica colloid, VB12/SBA-15, and VB12/MMT. Reproduced with permission.^[106] Copyright 2013, American Chemical Society. b) The preparation schematic diagram of 3D pillared-PCNSs and the corresponding electrochemical performances: CV curves, GCD curves at various current densities, and specific capacitances versus scan rates of the as-prepared carbon materials. Reproduced with permission.^[110] Copyright 2012, Wiley-VCH. c) The schematic diagram for one-step nano-templated CO₂ conversion into porous carbons, and the corresponding CV curves, specific capacitances at various current densities of the porous carbons. Reproduced with permission.^[123] Copyright 2018, Elsevier.

1 hundreds of nanometers, tens of micrometers in length, and
2 sheet thickness values of about 1 nm. Thus, the structural fea-
3 tures of porous carbons prepared using the hard templates
4 greatly depend on the properties of the templates used.

5 Magnesium oxide (MgO) can be easily synthesized with
6 morphologies of 2D sheets and 3D clusters, and conse-
7 quently, many porous carbons have been synthesized using
8 MgO templates. Fan et al. proposed a strategy to fabricate a
9 large number of new porous carbons using MgO templates
10 with different morphologies, such as MgO nanoparticles and
11 Mg(OH)₂ nanosheets (Figure 7b).^[110] Self-supporting lay-
12 ered 3D pillared-PCNSs with an average mesopore size of
13 7 nm were formed during the carbonization of coal tar pitch.
14 In this strategy, carbon layers were deposited on the MgO
15 nanosheets, so the porous carbon inherited the morphology
16 of MgO templates. The structure of 3D pillared-PCNSs can
17 be controlled by changing boiling times, which makes the
18 fabrication strategy easy to control. When used as an elec-
19 trode material for SC, the 3D pillared-PCNSs with SSA up to
20 883 m² g⁻¹, exhibited a high gravimetric specific capacitance
21 of 289 F g⁻¹ at 2 mV s⁻¹ and a high capacitance retention ratio
22 of 76% at a scan rate of 1000 mV s⁻¹ compared with the spe-
23 cific capacitance obtained at 5 mV s⁻¹. In some cases, carbon
24 sources can also be combined with chemicals that generate
25 gases during the pyrolysis process. In this way, the porogens
26 are bifunctional, and pore sizes less than the templates can
27 thus be generated. Hu et al. used a 3D flower-shaped MgO
28 as a template and synthesized nitrogen-doped porous carbon
29 using cellulose acetate as a decomposable carbon source
30 and urea as a nitrogen source.^[122] The as-synthesized hier-
31 archical porous graphene-like carbon displayed ultrathin
32 graphene-like sheets and an SSA of 937 m² g⁻¹. A high spe-
33 cific capacitance of 333 F g⁻¹ at 1 A g⁻¹ was achieved with
34 the hierarchical porous graphene-like carbon as SC electrode
35 material. The specific capacitance of hierarchical porous gra-
36 phene-like carbon at 10 A g⁻¹ retained 84% compared with the
37 capacitance measured at 1 A g⁻¹. Besides the high gravimetric
38 specific capacitances achieved with hard template methods,
39 the enhancement of volumetric capacitance can be achieved
40 by reducing the macropores and mesopores derived from hard
41 template methods. Bu et al. obtained a high-density porous
42 carbon named CCNC (collapsed carbon nanocage) by depos-
43 iting a thin shell on the MgO template and then collecting the
44 collapsed sample after removing the MgO template.^[21] The
45 CCNC with a high compaction density of 1.32 g cm⁻³ exhib-
46 ited an SSA of 1788 m² g⁻¹ and a pore volume of 0.79 cm³ g⁻¹.
47 Using ionic liquid electrolyte, the CCNC achieved a high volu-
48 metric energy density of 73 Wh L⁻¹ with a maximal volumetric
49 power density of 67 kW L⁻¹.

50 Because of the well-shaped tunnel or hollow oxides, the hard
51 template method can be easily combined with other novel syn-
52 thesis strategies. Kim et al. proposed a single-step process to
53 convert CO₂ into hierarchical porous carbon by using NaBH₄ as
54 a reducing agent and CaCO₃ as a nano-template (Figure 7c).^[123]
55 The NaBH₄ and CaCO₃ were mechanically mixed and heated
56 up to high temperatures under a CO₂ gas flow. The as-prepared
57 porous carbon showed an SSA up to 1262 m² g⁻¹ with a broad
58 pore-size distribution ranging from 10 to 50 nm. The gravi-
59 metric specific capacitance of porous carbon was 170 F g⁻¹ at

20 A g⁻¹ with a high capacitance retention of 63% with respect
to the capacitance obtained at 1 A g⁻¹.

One unique template mentioned here is zinc metal. Zn
metal has a special feature that can be removed through evapo-
ration under high temperatures.^[90,91] In the case of Zn species
used as templates, the removals of templates are not necessary
if the preparation goes through high-temperature treatment
due to the relatively low boiling point of zinc (907 °C).^[114] Zinc
metal can be directly used as a template for the synthesis of gra-
phitic porous carbons, in which various organics can be used as
carbon sources. At an annealing temperature of 550 °C, zinc
metal and sucrose mixture were directly carbonized into porous
graphitic carbons through a one-step pyrolysis process.^[124]
In this case, the zinc metal may act as a soft template, as the
melting temperature of zinc is as low as 420 °C. Zinc metal
template strategy can also be used to synthesize mesoporous
zinc-guided graphene (ZNG) monolith using glucose as carbon
source,^[125] in which metal zinc introduces a metal-carbon
interaction tiering process beyond the templating role of zinc.
The ZNG possessed an SSA as high as 2020 m² g⁻¹ and small
pores of 2.0–3.0 nm, which enabled a high specific capaci-
tance of 336 F g⁻¹ in 1 mol L⁻¹ H₂SO₄ electrolyte. Zinc metal
can be used as a template and graphitic carbon nitride (g-C₃N₄)
as a carbon source to synthesize porous graphenes.^[126] As the
g-C₃N₄ cannot be converted to carbon at high annealing tem-
peratures, the interaction between zinc and g-C₃N₄ is important
for the growth of graphene over the zinc catalyst, which needs
further investigation. By introducing CO₂ as a carbon source,
Xing et al. used Mg powder as a reduction agent to convert CO₂
into carbon, and Zn as the metal reductant to induce micropo-
rous structure. The resultant nanoporous graphene exhibited a
high SSA of 1900 m² g⁻¹ and a specific capacitance of 190 F g⁻¹
at 10 A g⁻¹.^[127]

Carbide is another hard template for porous carbon syn-
thesis. CDCs are produced by chlorine gas etching of metal
carbides, in which metals and metalloids are removed as vola-
tile chlorides. CDC turns out to be a nanoporous carbon with
a narrow pore-size distribution, usually around 0.5–3 nm, and
high SSA, beyond 2000 m² g⁻¹.^[128,129] Particularly, the SSA and
pore-size distribution of CDCs depend on the carbide precu-
sors and synthesis parameters. By controlling the synthesis
parameters, such as chlorination temperature, the CDCs usu-
ally show a narrow pore-size distribution (0.6–1.1 nm).^[128]
To achieve hierarchical porous CDCs, the composite precu-
sors of carbide and Si,^[130] polymer,^[131] as well as any other
materials^[132–134] have been investigated. Gogotsi et al. fabricated
a CDC with hierarchical pores by high-temperature chlorina-
tion of macroporous polymer-derived silicon carbide.^[135] The
as-prepared CDC exhibited a high SSA exceeding 2300 m² g⁻¹,
high micropore and mesopore volume of 1.1 cm³ g⁻¹, and high
macropore volume of 7.45 cm³ g⁻¹.

Through the hard-template method, porous carbons with
uniform and controllable pores can be synthesized easily.
However, the preparation of the template itself is costly, time-
consuming, and tedious. Another challenge is the ability to
tailor the wall thickness of pores, which is the key factor for
controlling the pore sizes of as-prepared carbon materials.^[136]
Besides, inorganic templates have to be removed by acid or
alkali etching, which hinders their practical applications.^[18]

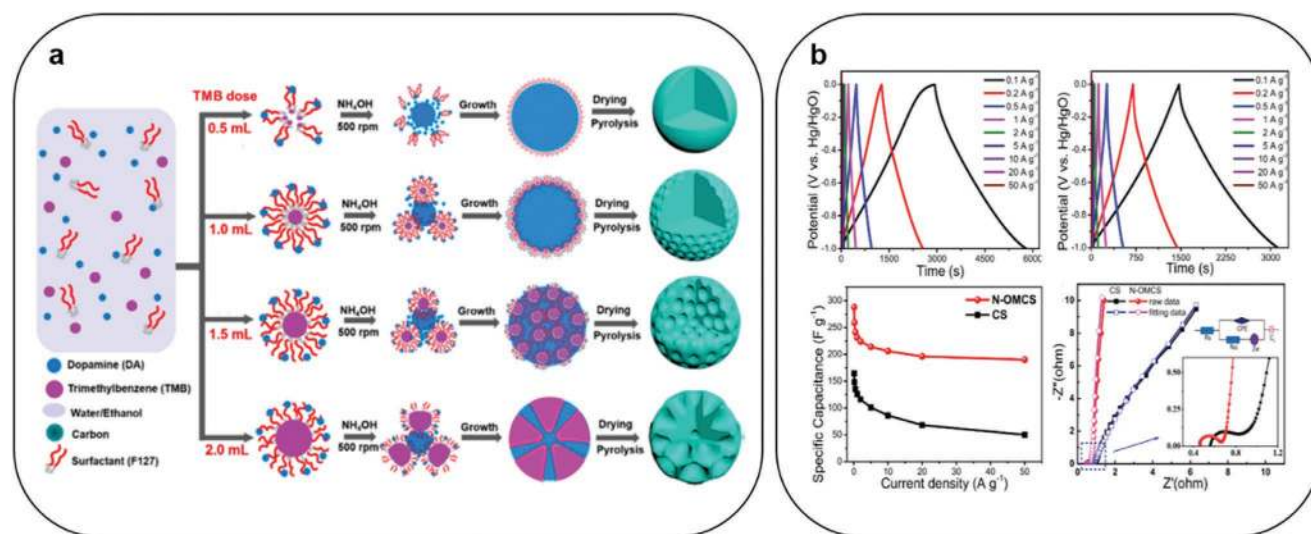


Figure 8. a) Versatile nanoemulsion assembly approach to synthesize functional mesoporous carbons. Reproduced with permission.^[147] Copyright 2019, American Chemical Society. b) GCD curves (above), specific capacitances as a function of current density, and Nyquist plots (below) of mesoporous carbon spheres. Reproduced with permission.^[149] Copyright 2017, Elsevier.

The unique templates (like zinc) give us more opportunities to carbonize those carbon sources that cannot be carbonized using traditional methods. By using these novel templates, the interaction between carbon sources and templates need to be studied thoroughly.

4.2. Soft Templates

In a soft template synthesis strategy, the templates are usually organic molecules or supermolecules with functional groups.^[84,121] In the particular solvent, the functional groups of soft templates can provide strong interaction force, such as hydrogen bonding,^[137,138] hydrophilic and hydrophobic interactions,^[139,140] or electrostatic interactions.^[141,142] Once the proper solvent is added, the soft templates turn into micelles. The micelles combined with carbon sources result in heterogeneous composites that turn into carbon materials with special porous architectures during the carbonization process.^[143–145] In particular, the pore size of carbon can be enlarged or decreased by controlling the ratio of solvent and micelle.

Although the mesoporous carbon can be prepared by carbonizing the mixture of carbon source and soft template, the requirements to develop soft templates are stringent and complex. The first attempt to synthesize mesoporous carbon with cetyltrimethylammonium bromide is based on the Coulombic interaction between the surfactant with positive charge and the phenolic resin with negative charge.^[143] However, no mesoporous carbon was obtained because the micelles collapse before the formation of a carbon skeleton at temperatures of about 200 °C. A successful soft template must satisfy several important requirements:^[120] 1) the ability to assemble into nanostructures, 2) inclusion of at least one component can turn into micro- or mesopores, and 3) sustaining the soft-template progenes before the formation of the carbon skeleton. According to these basic principles, the soft templates

like polystyrene-*b*-poly(4-vinylpyridine) (PS-P4VP),^[146] the poly(ethylene oxide)-*b*-poly(propylene oxide)-*b*-poly(-ethylene oxide) (PEO-PPO-PEO) (F127,^[147–149] F108,^[150] and P123^[149,151]) and some surfactants have been developed rapidly.

Liang et al. developed a method to form strong covalent interactions between carbon precursors and soft templates during the self-assembly process.^[152] The commercial triblock copolymer EO106-PO70-EO106 (F127) and the phenol-formaldehyde resol were combined with a stable covalent bond which was formed by the replacement of the chain end of F127 from aldehyde group into hydroxyl-methyl group. With the enhanced interaction between resol and soft template, the as-prepared ordered cubic mesoporous carbon exhibited an SSA of 637 m² g⁻¹ and a pore volume of 0.32 cm³ g⁻¹ which endows it a specific capacitance of 159 F g⁻¹ at 10 mV s⁻¹. Peng et al. explored a synthesis route to fabricate a series of highly uniform polymer nanospheres, with various surface morphologies (smooth, golf ball type, multichambered, and dendritic nanospheres) (Figure 8a).^[147] In this synthesis route, F127 was employed as a soft template and the organic molecule, 1,3,5-trimethylbenzene, was used to affect the interfacial interaction between the soft templates and carbon precursors. Through this method, carbon nanospheres achieved an ultralarge pore size of 37 nm, a small particle size of 128 nm, an SSA of 635 m² g⁻¹, and a high N doping ratio of 6.8%. In some cases, ordered mesoporous carbon spheres can be synthesized by the simple one-step route. Wang et al. used F127 as the soft template for the preparation of mesoporous carbon spheres in a one-step pyrolysis strategy.^[149] The as-obtained mesoporous carbon spheres possessed an SSA of 439 m² g⁻¹ and a uniform mesopore size of 5 nm. When used as SC electrodes, the mesoporous carbon spheres delivered a gravimetric specific capacitance of 288 F g⁻¹ at 1 A g⁻¹ with capacitance retention of 66% at 50 A g⁻¹ (Figure 8b). Besides block polymers, surfactants like Triton X-100 can also be used as soft templates to prepare hollow carbon nanospheres (HCNs).^[153]

1 The hollow carbon spheres derived from the Triton X-100
2 template method exhibited an SSA around $893.3 \text{ m}^2 \text{ g}^{-1}$ with
3 a corresponding total pore volume of $0.76 \text{ cm}^3 \text{ g}^{-1}$. The soft
4 template methods are in principle more attractive than hard
5 templates for the synthesis of mesoporous carbons since we
6 do not need to remove the soft templates after carbonization.
7 The main bottleneck is that the as-prepared porous carbon is
8 mesopore-dominated, and it is hard to obtain high SSA and
9 high specific capacitance. To pursue high SSAs, researchers
10 also tried to combine chemical activation and soft template
11 methods.^[154]

14 4.3. New Emerging Templates

16 Recently, novel templates such as ice (water),^[155–157] Mxene
17 ($\text{Ti}_3\text{C}_2\text{T}_x$),^[158,159] as well as melamine^[160–162] have been adapted
18 to fabricate functional porous carbons. For example, ice tem-
19 plates can be applied to various carbon sources to fabricate the
20 3D macrostructures according to the following procedures:^[163]
21 1) the precursors are dissolved in water or in hydroalcoholic
22 mixture with a suitable catalyst; 2) the precursors undergo
23 gelation at mild temperatures; 3) the gel is frozen and the
24 frozen solvent is removed by freeze-drying or solvent exchange;
25 4) the dry gel is carbonized in an inert atmosphere to produce
26 carbon cryogels. Both of the initial composition of suspension
27 and the parameters during the freezing process are critical for
28 the 3D macroporous carbon fabrication. Park et al. achieved an
29 ordered 3D lamellar microstructure CNTs by employing ice as
30 a template.^[155] By changing the concentration of chitosan in the
31 CNT suspension, disordered, lamellar, and cellular macropo-
32 rous carbonaceous structures can be synthesized successfully.
33 Zhang et al. prepared a hierarchically porous sulfur-containing
34 activated carbon by ice-templating an aqueous sodium poly
35 (4-styrenesulfonate) with thermal treatment (Figure 9a).^[157]
36 In the thermal treatment, the carbon precursor generates
37 Na_2SO_4 which contributes to the porous structure and SSA
38 of porous carbon. The derived porous carbon exhibited a
39 macropore volume of $3.19 \text{ cm}^3 \text{ g}^{-1}$ with the macropores pre-
40 dominantly locating in the ranges of 1–3, 5–7, and around
41 $100 \mu\text{m}$. The macropore SSA created by ice templating was
42 measured to be $73.66 \text{ m}^2 \text{ g}^{-1}$, with an average pore diameter of
43 $2.80 \mu\text{m}$. Because ice template is good at introducing macropo-
44 rous structures into carbon materials, the resultant porous
45 carbon is usually of low SSA. Chemical activation is needed
46 to enhance the SSA and specific capacitance of these carbons.
47 Umar et al. prepared a hierarchical porous carbon with macro
48 and mesoporous architectures using ice templates, and the
49 micropores on mesoporous carbon walls were achieved by
50 chemical activation.^[164] When this hierarchical porous carbon
51 was used as an electrode in solid-state SC, a specific capacitance
52 of 142.1 F g^{-1} was obtained at 0.5 A g^{-1} .

53 MXene is a series of 2D transition metal carbides, carbon-
54 itrides, and nitrides whose formula is $\text{M}_{n+1}\text{X}_n\text{T}_x$.^[165] Here M
55 represents a transition metal, X represents carbon or nitrogen,
56 and T_x represents the surface termination. MXene itself is a
57 pseudocapacitive electrode material. Furthermore, MXenes
58 can be used as hard templates for the preparation of porous
59 carbons due to its 2D morphology and abundant surface

terminations. Moreover, when MXene is used as a template, 1
polar organic molecules can spontaneously intercalate into 2
the interlayer spaces and occupy the active sites on the sur- 3
face of MXene. Wang et al. used Ti_3C_2 , the most well-studied 4
MXene, as a 2D host and injected the low-molecular-weight 5
phenolic resol and the amphiphilic triblock copolymer F127 6
into MXene.^[158] After carbonization and chlorination, they 7
obtained MXene-derived carbon (MDC-OMC) with 2D–2D het- 8
erostructure (Figure 9b). The MDC-OMC possessed an SSA of 9
 $1021 \text{ m}^2 \text{ g}^{-1}$ and exhibited a specific capacitance of 249 F g^{-1} 10
at 1 A g^{-1} in a 6 mol L^{-1} KOH electrolyte. MDC-OMC still 11
displayed a high specific capacitance of 188 F g^{-1} at 40 A g^{-1} . 12
Melamine is a template that can be incorporated into the 13
carbon framework. Melamine decomposes to $\text{g-C}_3\text{N}_4$ and finally 14
decomposes completely resulting in macropores. He et al. syn- 15
thesized a honeycomb-like porous carbon (HPC) using coal tar 16
pitch as a carbon precursor with melamine as a template cou- 17
pled with the KOH activation technique.^[161] Melamine decom- 18
posed at high temperatures ($> 650 \text{ }^\circ\text{C}$) and formed macro- and 19
mesopores in the HPC framework. The HPCs exhibited an 20
SSA of $2038 \text{ m}^2 \text{ g}^{-1}$ and pore volume of $1.07 \text{ cm}^3 \text{ g}^{-1}$ which 21
endowed its specific capacitances of 221 F g^{-1} at 0.05 A g^{-1} 22
and 179 F g^{-1} at 20 A g^{-1} . In addition to the above templates, 23
some particular metal nanoparticles can be used as templates 24
for porous carbon synthesis. Hou et al. synthesized a carbon 25
nano-cage by CO_2 reduction with the Mg metal ribbon as a 26
reducing agent and template.^[166] The obtained carbon material 27
displayed an SSA of $806 \text{ m}^2 \text{ g}^{-1}$, a narrow pore size centered 28
at 6–7 nm, and a pore volume of $1.51 \text{ cm}^3 \text{ g}^{-1}$. This carbon 29
nano-cage showed a high specific capacitance up to 304 F g^{-1} 30
at 2 mV s^{-1} and a high specific capacitance of 96 F g^{-1} at 31
 1000 mV s^{-1} . 32

Basically, compared with activated carbons, the features of 33
porous carbons derived from template methods usually poss- 34
ess macro- and mesopores and relatively low SSA (several 35
hundreds of square meters per gram).^[92,96] The new emerging 36
template methods are capable of fabricating 3D functional 37
macroporous carbons or graphene-like materials. For the fab- 38
rication of carbon materials with high SSA, high pore volume, 39
and high ratio of micropores, chemical activation methods need 40
to be applied, which limits the commercial potential of tem- 41
plate-based methods for the synthesis of porous carbons as SC 42
electrodes.^[80,167,168] On the other hand, the template methods 43
can be used to fabricate high-frequency response SCs based on 44
their macroporous structures. 45

47 5. Self-Template Methods

48 Both activation agents and templates used in the above methods 49
are porogens that are needed to be added. There are also some 50
porous carbon fabrication strategies that use self-generated 51
porogens,^[169] which we henceforth designate as self-template 52
methods. In this section, we discuss the strategies used to fab- 53
ricate porous carbon materials by directly carbonizing the self- 54
templated materials,^[170] such as ethylenediamine tetraacetates 55
(EDTA)-based salts,^[171,172] glycolates,^[173] MOFs^[174] and their 56
derivatives,^[175] biomass-based organic salts,^[176] as well as other 57
special self-templated organic materials. 58
59

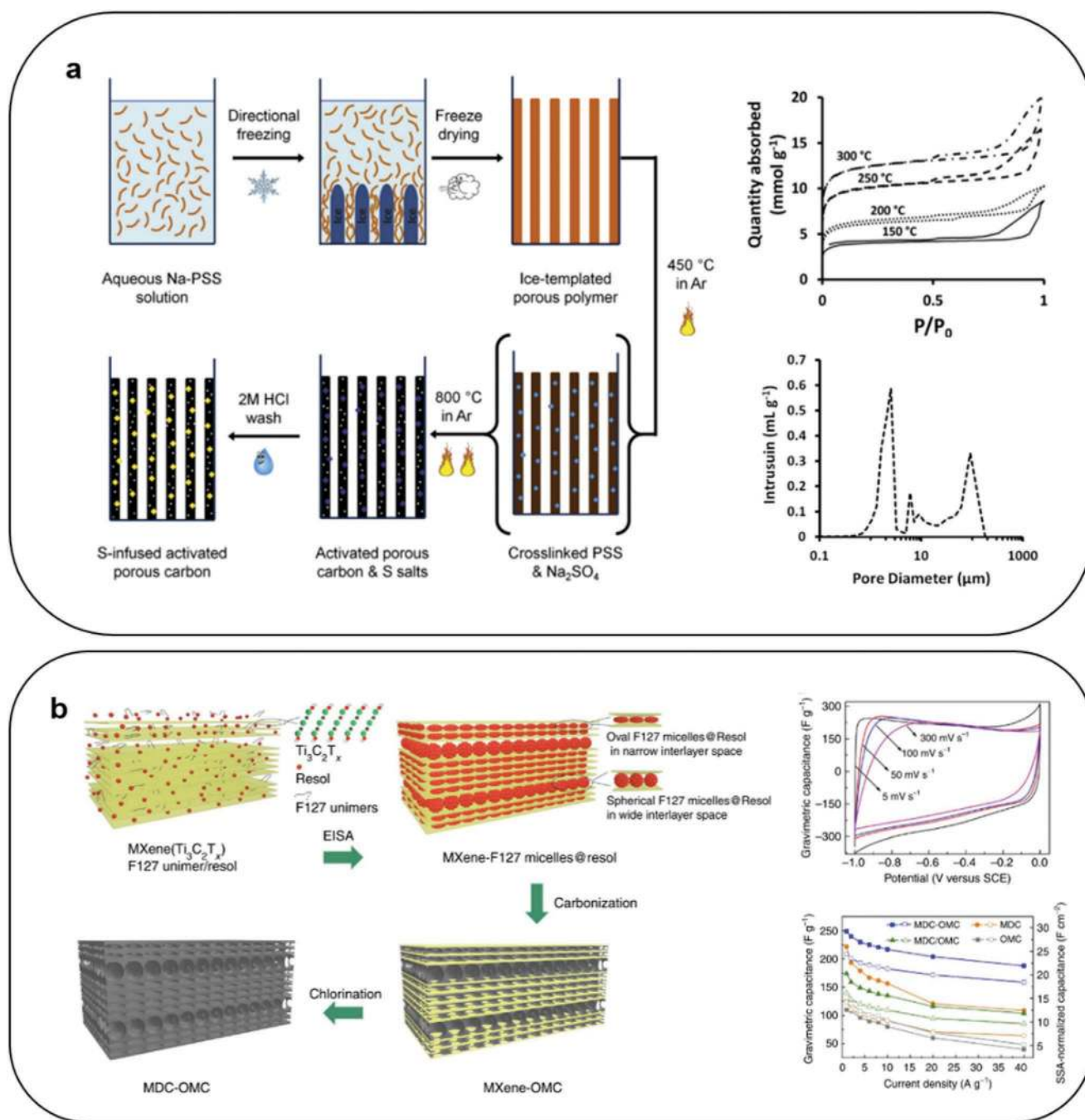


Figure 9. a) The preparation schematic diagram of ice-templated hierarchical activated carbon (left); N₂ adsorption and desorption isothermals at different degas temperatures and pore-size distribution of ice-templated hierarchical activated carbon (right). Reproduced with permission.^[157] Copyright 2015, Elsevier. b) The preparation schematic diagram of the MDC-OMC composite using MXene as template (left), the corresponding CV curves at various scan rates and the capacitances at different current densities for the MDC-OMC (right). Reproduced with permission.^[158] Copyright 2017, Nature Publishing Group.

5.1. Organic Salts as Carbon Sources

As an example of organic salt methods, interconnected porous carbon nanosheets (IPCNs) with SSA up to 1736 m² g⁻¹ were synthesized by the carbonization of potassium and sodium citrate salts.^[177] The IPCN was determined to have a thickness of 20–50 nm and a length of 0.5–2 μm. By optimizing

the ratio of potassium citrate and sodium citrate at 2:8, IPCN with a high specific capacitance of 200 F g⁻¹ at 5 mV s⁻¹ was achieved (Figure 10a). In another study, zinc and calcium citrates with combination melamine were used to prepare the N-doped mesoporous carbon with SSAs of 1190–1350 m² g⁻¹ and mesopore size around 11 nm.^[178] By carbonizing the pure sodium citrate, the ultrathin porous carbon shells with SSAs of

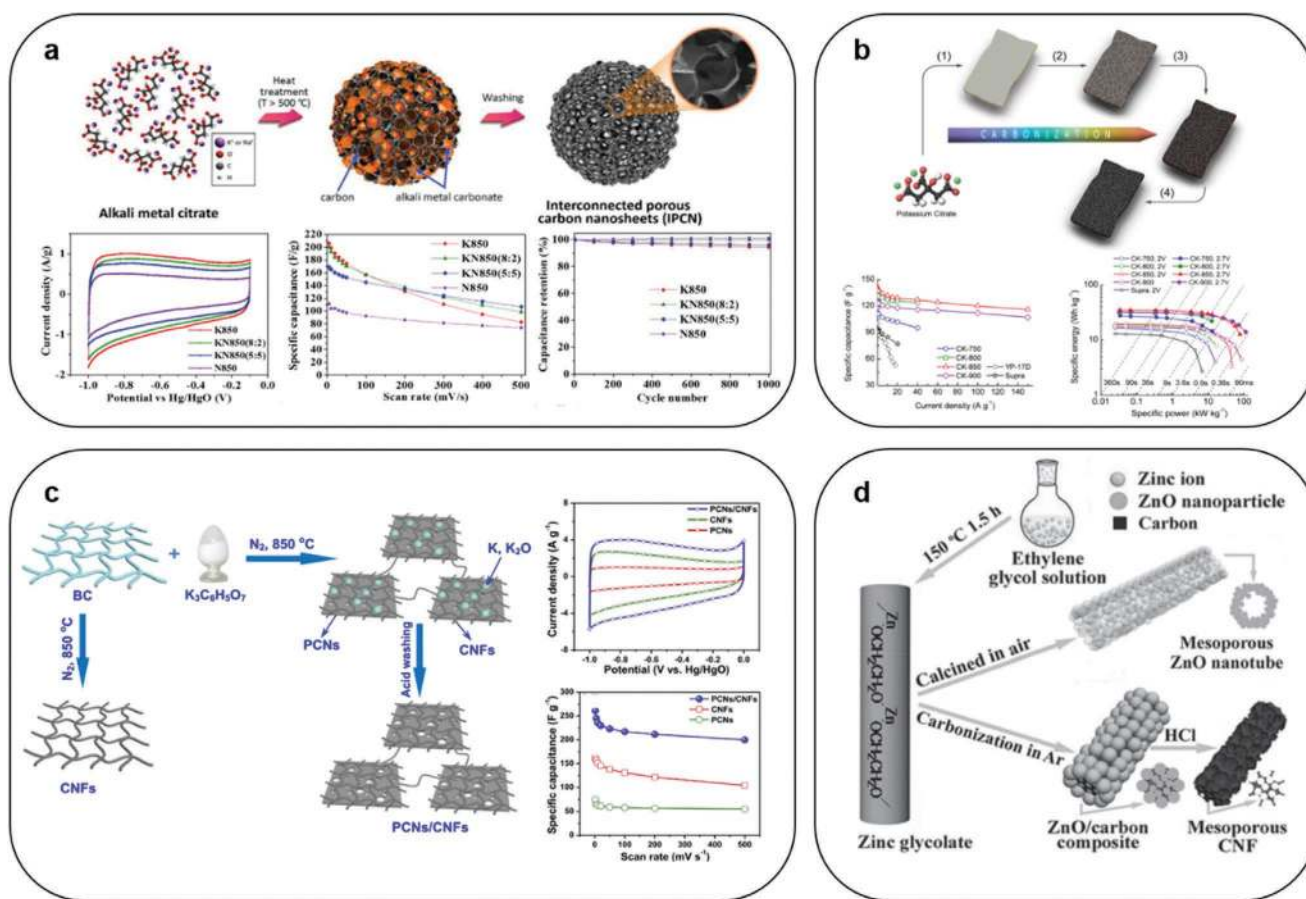


Figure 10. a) The preparation schematic diagram of IPCN (above), the corresponding CV curves at 5 mV s^{-1} , the specific capacitances at different scan rates and cycling stability tested in 6 mol L^{-1} KOH (below). Reproduced with permission.^[177] Copyright 2017, Elsevier. b) The synthesis scheme for PCNs from potassium citrate (above); the corresponding GCD curves and Ragone plot of the PCNs samples tested in 1 M tetraethylammonium tetrafluoroborate in acetonitrile (TEABF₄/AN) electrolyte (below). Reproduced with permission.^[182] Copyright 2014, American Chemical Society. c) Scheme illustration of the synthesis of the PCN/CNF composite (left), the corresponding CV curves at 20 mV s^{-1} , specific capacitances at different scan rates of PCN/CNF composite tested in 6 M KOH electrolyte (right). Reproduced with permission.^[183] Copyright 2016, Elsevier. d) The schematic illustration of the formation process of CNFs. Reproduced with permission.^[173] Copyright 2011, Wiley-VCH.

400–600 $\text{m}^2 \text{g}^{-1}$ and pore size of 1 nm were achieved.^[179] The ultrathin porous carbon shells exhibited a gravimetric specific capacitance up to 251 F g^{-1} at 1 A g^{-1} and 228 F g^{-1} at 20 A g^{-1} . A hierarchical microporous/mesoporous carbon nanosheet with a high SSA of 1890 $\text{m}^2 \text{g}^{-1}$ was fabricated by direct pyrolysis of sodium gluconate.^[180] Due to their hierarchical microporous/mesoporous structure, this carbon nanosheet exhibited a high specific capacitance of 140 F g^{-1} at 150 A g^{-1} . Xu et al. prepared a nitrogen-doped porous carbon by the pyrolysis of EDTA disodium magnesium salt.^[172] The obtained nitrogen-doped porous carbon exhibited an SSA of 1811 $\text{m}^2 \text{g}^{-1}$ and a pore volume of 1.16 $\text{cm}^3 \text{g}^{-1}$, while the specific capacitances of the nitrogen-doped porous carbon were 281 F g^{-1} at 0.05 A g^{-1} and 196 F g^{-1} at 20 A g^{-1} . Similarly, EDTA disodium zinc salt was used as a self-templated carbon precursor.^[181] Porous carbon derived from EDTA disodium zinc salt possessed a high SSA of 1368 $\text{m}^2 \text{g}^{-1}$ and exhibited a high specific capacitance of 275 F g^{-1} and an excellent rate capability (207 F g^{-1} at 100 A g^{-1}). Through the direct pyrolysis of potassium citrate, highly porous interconnected carbon nanosheets (PCNs) with SSA of

2220 $\text{m}^2 \text{g}^{-1}$ were fabricated at 850 $^{\circ}\text{C}$.^[182] The synthesis scheme from potassium citrate to PCNs is described in Figure 10b. The potassium citrate-derived 2D PCNs exhibited a microporous architecture with pore sizes centered around 0.7–0.85 and 0.95–1.6 nm and thickness less than 80 nm. The PCNs showed a good rate performance, where specific capacitances of 134 F g^{-1} at 5 A g^{-1} and 120 F g^{-1} at 150 A g^{-1} were obtained using commercial 1 M TEABF₄/AN electrolyte. In another study, bacterial cellulose (BC) and potassium citrate were mixed to fabricate CNFs-bridged PCNs.^[183] As shown in Figure 10c, the potassium citrate serves as the self-templated carbon precursor while the BC bridge turns into CNFs which provides the 3D structure to integrate porous carbon. The as-prepared PCN/CNF composite exhibited an SSA of 1037 $\text{m}^2 \text{g}^{-1}$ and a specific capacitance up to 261 F g^{-1} in aqueous electrolyte. Similarly, porous carbon with a high surface area of 1094 $\text{m}^2 \text{g}^{-1}$ and pore sizes distributed in a wide range from 1 to 100 nm were fabricated by direct calcination of sodium citrate.^[184] Li et al. synthesized mesoporous CNFs with the thermal treatment of zinc glycolate at 600 $^{\circ}\text{C}$ (Figure 10d).^[173] Zinc glycolate decomposed

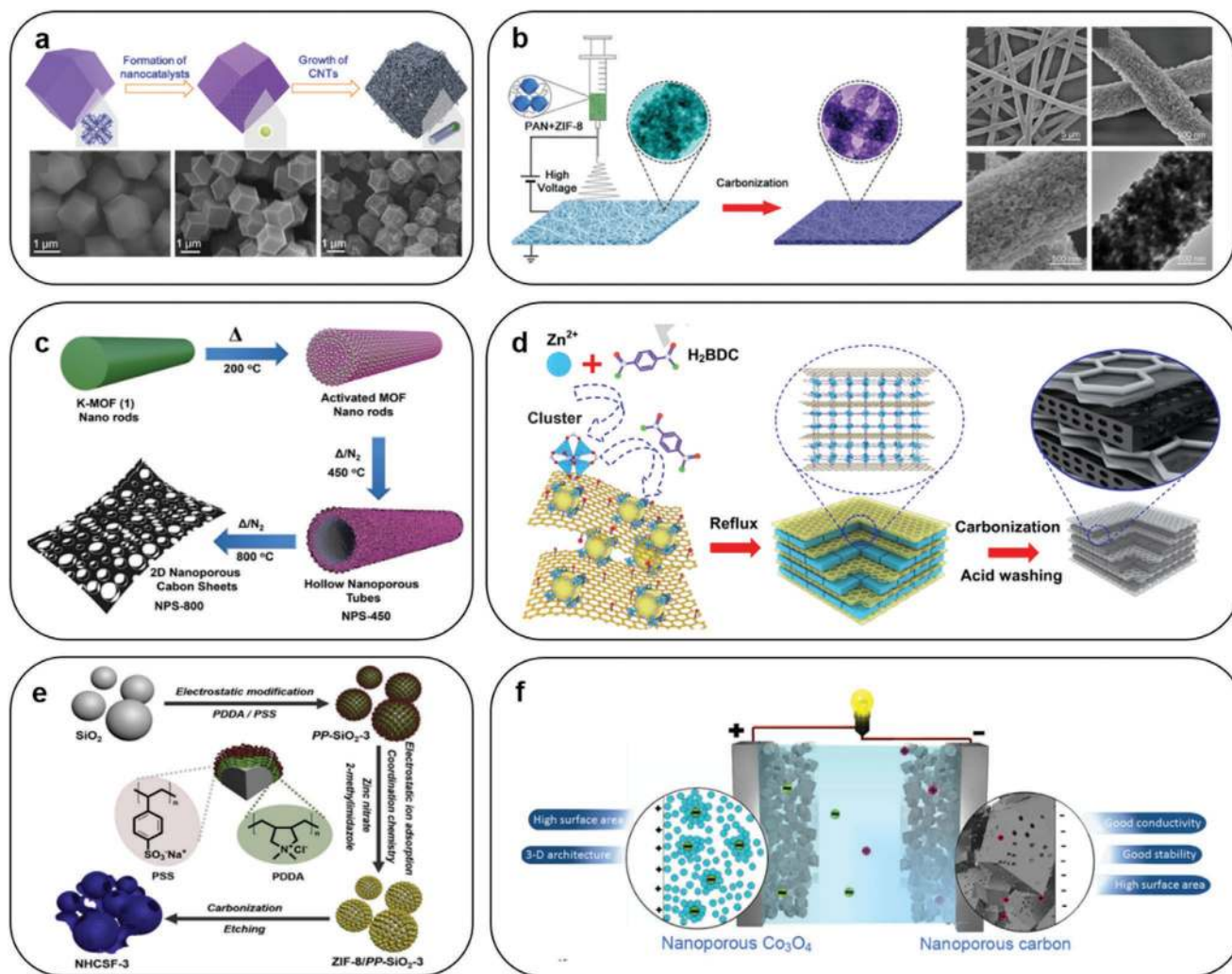


Figure 11. a) Synthesis and characterization of N-doped CNT-assembled hollow dodecahedra from zeolitic imidazolate frameworks (ZIF-67). Reproduced with permission.^[185] Copyright 2017, American Chemical Society. b) Schematic illustration of the synthesis of HPCNFs-N, SEM, and TEM images of the PAN/ZIF-8 composite nanofibers. Reproduced with permission.^[186] Copyright 2017, The Royal Society of Chemistry. c) Schematic illustration of the synthesis of K-MOF rods under solvothermal conditions and morphologically controlled synthesis of 2D hierarchical nanoporous carbon sheets derived from K-MOF under various carbonization conditions. Reproduced with permission.^[187] Copyright 2018, Wiley-VCH. d) Schematic illustration showing the fabrication process for porous carbon using MOFs and graphene oxide as precursors. Reproduced with permission.^[188] Copyright 2016, Elsevier. e) Scheme depicting the fabrication of NHCSF from ZIF-8/PP-SiO₂ precursor. Reproduced with permission.^[189] Copyright 2018, Elsevier. f) Schematic illustration of asymmetrical SC containing nanoporous Co₃O₄ and nanoporous carbon as the positive and negative electrodes, respectively. Reproduced with permission.^[190] Copyright 2015, American Chemical Society.

into ZnO/carbon composite in which ZnO was homogeneously dispersed in the carbon matrix with average particle sizes of ≈ 4 nm. After acid etching, the ZnO/carbon composite was transformed into mesoporous CNFs. The mesoporous CNFs exhibited a high SSA of $1725 \text{ m}^2 \text{ g}^{-1}$ with a large pore size of 3.4 nm, and a high specific capacitance of 280 F g^{-1} .

5.2. MOF Derivatives as Carbon Sources

Due to the versatile, tunable porous structure and composition of MOFs, MOF is a promising material platform for the synthesis of various porous and functional carbon materials. The metal components inside MOFs can be directly used as

self-templates during the pyrolysis processes of MOFs. An assembled CNTs array was obtained by the carbonization of MOF at a low pyrolysis temperature of $430 \text{ }^\circ\text{C}$.^[185] Various morphologies of the assembled carbon can be achieved by modulating Co, Fe, and Zn MOFs. As shown in Figure 11a, the as-prepared CNTs exhibited a uniform assembled morphology with a high SSA of $1389 \text{ m}^2 \text{ g}^{-1}$. Chen et al. prepared hollow particle-based N-doped CNFs (HPCNFs-N) by the electrospinning of PAN/ZIF-8 composite (Figure 11b).^[186] The HPCNFs-N exhibited a high SSA of $417.9 \text{ m}^2 \text{ g}^{-1}$ and specific capacitances of 307.2 and 193.4 F g^{-1} at 1 and 50 A g^{-1} , respectively. PCNSs can be fabricated by pyrolysis of K-MOF nanorods at temperatures of 200, 450, and $800 \text{ }^\circ\text{C}$ (Figure 11c).^[187] The carbon nanosheets possessed the highest SSA of $1678 \text{ m}^2 \text{ g}^{-1}$ among

1 various MOF-derived porous carbons, which may be ascribed
2 to the small-sized potassium compounds after pyrolysis and
3 the possible activation effect of potassium oxide and carbon-
4 ates. Carbon nanosheets presented a specific capacitance
5 up to 233 F g⁻¹ at a low scan rate of 5 mV s⁻¹ in the H₂SO₄
6 electrolyte. Wang et al. synthesized a “brick-and-mortar” type
7 sandwiched porous carbon (C-GMOF) by using MOF-5-derived
8 porous carbon film as “mortar” and the graphene nanosheets
9 as “brick” (Figure 11d).^[188] The C-GMOF showed a relatively
10 low SSA (979 m² g⁻¹) and a relatively wide pore distribution
11 (1–8 nm) compared with porous carbon derived from MOF-5
12 (C-MOF) (1117 m² g⁻¹ and 1–4 nm). The assembled “brick-
13 and-mortar” C-GMOF exhibited high specific capacitances of
14 345 F g⁻¹ at 2 mV s⁻¹ and 201 F g⁻¹ at 2 V s⁻¹. Since MOFs
15 are synthesized in a solvent environment, the design of MOF
16 composites with advanced structures can be realized by com-
17 bining MOFs with other functional materials. A hollow carbon
18 shell framework (NHCSF) was fabricated by the carbonization
19 of core-shell hybrid precursors (ZIF-8-PP-SiO₂).^[189] The core-
20 shell hybrid precursors were obtained by depositing a zeolitic
21 imidazolate framework (ZIF 8) on the polyelectrolyte-derived
22 silica (Figure 11e). The as-prepared NHCSFs with SSAs of
23 585–847 m² g⁻¹ displayed high capacitances up to 253.6 F g⁻¹
24 at 1 A g⁻¹ and 200.4 F g⁻¹ at 50 A g⁻¹. With the molecular scale
25 special tunable structure of MOF, Salunkhe et al. assembled
26 an SC by using the nanoporous carbon and nanoporous cobalt
27 oxide materials derived from a single ZIF-67 (Figure 11f).^[190]
28 The ZIF-derived carbon possessed an SSA of 350 m² g⁻¹, and
29 the SC exhibited a capacitance of 101 F g⁻¹ at 2 A g⁻¹.

32 5.3. Other Self-Template-Derived Methods

34 Biomass is abundant, cheap, readily available, and most impor-
35 tantly, is renewable. High value-added utilization of biomass
36 is regarded as a green solution for waste disposal problems in
37 the agricultural industries.^[176] Moreover, by taking advantage of
38 the unique bio-organized natural structures of biomass, carbon
39 materials with hierarchical porous architectures, and excellent
40 electrochemical performances of SCs can be achieved.^[191] BC
41 is a common biomass precursor with 3D networks consisting
42 of superfine nanofibers (≈50 nm in diameter).^[192] A 3D net-
43 work structure consisting of numerous intertwined CNFs with
44 a diameter of 30–60 nm was obtained by freeze-drying and
45 carbonization of the BC aerogel. After coating, the polyaniline-
46 coated BC nanofibers exhibited a high specific capacitance
47 of 238.4 F g⁻¹ at 0.5 A g⁻¹. Zhang et al. prepared a rice husk-
48 derived carbon (RHC) through direct pyrolysis of rice husk
49 in a sealed tube furnace without the injection of N₂.^[193] RHC
50 showed an SSA of 337 m² g⁻¹, a pore size centered at 0.7 and
51 3.6 nm, and a pore volume of 0.207 cm³ g⁻¹. Nano-SiO₂ parti-
52 cles inside RHC were etched by NaOH to prepare RHPC that
53 exhibited an SSA of 527 m² g⁻¹, a pore size centered at 0.8 and
54 3.4 nm, a pore volume of 0.327 cm³ g⁻¹, and a specific capaci-
55 tance of 110 F g⁻¹ at 0.1 A g⁻¹. Zhang et al. also proposed a gen-
56 eral strategy for the preparation of porous carbon from general
57 lignocellulose-based biomasses.^[194] In this strategy, lignin was
58 extracted from onion by KOH etching and transformed into a
59 lignin potassium salt. The lignin potassium salt from onion

was pyrolyzed into porous carbon materials (OPC). OPC exhib-
1 ited a high SSA of 1910 m² g⁻¹ dominated by micropores and
2 a high gravimetric specific capacitance of 200 F g⁻¹. Using this
3 etching strategy, generally, any lignin-containing biomass can
4 be treated and transformed into porous carbons under pyroly-
5 sis. More generally, efficient methods need to be developed
6 to prepare porous carbons derived from celluloses using self-
7 template strategies.

11 6. Direct Pyrolysis Methods

13 6.1. Direct Pyrolysis of Conjugated Copolymers

15 The pursuit of facile and green preparation techniques for
16 porous carbon materials for SC electrodes remains an active
17 research area. Although traditional carbonization-activation
18 methods can prepare porous carbons with controllable SSAs,
19 and pore-size distributions, the templates or the residues of
20 activation agents after carbonization and activation need to
21 be removed completely. Hence, activation-free methods are
22 becoming more attractive. In typical pyrolysis processes of
23 organics, organic sources decompose and release gases (e.g.,
24 H₂O, CO₂, NH₃, and CO), where the pyrolysis gases function
25 as porogens. However, most pyrolysis gases are released at
26 relatively low temperatures when the evolving carbon skeleton
27 is not robust enough to sustain pores. As a result, when poly-
28 aniline (PANI) or PPy were used as precursors for nitrogen-
29 doped carbons, PANi or PPy-derived carbons showed low SSAs
30 around 100–300 m² g⁻¹, which are too low to be used in SC
31 applications.^[195,196] Nevertheless, when aniline and pyrrole are
32 co-polymerized into a PANi-co-PPy (PACP) conjugated copol-
33 ymer, PACP acts as a unique precursor for porous carbons.
34 Wu et al. synthesized PACP hollow spheres with the assist-
35 ance of Triton X-100 soft template and used it as a precursor
36 for porous HCNs (Figure 12a).^[197] By controlling the pyrolysis
37 parameters, such as carbonization temperature, heat ramping
38 rate, and carbonization time, the SSA and pore-size distribu-
39 tion of HCNs can be finely engineered. Compared with tradi-
40 tional template-assisted carbonization and activation methods
41 for the synthesis of HCNs, the direct pyrolysis of PACP showed
42 unique simplicity and low-cost advantages. HCN-900-20H2R
43 sample (carbonization temperature is 900 °C, carbonization
44 time is 20 h, and the heat ramping rate is 2 °C min⁻¹) showed
45 unexpectedly high SSA of 3022 m² g⁻¹ which guarantees a
46 moderate gravimetric specific capacitance of 200 F g⁻¹ and good
47 rate capability (Figure 12b). The ultrahigh SSA did evolve from
48 the unique structure of PACP, since PACP itself only showed
49 a low SSA of 33 m² g⁻¹. Although there was still lack of fun-
50 damental understanding of the mechanism behind the forma-
51 tion of such a high SSA, this method opened a new pathway for
52 designing porous carbons with high pore volume and SSA by
53 direct copolymer pyrolysis. Kang et al. used PACP as precursor
54 and MnO₂ (initiator) nanowire sacrificial template to synthe-
55 size hierarchically porous carbon nanotubes (HPCNTs). The
56 HPCNT showed a high SSA of 1419 m² g⁻¹, a high gravimetric
57 specific capacitance of 280 F g⁻¹, and high rate capability.^[198]
58 In contrast, CNTs derived from PANi and PPy showed much
59 lower SSA. The ultrahigh SSAs of HPCNT was derived from

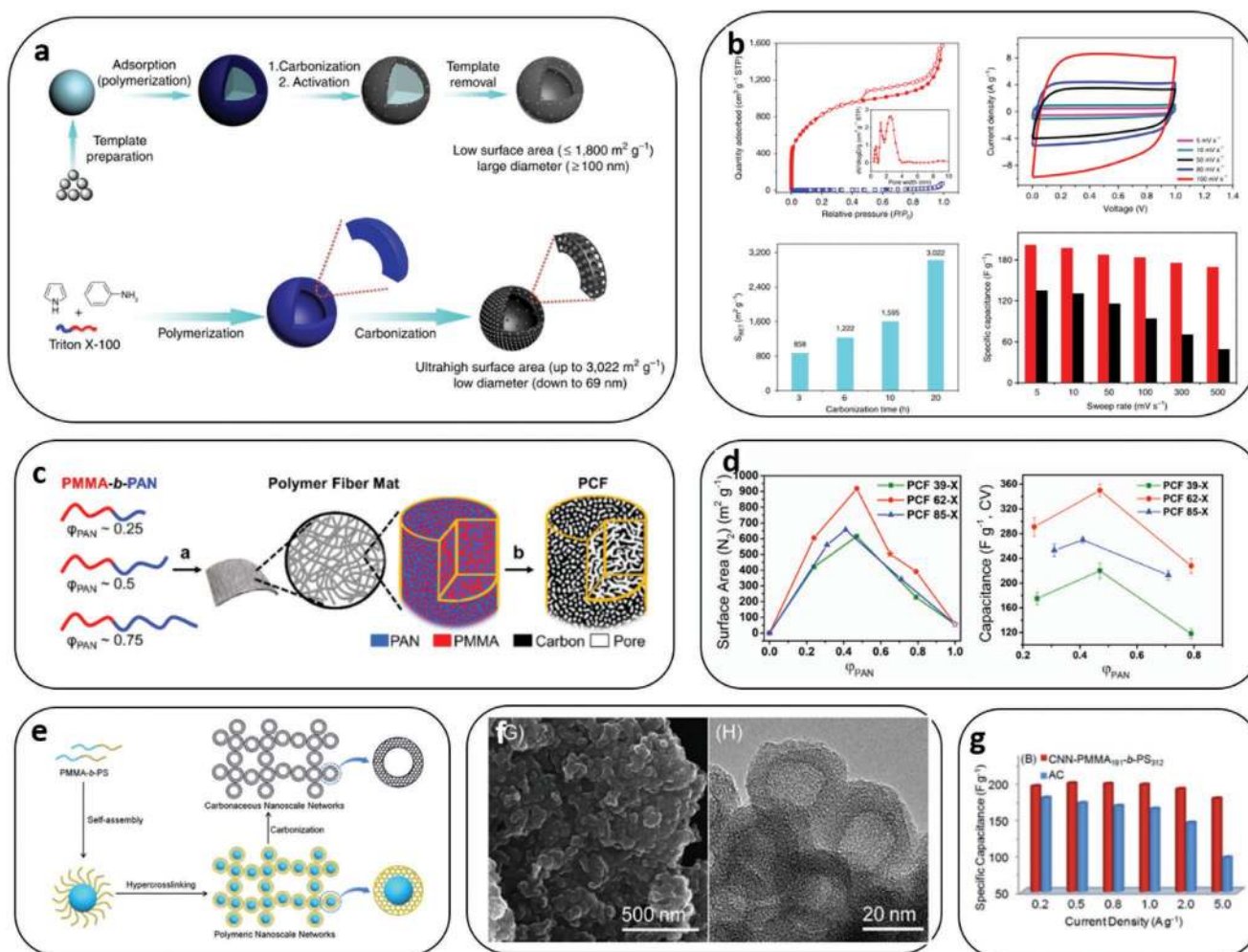


Figure 12. a) The schematic for the synthesis of high-specific-surface-area HCNs using traditional template-assisted carbonization and activation methods (above), and the direct pyrolysis carbonization of PACP (below). b) Physicochemical and electrochemical properties of HCNs, N_2 adsorption/desorption isotherms, and pore-size distribution of HCN-900-20H2R, CV curves of HCN-900-10H5R, the dependence of SSA on the carbonization temperature, dependence of specific capacitance of HCN-900-10H5R on the scan rate. Reproduced with permission.^[197] Copyright 2015, Nature Publishing Group. c) The schematic for the synthesis of PCFs using PMMA-*b*-PAN block copolymer with the volume fraction of PAN. d) The dependence of SSA obtained from N_2 adsorption/desorption, and the gravimetric capacitances of PCFs on the volume fraction of PAN. Reproduced with permission.^[205] Copyright 2019, American Chemical Society. e) The schematic illustration of the preparation of PNNs and CNNs from PMMA-*b*-PS block copolymer. f) The SEM and TEM images of CNN-PMMA₁₉₁-*b*-PS₃₁₂. g) The dependence of the specific capacitance of CNN-PMMA₁₉₁-*b*-PS₃₁₂ on charge-discharge current densities. Reproduced with permission.^[207] Copyright 2014, The Royal Society of Chemistry.

the robust conjugated structure of PACP. Various covalent organic frameworks and conjugated copolymers can be used as precursors for the synthesis of porous carbons. During the past few years, many conjugated copolymers have been adopted as precursors for porous carbons in direct pyrolysis methods, such as triazine-based copolymers,^[167,199,200] polyimides,^[201,202] Schiff-base porous organic polymers,^[203] and other aromatic polymers.^[204] The general common feature of these polymers is that they have two or more different monomers. We speculate that the thermal stabilities of the monomers are very different. The monomer with higher thermal stability can function as a carbon skeleton, while the second monomer with lower thermal stability can act as a porogen. Based on this hypothesis, block copolymers possessing two polymer chains with different thermal stabilities can also be used as precursors for

the preparation of porous carbons with high SSA and high specific capacitance.

6.2. Direct Pyrolysis of Block Copolymers

Poly(methyl methacrylate) (PMMA) is usually used as a template to prepare hollow carbon spheres since it can be completely decomposed at $\approx 345 \text{ }^\circ\text{C}$. Using PMMA as an inner molecular sacrificial template, PMMA-based block copolymers can be used as precursors for highly porous carbons. Liu et al. prepared PMMA-*b*-PAN copolymer and carbonized it into highly porous carbons (Figure 12c).^[205] By controlling the molecular weight of PMMA, tunable mesopore sizes ranging from 10.9 to 18.6 nm of the obtained porous carbons can be achieved.

1 With a PAN volume fraction of 0.5, the obtained porous carbon
2 fibers (PCFs) exhibited a high SSA of $918 \text{ m}^2 \text{ g}^{-1}$ and high spe-
3 cific capacitance of 345 F g^{-1} in 3 mol L^{-1} KOH aqueous elec-
4 trolyte (Figure 12d). The PMMA-*b*-PAN can be fabricated into a
5 nanofiber mat by electrospinning technique. The fiber mat thus
6 can be tuned into highly porous PCFs by direct pyrolysis. The
7 PCFs possess abundant macropores, which enables them to be
8 used as substrates of MnO_2 electrodes.^[206]

9 Based on the atom transfer radical polymerization tech-
10 niques, the PMMA-*b*-PAN copolymer can be transformed
11 into microemulsion hollow spheres and highly nanoporous
12 carbon materials after pyrolysis (Figure 12e).^[207] Poly(methyl
13 methacrylate)-*b*-polystyrene (PMMA-*b*-PS) block copoly-
14 mers were also used to self-assemble into uniform spherical
15 micelles (Figure 12f). What is more, the inter-sphere hyper-
16 crosslinking of PS chains on the colliding micelles connects
17 the nanosphere network units in various directions forming
18 the 3D polymeric nanoscale networks (PNNs). Thus, 3D
19 PNNs could be further transformed into carbonaceous
20 nanoscale networks (CNNs) after pyrolysis. CNNs derived
21 from PMMA₁₉₁-*b*-PS₃₁₂ showed a BET SSA and micropor-
22 ous surface area of 839 and $561 \text{ m}^2 \text{ g}^{-1}$, respectively. Given
23 the high BET SSA and microporous surface area of PNN-
24 PMMA₁₉₁-*b*-PS₃₁₂ (288 and $116 \text{ m}^2 \text{ g}^{-1}$), the formation of
25 higher SSA and micropore surface area of CNNs could be
26 attributed to the pore formation during the pyrolysis of PNN-
27 PMMA₁₉₁-*b*-PS₃₁₂. CNNs showed a high gravimetric specific
28 capacitance of 195 F g^{-1} at a current density of 0.2 A g^{-1} , as
29 shown in Figure 12g. There are renewed efforts in designing
30 numerous block copolymers with different combinations for
31 the preparation of porous carbons. In recent years, nanopor-
32 ous carbon materials have been prepared from PS-*b*-PEO,^[144]
33 PAN-*b*-PBA,^[208] PS₂₃₅-*b*-PEO₄₅,^[209] PS-*b*-PAN,^[210] and PDA/
34 PS-*b*-PEO.^[145] As we can see, the SSAs of most porous car-
35 bons derived from these block copolymers are still limited to
36 be $<1500 \text{ m}^2 \text{ g}^{-1}$. The limited SSA of the decomposition of
37 copolymers should be further enhanced by controlling the
38 molecular design.

6.3. Direct Pyrolysis of Ionic Liquids and Ionized Organics

43 Another popular way to synthesize porous carbon from
44 polymer-based materials is the direct pyrolysis of poly(ionic
45 liquid)s (PILs). PILs have both the advantages of IL and poly-
46 mers. PIL renders the choices of anion and cations, and the
47 nano-objective engineering of the resultant carbon materials
48 can be achieved by polymerization methods. The heteroatom-
49 rich PILs can be tuned into heteroatom-rich carbon structures.
50 What is more, for SC applications, tuning porous structures of
51 carbon materials can be achieved by tuning the chemical com-
52 position (porogens) and the parameters during direct pyrol-
53 ysis of PILs. Gan et al. prepared *p*-phenylenediamine (pPD)
54 sulfuric acid ($[\text{pPD}][2\text{HSO}_4]$) PIL by a solution polymeriza-
55 tion reaction.^[211] $[\text{pPD}][2\text{HSO}_4]$ was also prepared without
56 oxidative polymerization for comparison. Highly microporous
57 carbon nanoparticles with nitrogen and sulfur doping (N/S-
58 UCNs) were obtained by direct pyrolysis of $[\text{pPD}][2\text{HSO}_4]$.
59 Furthermore, the N/S-UCN prepared at $800 \text{ }^\circ\text{C}$ exhibited a

high SSA of $1018 \text{ m}^2 \text{ g}^{-1}$ which endowed it with a high capaci-
1 tance of 225 F g^{-1} at 2 A g^{-1} . One drawback of this research
2 is that the intrinsic mechanism for obtaining high surface
3 area porous carbon is not fully understood. Porous carbons
4 derived from $[\text{pPD}][2\text{HSO}_4]$ ($1018 \text{ m}^2 \text{ g}^{-1}$) showed higher
5 SSA than porous carbons derived from nonpolymerized $[\text{pPD}]$
6 $[2\text{HSO}_4]$ ($834 \text{ m}^2 \text{ g}^{-1}$). Since $[\text{pPD}][2\text{HSO}_4]$ is more stable
7 than $[\text{pPD}][2\text{HSO}_4]$ due to the polymerization, the pPD can
8 act as a carbon skeleton while the HSO_4^- species act as pore-
9 forming agent. Similarly, Gan et al. mixed 5-carboxybenzene-
10 1,3-diamine (DABA) and H_2SO_4 in a dimethylformamide
11 solvent and obtained protic salt $[\text{DABA}][2\text{HSO}_4]$ without
12 polymerization.^[212] N/S-co-doped porous carbon (NSC) was
13 obtained from the direct pyrolysis of $[\text{DABA}][2\text{HSO}_4]$. NSC-900
14 displayed a high SSA of $1543 \text{ m}^2 \text{ g}^{-1}$, and a high gravimetric
15 specific capacitance of 285 F g^{-1} at 1 A g^{-1} . Gan et al. also
16 developed a similar protic salt using *p*-phenylenediamine and
17 toluenesulfonic acid for porous carbon preparation.^[213] The
18 synthesis of protic salt is a more facile way for the preparation
19 of porous carbons since it avoids polymerization and tedious
20 reaction processes. Because inorganic acid and amine-based
21 precursors are abundant and cost-effective, this approach can
22 be developed to fabricate porous carbon with much higher
23 SSA and higher specific capacitances. Chitosan is an abun-
24 dant natural biopolymer with abundant amine functional
25 groups. Methanesulfonic acid and chitosan were used to pre-
26 pare an ionic organic compound.^[214] After carbonizing this
27 ionic organic compound at $750 \text{ }^\circ\text{C}$, a N/S doped carbon with
28 an SSA of $1094 \text{ m}^2 \text{ g}^{-1}$ was obtained.

30 A nitrogen-doped, graphitic nanoporous carbon membrane
31 (HNDCM) was prepared from PILs composed of cationic
32 poly[1-cyanomethyl-3-vinylimidazolium bis (trifluorometh-
33 anesulfonyl)imide] (PCMVImTf₂N) and anionic neutralized
34 poly(acrylic acid) (PAA), as shown in Figure 13a.^[215] In the
35 structure of (PCMVImTf₂N)(PAA), PAA acts as a crosslinker to
36 chemically lock PCMVImTf₂N in a porous network via electro-
37 static complexation. Tf₂N⁻ ions are believed to be the porogens.
38 Due to the considerable mass loss in the form of volatile spe-
39 cies during carbonization, the HNDCM prepared at $1000 \text{ }^\circ\text{C}$
40 showed an SSA of $907 \text{ m}^2 \text{ g}^{-1}$ with a high pore volume of
41 $0.79 \text{ cm}^3 \text{ g}^{-1}$.

42 Recently, Zhao et al. developed a B/N co-doped nanoporous
43 carbon membrane (B/N-GCM) from the pyrolysis of membrane
44 composing of PAA matrix and poly[1-cyanomethyl-3-vinylim-
45 idazolium bis(trifluoromethane sulfonyl)imide] (PCMVImTFSI)
46 PIL (Figure 13b).^[216] Zhao et al. demonstrated the pore-forming
47 mechanism was directly related to the contents of TFSI ions. In
48 other words, TFSI acts as the porogen during pyrolysis. B, N-co-
49 doped nanoporous carbon membranes (B/N-GCM) derived
50 from (PCMVImTFSI)(PAA) showed a high SSA of $1500 \text{ m}^2 \text{ g}^{-1}$
51 with an ultrahigh areal capacitance of 3 F cm^{-2} .

52 The advantages of the carbonization of PILs for the prepara-
53 tion of porous carbon are obvious. The porogens are evenly
54 distributed in the polymer matrix due to the electrostatic
55 forces between anion and cations so that the morphology and
56 porous microstructure of porous carbons can be tuned by
57 porogens easily. The polymer matrix can be easily tuned into
58 flexible matrix or fiber morphology for flexible and integrated
59 SC devices.^[217,218]

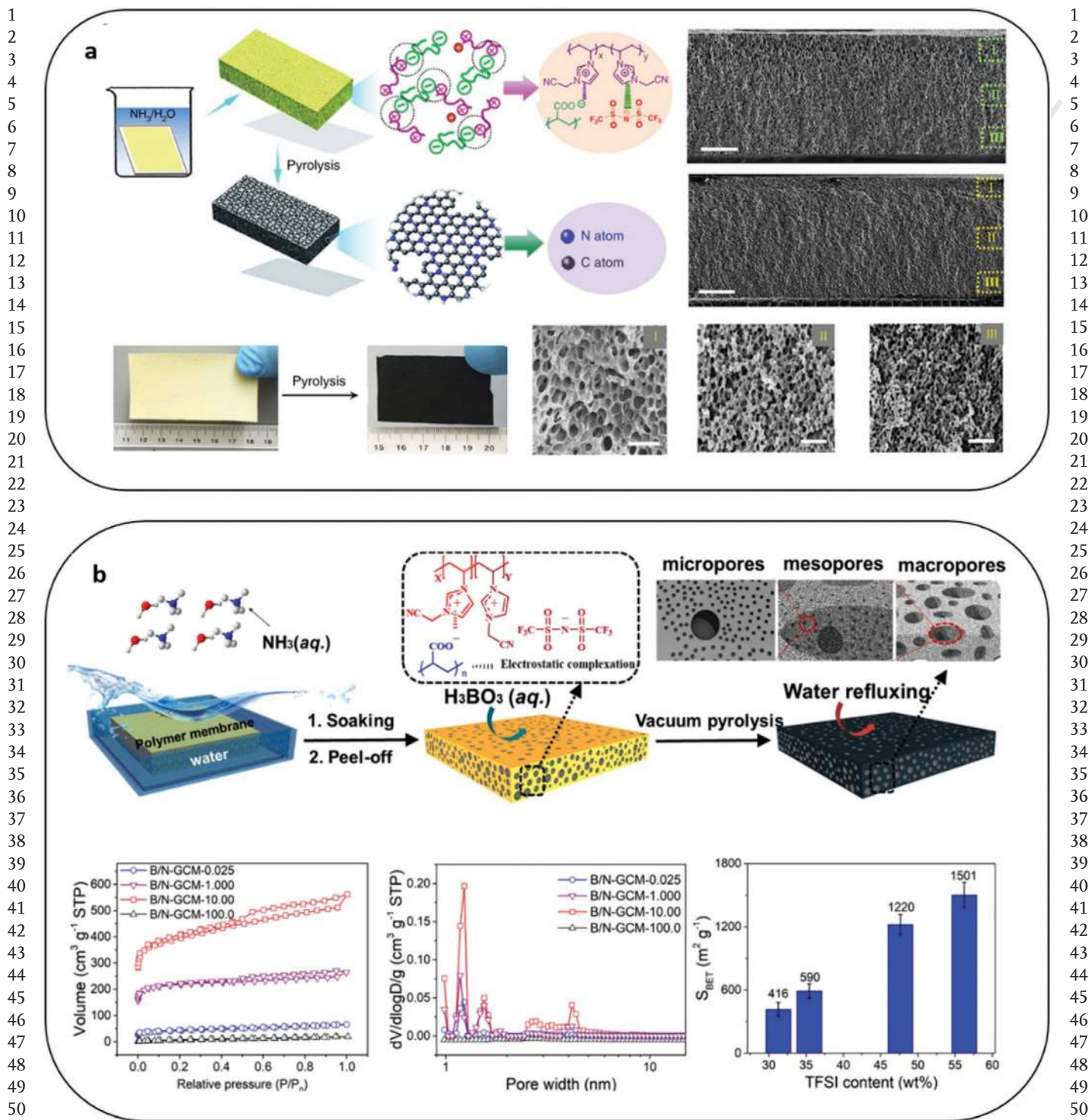


Figure 13. a) The schematic illustration of the preparation of nanoporous carbon membrane from cationic poly[1-cyanomethyl-3-vinylimidazolium bis(trifluoromethanesulfonyl)imide] (PCMVImTf₂N) and anionic neutralized poly(acrylic acid) (PAA), the SEM images of the cross-section of the obtained membrane (above), the digital photograph of the polymer and obtained B/N-GCM membrane, and the SEM images of its top view (below). Reproduced with permission.^[215] Copyright 2017, Nature Publishing Group. b) The schematic fabrication process of hierarchically structured B, N-co-doped nanoporous carbon membranes (B/N-GCM) and the typical pore-parameters as a function of doping ratio of TFSI in the membrane (above), the N₂ adsorption/desorption isotherms, pore-size distribution, and SSA as a function of TFSI content. Reproduced with permission.^[216] Copyright 2019, American Chemical Society.

7. New Porogen Engineering Methods

7.1. Self-Activation of Carbohydrate

Although the direct pyrolysis of co-polymer can be used to synthesize porous carbon with high SSAs, the copolymer precursors are expensive and nonrenewable. Besides, it takes a long time and tedious procedures are needed to prepare these copolymer precursors. Given the abundance of carbohydrates, preparing porous carbons directly by carbohydrate pyrolysis can reduce the usage of activating agents and avoid using nonrenewable petrochemicals. Biomass-based char shows low SSA because the carbon skeleton forms at temperatures higher than the temperatures at which decomposition gases are released. The low interatomic distance between carbon atoms and heteroatom functional groups enables significant shrinkage during pyrolysis, which results in the nonporous nature of biomass chars. In consideration of this, one effective way is to exfoliate the carbon skeleton into sheets and enlarge the interatomic spacing between oxygen functional groups by oxidation. Li et al. synthesized sheet-like porous carbons by a facile hydrothermal-assisted carbonization process.^[219] In the hydrothermal process, H₂O₂ and acetic acid (HAc) were added into the reactor which contains biomass precursor. Subsequently, the resultant porous carbon was obtained by carbonization. The resultant carbon (C-H₂O₂/HAc, **Figure 14a**) showed a sheet-like structure, a high SSA of 1015 m² g⁻¹, and a high specific capacitance of 340 F g⁻¹ at a current density of 0.5 A g⁻¹ (**Figure 14b**). During the hydrothermal process, H₂O₂ acts as a driller which assists in forming mesopores, while HAc exfoliates bulk carbon particles into lamellar carbon sheets. Functional groups such as C(O)OH and C=O decompose to generate gas, which prevents the formation of dense structure and introduces the unique porous structure into carbon skeleton during carbonization. This study offered a general method for the pyrolysis of carbohydrates to prepare porous carbon for SC applications. In principle, any carbon precursors with oxygen functional groups that can enlarge the interatomic spaces of carbon atoms can be carbonized directly to synthesize porous carbon.

Direct pyrolysis strategy is an advance for the preparation of porous carbons since it eliminated the post-synthesis activation process. Ji et al. also discovered a general strategy to prepare porous carbon from the direct pyrolysis of cellulose (the most abundant biomass on the earth).^[220] In this strategy, the argon gas flow rate was controlled during pyrolysis. They found that the BET SSA and the pore volume of the obtained porous carbon showed a negative correlation with the argon flow rate (**Figure 14c**). Through high-resolution transmission electron microscope (HRTEM; **Figure 14d**), it can be observed that a more mesoporous structure was obtained under a 20 sccm argon flow compared with a 100 sccm argon flow. Apparent textural differences of carbons were observed due to the different self-activation reactions under different argon gas flow rates. Namely, the decomposition gases (CO₂, H₂O) of cellulose can react with the carbon skeleton which is formed during pyrolysis (confirmed by the increase of H₂ concentration by mass spectroscopy (**Figure 14e**)) in the temperature range from 750 to 800 °C (Equations (3) and (4)). Argon gas with lower flow rate enables longer residence time, which results in a better

activation effect. Surprisingly, C-10 sample (Ar flow is 10 sccm) showed a high SSA of 2602 m² g⁻¹. With a high SSA and a pore-size distribution of 2–20 nm, C-10 had a specific capacitance of 132 F g⁻¹, good rate capability, and superior cycling stability.

These studies indicated that all carbohydrates can essentially be used as precursors to synthesize porous carbon by this self-activation strategy. Self-activation even can be applied in the activation of other carbon-rich biomasses.^[193,221,222] Defect mesopore-dominant porous carbon (termed as HDMPC) with SSA of 2192 m² g⁻¹ was prepared through direct pyrolysis of low-cost sheep bone in an argon atmosphere through self-activation strategy. When used as the cathode in a lithium-ion capacitor, HDMPC displayed a high capacity of 110 mAh g⁻¹ in the potential range of 2.0–4.5 V versus Li/Li⁺. Given the unique feature of the self-activation mechanism, more oxygen-abundant organic precursors can be pyrolyzed to synthesize porous carbons for SC applications.

7.2. CO₂ Laser Scribing

Laser scribing is a new technique based on the photochemical and photothermal reaction between laser spot and carbon precursors. In 2011, Ajayan et al. synthesized laser-reduced graphene oxide (rGO) on the GO membrane and directly used the rGOs as electrodes for sandwiched and in-plane microsupercapacitors.^[223] Laser-reduced rGO showed 3D morphology, high capacitance, and high conductivity. Later, in 2012, Kaner et al. demonstrated that GO can be reduced as laser-scribed graphene (henceforth termed as LSG) by a commercial LightScribe DVD laser.^[224] LSG with high conductivity (1738 S m⁻¹) and high SSAs (1520 m² g⁻¹) endows LSG with high areal capacitance and an ultralow time constant of 33 ms. Microsupercapacitors based on LSG electrodes showed a high energy density of 1 mWh cm⁻³ and superior rate capability. Tour et al. showed another example that commercial polyimide can be laser scribed into LSG by using a commercial CO₂ laser cutting machine (**Figure 15a**).^[225] Furthermore, they developed inert-gas-protected laser scribing and multiple laser scribing processes which enable the successful transformation from wood,^[226] cloth,^[227] bread into LSG (**Figure 15b**). Alshareef et al. developed the LSG from natural lignin and used LSG as electrodes for high-energy microsupercapacitors through a direct-write lignin laser lithography technique.^[228] Besides, Alshareef et al. developed high-power SC based on the LSG from laser-scribed amorphous carbon spheres.^[229] What is more, due to the hydrophobic nature of LSG, a wettability-driven assembly process was developed to fabricate microsupercapacitor using particulate active materials.^[230] Despite the above achievements, the SSAs of LSG derived from polyimide, lignin, and wood are limited to < 500 m² g⁻¹, which limits its application as electrodes for SCs. The interesting phenomena of transforming organic sources into LSG needs to be elaborated for the further development of LSG-based materials. Kaner et al. proposed a mechanism for the graphene formation during CO₂ laser scribing. Carbon dots absorb CO₂ laser energy which is very close to the absorbance of sp³ C–C, thus breaking the chemical bonds between C–C and forming sp²-dominated carbon dots (**Figure 15c**).^[231] The carbon dots then self-assembled into porous long-range

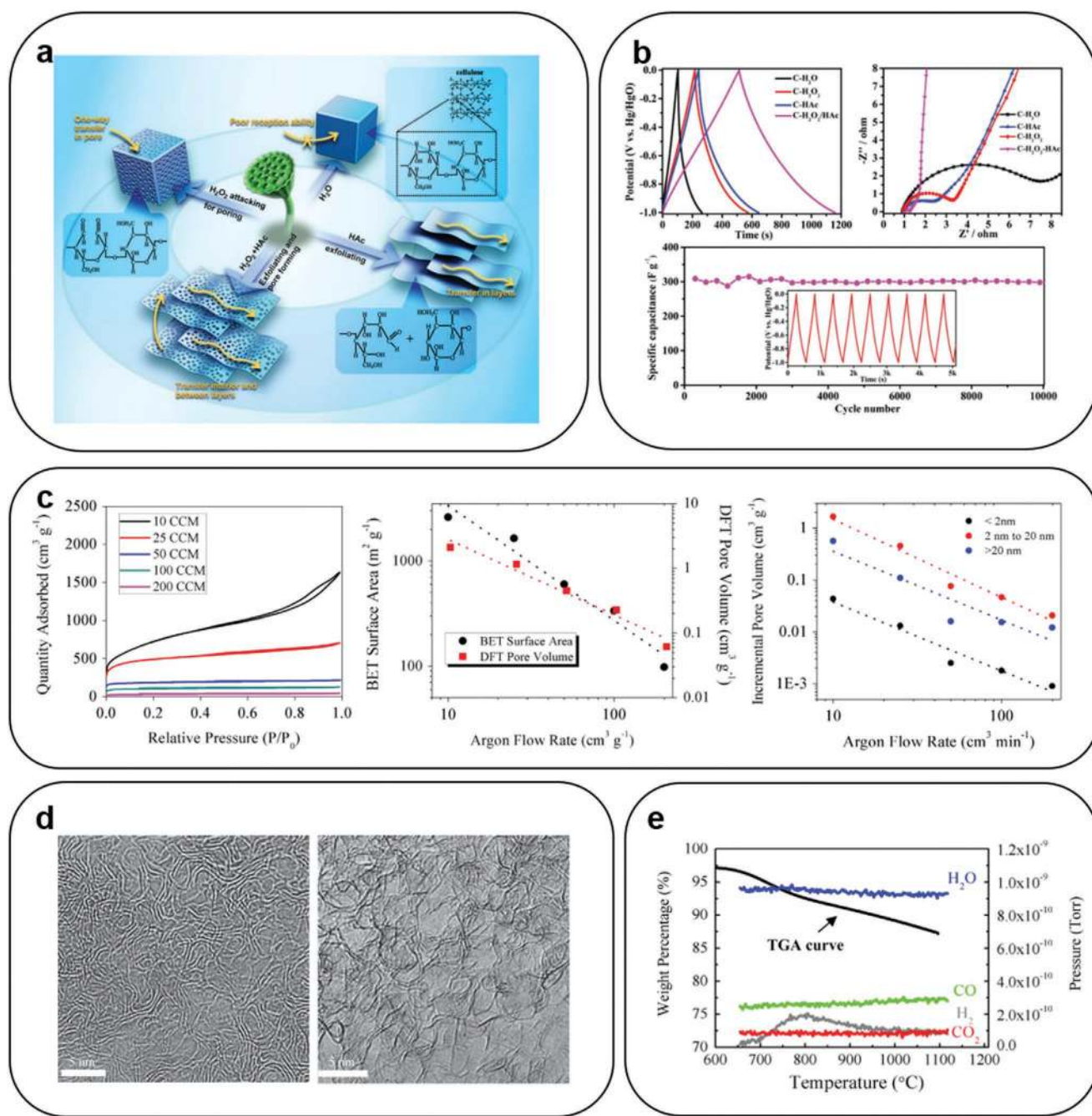


Figure 14. a) Mechanisms of the synthesis and the enhancements of the electrochemical performances of the porous graphene-like carbon using different hydrothermal protocols. b) The CV curves, GCD curves of different carbon materials using different recipe combinations in hydrothermal reactions, and the cycling performances of C-H₂O₂/HAc carbon under of current density of 1 A g⁻¹ using a three-electrode set-up. Reproduced with permission.^[219] Copyright 2018, Wiley-VCH. c) The influence of flow rate of argon gas during the pyrolysis of cellulose, the dependence of SSA on the flow rate of argon during pyrolysis, the pore volume as a function of the argon gas flow rate. d) HRTEM images showing the different microstructures of C-100 and C-20. e) The MS spectra during the pyrolysis of a 650 °C pre-heat-treated cellulose sample. Reproduced with permission.^[220] Copyright 2015, Elsevier.

turbostratic graphene nanodomains. The pursuit of high SSA from direct laser scribing organics, has significant potential because direct laser scribing is a fast technique that can also be used to fabricate LSG electrodes on metal current collectors without binders. Kaner et al. investigated a laser scribed mixture of carbon quantum dots and graphene oxide (Figure 15d).^[232] At

a carbon quantum dot concentration of 35%, the LSG exhibited the highest SSA around 1000 m² g⁻¹ and a specific capacitance of 190 F g⁻¹. Kaner et al. also discovered that the performances of commercially activated carbon electrode could be greatly enhanced by laser scribing (Figure 15e).^[233] After laser scribing, both the areal and gravimetric capacitances of activated carbon

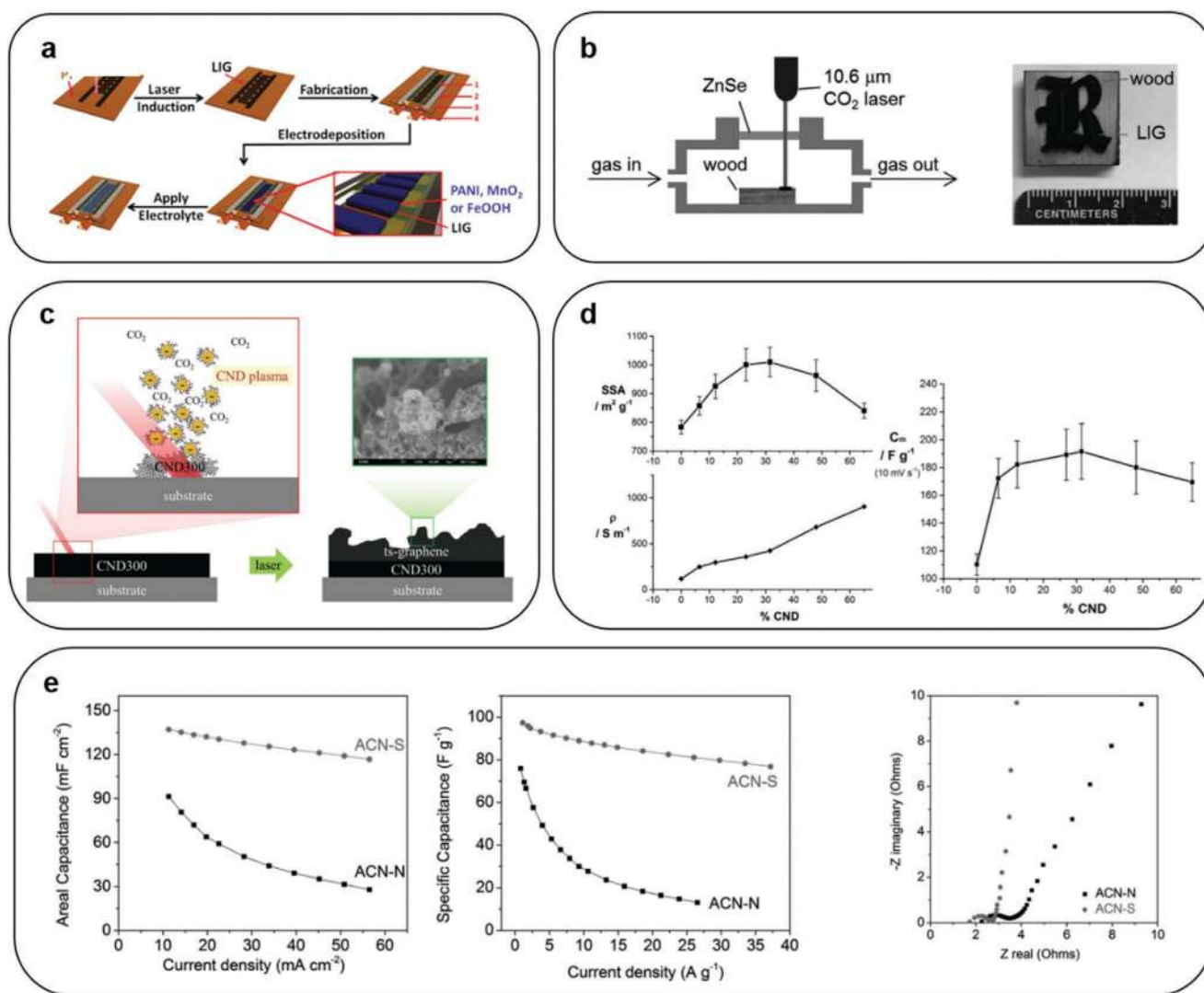


Figure 15. a) Scheme of the fabrication of microsupercapacitors with laser-induced graphene (LIG)–MnO₂. Reproduced with permission.^[225] Copyright 2015, Wiley-VCH. b) The formation of graphene can be done by laser scribing natural wood under inert-atmosphere protection. Reproduced with permission.^[226] Copyright 2017, Wiley-VCH. c) Proposed LSG formation mechanism by laser scribing of carbon quantum dots. Reproduced with permission.^[231] Copyright 2018, Wiley-VCH. d) The dependence of SSA, conductivity, the specific capacitance of the obtained LSG on the weight ratio of carbon quantum dots using a CO₂ laser scribing process. Reproduced with permission.^[232] Copyright 2019, The Royal Society of Chemistry. e) The electrochemical behaviors (dependence of areal capacitance and the gravimetric specific capacitance on current density, the electrochemical impedance spectroscopy) of laser-scribed activated carbon and activated carbon in acetonitrile electrolytes. Reproduced with permission.^[233] Copyright 2017, Wiley-VCH.

are enhanced apparently. What is more, the impedance of activated carbon electrode was reduced by laser scribing, as demonstrated by the Nyquist plot. Still, the mechanism and what happened to the commercial activated carbon need to be elaborated. Given the advantages of laser scribing, it is suitable to develop the LSG electrodes with both high areal capacitance and high rate capability for commercial SC applications. The SSAs of LSGs can be further enhanced by incorporating some porogens in the laser scribing process.

7.3. Dehalogenation Carbonization

Carbonization can be achieved by not only pyrolysis but also deoxygenation and dehydrogenation with concentrated sulfuric

acid treatment. However, the SSAs of carbons derived from dehydrogenation using H₂SO₄ was as low as 2.4 m² g⁻¹.^[28] Recently, dehalogenation became a general method that can transform halogen-containing polymers into porous carbons. Dai et al. discovered that polyvinylidene chloride (PVDC) could be directly transformed into a carbonaceous material using dehalogenation reaction by KOH in ethyl alcohol solution (Figure 16a).^[37] The dehalogenation of PVDC is composed of multiple processes. HCl molecules are eliminated by KOH etching. Then the partially cyclized structure was transformed into carbonaceous structure through either intramolecular cyclization or intermolecular dehalogenation (Figure 16b). The obtained ball-milled carbon (BMC) showed particulate morphology and sp² hybridized crystalline structure with

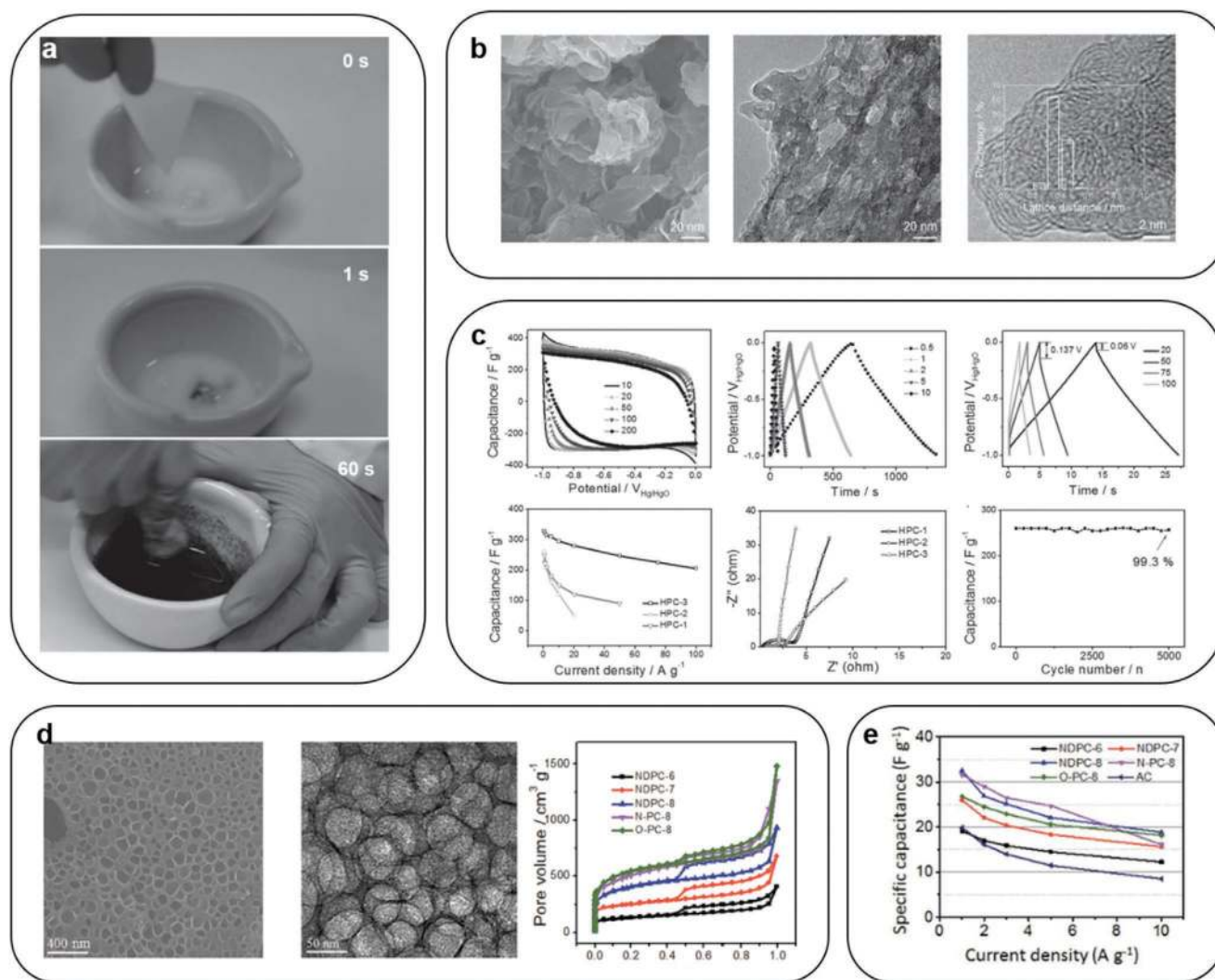


Figure 16. a) Hand-grinding processing mixture of PVDF/KOH powders in ethyl alcohol solution at different time. b) The SEM, TEM, and HRTEM images of BMC. c) The electrochemical performance of BMC (CV, GCD, and EIS). Reproduced with permission.^[37] Copyright 2016, Wiley-VCH. d) The SEM, TEM images, and the N_2 adsorption/desorption isotherms of nonporous porous carbon (NDPC). e) The rate capability of symmetric capacitor using NDPC as electrodes. Reproduced with permission.^[234] Copyright 2017, The Royal Society of Chemistry.

an interlayer spacing of 0.35 nm. BMC shows a high SSA of $1735 \text{ m}^2 \text{ g}^{-1}$ and a pore sizes below 5 nm. BMC exhibits a high specific capacitance of 328 F g^{-1} at 0.5 A g^{-1} (Figure 16c). Besides, BMC also shows high rate capability and good cycling stability. These studies show that dehalogenation-based carbonization can be used to prepare porous carbons with high surface areas. As a general process, various halogen-containing polymers can be used as carbon sources. Polyvinyl fluoride (PVDF) can be dehalogenated by NaNH_2 ^[29] and sodium ethoxide^[234] to prepare porous carbon. The dehalogenated PVDF using sodium ethoxide showed a high SSA of $1920 \text{ m}^2 \text{ g}^{-1}$ (Figure 16d). This porous carbon enables a 2 V symmetric SC with a capacitance 32.5 F g^{-1} in Li_2SO_4 electrolyte (Figure 16e).

8. Summary and Outlook

SCs are important energy storage devices that are playing increasingly important roles in nowadays energy storage

applications. SC modules are being evaluated for electrical transportation, uninterruptible power supplies, power tools, and high power electronics. At present, the capital cost of SC (price per watt-hour) is too high compared with mature rechargeable battery technologies such as LIBs and lead-acid batteries, partially due to the high cost of porous carbon active materials (around $30\text{--}50 \text{ \$ kg}^{-1}$). Searching new porous carbons that offer both low cost, moderate SSA (1500 to $2000 \text{ m}^2 \text{ g}^{-1}$), and decent performance is crucial for the further market penetration of SC. Thus, this review presents several strategies that are being developed to achieve porous carbons with higher performance and addresses the synthesis and development difficulties for each approach.

Porous carbon electrodes used in commercial SCs are currently mostly produced by physical activation. Physical activation (H_2 , CO_2 activation) produces porous carbons with micropore-dominated porous structures and limited SSAs. Air, as a free activation agent, has seldom been used in the

1 preparation of high-SSA porous carbon in physical activation
2 method because carbon faces combustion in the oxygen-rich
3 atmosphere. Diluted air in an inert atmosphere can exert as
4 a high-oxidative physical activation agent that enhances the
5 SSA of the resultant porous carbons obtained from physical
6 activation.

7 In chemical activation methods, a lot of KOH or NaOH is
8 used, which causes the emission of highly corrosive byproducts
9 and pollutants during activation. Thus, chemically activated
10 porous carbons require post-treatments in industrial produc-
11 tion. The chemical activation method needs to be redesigned
12 to develop porous carbons at a reasonable cost and minimal
13 environmental impact. Green chemical engineering processes
14 are essential for the sustainable preparation of chemically
15 activated porous carbons for SCs. During the past few years,
16 various new chemical activation agents have been developed,
17 but unfortunately, some of them are highly corrosive and even
18 toxic. In addition, the porous carbons obtained from these new
19 activation agents usually possess macropores that significantly
20 reduce the tap density of the resultant porous carbons. In that
21 case, porous carbons without macroporous structures prepared
22 by new chemical activation agents (CuCl₂ as a typical activation
23 agent) are of special interests for developing SCs. The porogen
24 mechanisms of these new chemical agents are also needed to
25 be studied thoroughly through in situ techniques. Besides, the
26 environmental impacts of these new chemical activation agents
27 still need to be re-evaluated.

28 Direct pyrolysis of self-template organic salts may be a solu-
29 tion for fabricating porous carbons used in SCs. Based on
30 some low-cost precursors such as alkaline metal citrate salts,
31 the self-template method can be cheap and easy to be applied
32 in the preparation of porous carbons with high SSA. The big-
33 gest disadvantage of this method can be the low tap density of
34 the obtained porous carbons due to its macroporous structures.
35 On the one hand, the macroporous structure of these porous
36 carbons can be crushed to increase the tap density. On the other
37 hand, the self-templated carbons with opened 3D macroporous
38 structures may be used as supports for pseudocapacitive mate-
39 rials (such as RuO₂, MnO₂) in aqueous SCs.

40 The pyrolysis of conjugated copolymers, block copolymers,
41 and PILs are new strategies that have been recently developed
42 to improve the quality of porous carbons for SC applications.
43 Through direct pyrolysis of copolymers, high SSAs and impres-
44 sive specific capacitance values have been obtained, but these
45 processes are admittedly complex and the precursors are expen-
46 sive. So cheaper polymer precursors, simplified and scalable
47 processes are needed to make these processes practical. The
48 intrinsic mechanism of these direct pyrolysis methods needs to
49 be studied so that better copolymers can be designed and used
50 to prepare porous carbons. The decomposition gases of these
51 heteroatom-rich polymers are toxic and need to be treated to
52 minimize their environmental impact, which adds cost to the
53 pyrolysis process. From the perspective of material synthesis,
54 the SSA of porous carbons can be further improved by tuning
55 the intermolecular design (such as decrease the molecular chain
56 of PMMA and PAN) and optimization of preparation param-
57 eters (pyrolysis time, pyrolysis temperature, and inert gas flow
58 rate). Because pyrolysis of polyaniline-co-polypyrrole generates
59 amine species, these amine species may be used as activation

agents simultaneously in the pyrolysis process. On the appli- 1
cation aspect, the copolymer (block polymer, PILs) pyrolysis 2
strategy is versatile for preparing free-standing PCF mats or 3
flexible porous carbon electrodes. These integrated electrodes 4
have great potentials for advanced flexible and wearable SCs. 5

6 Self-activation of carbohydrate biomasses has been playing
7 increasingly important roles in producing porous carbons. 8
The self-activation method is a successful example that 9
porous carbons can be prepared by the direct pyrolysis of bio- 10
carbohydrates. Thus, inert gas lines in a traditional physical 11
activation production line can be eliminated. Still, based on 12
the self-activation mechanism, reactors that can fully utilize the 13
decomposition gases (CO₂) for porous carbon production are 14
needed to be designed.

15 As a huge power density gap between SCs and electrolytic
16 capacitors still exists, the development of high-power SCs is
17 still another major trend. SCs with high energy density and
18 high power density require that the porous carbon materials
19 have not only high SSA but also high conductivity enabled by
20 highly graphitic structure. High graphitization (conductivity)
21 and high SSA are contradictory factors since amorphous car-
22 bons with relatively low conductivities (<1 S cm⁻¹) are obtained
23 from the traditional pyrolysis process. Laser scribing opens a
24 new pathway for graphene-based electrode materials with high
25 conductivity (as high as 60 S cm⁻¹) for SCs.^[228] Given the lim-
26 ited SSA of state-of-art LSG electrodes, we still need other ways
27 to improve the SSA of LSG. In the next stage of development
28 of LSG electrodes for SCs, various porogens, such as alkaline
29 metal hydroxides, metal-organic salts, and organics that cannot
30 be laser-carbonized (such as PMMA), may be added into the
31 carbon precursors to synthesize porous, graphitic carbon mate-
32 rials in the laser scribing process.

33 In the development of porous carbons for commercial SC
34 applications, we also need to consider the tap density of porous
35 carbons. Tap density is a critical parameter that is seldom
36 investigated by researchers. The tap density of porous carbon
37 is directly related to the volumetric energy density of the SCs.
38 Using graphene materials with high pack density as electrode
39 materials, SC can achieve a high volumetric energy density of
40 13.1 Wh L⁻¹.^[235,236] However, due to the existence of a huge
41 amount of micropores, the tap densities of activated carbon are
42 limited to 0.35 cm³ g⁻¹. The tap density decreases as the SSA
43 increases, so the tap density should be optimized concurrently
44 with SSA for new production processes. For achieving higher
45 energy density SCs, we may design asymmetric hybrid lithium
46 (sodium, potassium) ion SCs that use porous carbon as the
47 cathode to increase the operating voltage and energy density.
48 The major role of porous carbon in hybrid SCs is to provide
49 a high surface area that provides high double-layer capacitance
50 with high power capability. The designing of asymmetric hybrid
51 lithium (sodium, potassium) SCs requires optimization of the
52 relationship between pore architecture and active electrolyte
53 ions. For practical applications, the stability of porous carbon in
54 mobile ion SCs need to be investigated.

55 SCs have become important energy storage devices with
56 potential in many types of applications. With the development
57 of novel, facile, and green methods for synthesis of high-quality
58 porous carbons, we can achieve SCs with higher storage energy
59 density and lower costs soon.

1 Acknowledgements

2 J.Y. and W.L.Z. contributed equally to this work. ~~The research reported in~~
3 ~~this publication is supported by King Abdullah University of Science and~~
4 ~~Technology (KAUST).~~

7 Conflict of Interest

9 The authors declare no conflict of interest.

12 Keywords

14 activation, carbonization, porous carbon, pyrolysis, self-activation,
15 self-template, supercapacitors

16 Received: December 10, 2019

17 Revised: January 10, 2020

18 Published online:

- 21
-
- 22 [1] J. R. Miller, P. Simon, *Science* **2008**, 321, 651.
23 [2] S. Zhang, N. Pan, *Adv. Energy Mater.* **2015**, 5, 1401401.
24 [3] M. F. El-Kady, Y. Shao, R. B. Kaner, *Nat. Rev. Mater.* **2016**, 1, 16033.
25 [4] A. K. Talukder, *Electrochem. Soc. Interface* **2008**, 17, 53.
26 [5] B. Dunn, B. Dunn, H. Kamath, J. Tarascon, *Sci. Mag.* **2011**, 334,
27 928.
28 [6] J. R. Miller, *Science* **2012**, 335, 1312.
29 [7] K. Fic, A. Platek, J. Piwek, E. Frackowiak, *Mater. Today* **2018**, 21,
30 437.
31 [8] K. S. W. Sing, D. H. Everett, R. A. W. Haul, L. Moscou, R. A. Pierotti,
32 J. R. Rouquerol, T. Siemieniowska, *Pure Appl. Chem.* **1985**, 57, 603.
33 [9] F. Rodríguez-Reinoso, M. Molina-Sabio, *Carbon* **1992**, 30, 1111.
34 [10] J. Wang, S. Kaskel, *J. Mater. Chem.* **2012**, 22, 23710.
35 [11] M. Rodenas, D. Amoros, A. Solano, *Carbon* **2003**, 41, 267.
36 [12] Y. Zhu, S. Murali, M. D. Stoller, K. J. Ganesh, W. Cai, P. J. Ferreira,
37 A. Pirkle, R. M. Wallace, K. A. Cychosz, M. Thommes, D. Su,
38 E. A. Stach, R. S. Ruoff, *Science* **2011**, 332, 1537.
39 [13] D. Liu, W. Zhang, H. Lin, Y. Li, H. Lu, Y. Wang, *J. Cleaner Prod.*
40 **2016**, 112, 1190.
41 [14] J. A. Maciá-Agulló, B. C. Moore, D. Cazorla-Amorós,
42 A. Linares-Solano, *Carbon* **2004**, 42, 1367.
43 [15] A. Hamasaki, A. Furuse, Y. Sekinuma, K. Fujio, M. Iide, S. Ozeki,
44 *Sci. Rep.* **2019**, 9, 7489.
45 [16] Z. Miao, Y. Huang, J. Xin, X. Su, Y. Sang, H. Liu, J. J. Wang, *ACS*
46 *Appl. Mater. Interfaces* **2019**, 11, 18044.
47 [17] S. Liu, Y. Liang, W. Zhou, W. Hu, H. Dong, M. Zheng, H. Hu,
48 B. Lei, Y. Xiao, Y. Liu, *J. Mater. Chem. A* **2018**, 6, 12046.
49 [18] J. Liu, N. P. Wickramaratne, S. Z. Qiao, M. Jaroniec, *Nat. Mater.*
50 **2015**, 14, 763.
51 [19] J. Chmiola, G. Yushin, Y. Gogotsi, C. Portet, P. Simon,
52 P. L. Taberna, *Science* **2006**, 313, 1760.
53 [20] Y. Zhai, Y. Dou, D. Zhao, P. F. Fulvio, R. T. Mayes, S. Dai, *Adv.*
54 *Mater.* **2011**, 23, 4828.
55 [21] Y. Bu, T. Sun, Y. Cai, L. Du, O. Zhuo, L. Yang, Q. Wu, X. Wang,
56 Z. Hu, *Adv. Mater.* **2017**, 29, 1700470.
57 [22] G. Xu, P. Nie, H. Dou, B. Ding, L. Li, X. Zhang, *Mater. Today* **2017**,
58 20, 191.
59 [23] F. Xu, D. Wu, R. Fu, B. Wei, *Mater. Today* **2017**, 20, 629.
[24] R. Ye, D. K. James, J. M. Tour, *Adv. Mater.* **2019**, 31, 1803621.
[25] J. Luo, H. Zhang, Z. Zhang, J. Yu, Z. Yang, *Carbon* **2019**, 155, 1.
[26] S. S. Lam, R. K. Liew, Y. M. Wong, P. N. Y. Yek, N. L. Ma, C. L. Lee,
H. A. Chase, *J. Cleaner Prod.* **2017**, 162, 1376.
[27] Y. Liu, X. Yang, H. Liu, Y. Ye, Z. Wei, *Appl. Catal., B* **2017**, 218, 679.
[28] D. Damodar, A. Kunamalla, M. Varkolu, S. K. Maity,
A. S. Deshpande, *ACS Sustainable Chem. Eng.* **2019**, 7, 12707.
[29] M. Guo, Y. Li, K. Du, C. Qiu, G. Dou, G. Zhang, *Appl. Surf. Sci.*
2018, 440, 606.
[30] X. Zheng, J. Luo, W. Lv, D. W. Wang, Q. H. Yang, *Adv. Mater.* **2015**,
27, 5388.
[31] Z. Liu, F. Mo, H. Li, M. Zhu, Z. Wang, G. Liang, C. Zhi, *Small*
Methods **2018**, 2, 1800124.
[32] R. J. White, V. Budarin, R. Luque, J. H. Clark, D. J. MacQuarrie,
Chem. Soc. Rev. **2009**, 38, 3401.
[33] L. Borchardt, M. Oschatz, S. Kaskel, *Mater. Horiz.* **2014**, 1, 157.
[34] T. M. Alslaibi, I. Abustan, M. A. Ahmad, A. A. Foul, *Chem. Technol.*
Biotechnol. **2013**, 88, 1183.
[35] Z. Rozlívková, M. Trchová, M. Exnerová, J. Stejskal, *Synth. Met.*
2011, 161, 1122.
[36] W. Chaiwat, I. Hasegawa, J. Kori, K. Mae, *Ind. Eng. Chem. Res.*
2008, 47, 5948.
[37] G. Zhang, L. Wang, Y. Hao, X. Jin, Y. Xu, Y. Kuang, L. Dai, X. Sun,
Adv. Funct. Mater. **2016**, 26, 3340.
[38] A. Zheng, Z. Zhao, S. Chang, Z. Huang, X. Wang, F. He, H. Li,
Bioresour. Technol. **2013**, 128, 370.
[39] M. Pala, I. C. Kantarli, H. B. Buyukisik, J. Yanik, *Bioresour. Technol.*
2014, 161, 255.
[40] W. H. Chen, S. C. Ye, H. K. Sheen, *Bioresour. Technol.* **2012**, 118,
195.
[41] S. W. Han, D. W. Jung, J. H. Jeong, E. S. Oh, *Chem. Eng. J.* **2014**,
254, 597.
[42] M. M. Tang, R. Bacon, *Carbon* **1964**, 2, 211.
[43] A. K. Kercher, D. C. Nagle, *Carbon* **2003**, 41, 15.
[44] K. Yang, J. Peng, H. Xia, L. Zhang, C. Srinivasakannan, S. Guo,
J. Taiwan Inst. Chem. Eng. **2010**, 41, 367.
[45] M. S. Contreras, C. A. Páez, L. Zubizarreta, A. Léonard, S. Blacher,
C. G. Olivera-Fuentes, A. Arenillas, J. P. Pirard, N. Job, *Carbon*
2010, 48, 3157.
[46] D. W. Kim, H. S. Kil, K. Nakabayashi, S. H. Yoon, J. Miyawaki,
Carbon **2017**, 114, 98.
[47] M. J. Prauchner, F. Rodríguez-Reinoso, *Microporous Mesoporous*
Mater. **2012**, 152, 163.
[48] R. M. Navarro, M. A. Peña, J. L. G. Fierro, *Chem. Rev.* **2007**, 107,
3952.
[49] K. Suresh Kumar Reddy, A. Al Shoaibi, C. Srinivasakannan, *New*
Carbon Mater. **2012**, 27, 344.
[50] Ö. Şahin, C. Saka, *Bioresour. Technol.* **2013**, 136, 163.
[51] G. Lin, R. Ma, Y. Zhou, Q. Liu, X. Dong, J. Wang, *Electrochim. Acta*
2018, 261, 49.
[52] K. Zou, Y. Deng, J. Chen, Y. Qian, Y. Yang, Y. Li, G. Chen, *J. Power*
Sources **2018**, 378, 579.
[53] M. A. Islam, M. J. Ahmed, W. A. Khanday, M. Asif, B. H. Hameed,
J. Environ. Manage. **2017**, 203, 237.
[54] M. A. Lillo-Ródenas, D. Lozano-Castelló, D. Cazorla-Amorós,
A. Linares-Solano, *Carbon* **2001**, 39, 751.
[55] H. Saygili, F. Güzel, *J. Cleaner Prod.* **2016**, 113, 995.
[56] D. Prahas, Y. Kartika, N. Indraswati, S. Ismadi, *Chem. Eng. J.* **2008**,
140, 32.
[57] H. Yin, B. Lu, Y. Xu, D. Tang, X. Mao, W. Xiao, D. Wang,
A. N. Alshawabkeh, *Environ. Sci. Technol.* **2014**, 48, 8101.
[58] F. Zhang, T. Liu, M. Li, M. Yu, Y. Luo, Y. Tong, Y. Li, *Nano Lett.*
2017, 17, 3097.
[59] M. Gao, S. Y. Pan, W. C. Chen, P. C. Chiang, *Mater. Today Energy*
2018, 7, 58.
[60] D. Kang, Q. Liu, J. Gu, Y. Su, W. Zhang, D. Zhang, *ACS Nano* **2015**,
9, 11225.
[61] X. Fan, C. Yu, J. Yang, Z. Ling, C. Hu, M. Zhang, J. Qiu, *Adv. Energy*
Mater. **2015**, 5, 1401761.

- [62] C. Wang, D. Wang, S. Zheng, X. Fang, W. Zhang, Y. Tian, H. Lin, H. Lu, L. Jiang, *Chem. Res. Chin. Univ.* **2018**, *34*, 983.
- [63] F. Zhang, T. Liu, G. Hou, T. Kou, L. Yue, R. Guan, Y. Li, *Nano Res.* **2016**, *9*, 2875.
- [64] M. Sevilla, R. Mokaya, A. B. Fuertes, *Energy Environ. Sci.* **2011**, *4*, 2930.
- [65] M. Sevilla, P. Valle-Vigón, A. B. Fuertes, *Adv. Funct. Mater.* **2011**, *21*, 2781.
- [66] W. Zhang, H. Lin, Z. Lin, J. Yin, H. Lu, D. Liu, M. Zhao, *ChemSusChem* **2015**, *8*, 2114.
- [67] W. Zhang, M. Zhao, R. Liu, X. Wang, H. Lin, *Colloids Surf., A* **2015**, *484*, 518.
- [68] W. Zhang, D. Liu, H. Lin, H. Lu, J. Xu, D. Liu, *Colloids Surf., A* **2016**, *511*, 294.
- [69] Y. X. Tian, C. Xiao, J. Yin, W. Zhang, J. P. Bao, H. Lin, H. Lu, *ChemistrySelect* **2019**, *4*, 2314.
- [70] M. Yu, D. Lin, H. Feng, Y. Zeng, Y. Tong, X. Lu, *Angew. Chem., Int. Ed.* **2017**, *56*, 5454.
- [71] Y. Han, Y. Lu, S. Shen, Y. Zhong, S. Liu, X. Xia, Y. Tong, X. Lu, *Adv. Funct. Mater.* **2019**, *29*, 1806329.
- [72] C. Wang, D. Wu, H. Wang, Z. Gao, F. Xu, K. Jiang, *J. Mater. Chem. A* **2018**, *6*, 1244.
- [73] Y. Chen, Z. Zhang, Y. Lai, X. Shi, J. Li, X. Chen, K. Zhang, J. Li, *J. Power Sources* **2017**, *359*, 529.
- [74] Y. Chen, S. Ji, H. Wang, V. Linkov, R. Wang, *Int. J. Hydrogen Energy* **2018**, *43*, 5124.
- [75] Z. Xu, Y. Zhou, Z. Sun, D. Zhang, Y. Huang, S. Gu, W. Chen, *Chemosphere* **2020**, *241*, 125120.
- [76] J. Li, L. Tian, F. Liang, J. Wang, L. Han, J. Zhang, S. Ge, L. Dong, H. Zhang, S. Zhang, *Carbon* **2019**, *141*, 739.
- [77] H. Zhu, X. Wang, X. Liu, X. Yang, *Adv. Mater.* **2012**, *24*, 6524.
- [78] S. I. Yun, S. H. Kim, D. W. Kim, Y. A. Kim, B. H. Kim, *Carbon* **2019**, *149*, 637.
- [79] Y. Lv, L. Gan, M. Liu, W. Xiong, Z. Xu, D. Zhu, D. S. Wright, *J. Power Sources* **2012**, *209*, 152.
- [80] J. Li, N. Wang, J. Tian, W. Qian, W. Chu, *Adv. Funct. Mater.* **2018**, *28*, 1806153.
- [81] G. Zhang, X. Ou, C. Cui, J. Ma, J. Yang, Y. Tang, *Adv. Funct. Mater.* **2019**, *29*, 1806722.
- [82] W. Gao, X. Feng, T. Zhang, H. Huang, J. Li, W. Song, *ACS Appl. Mater. Interfaces* **2014**, *6*, 19109.
- [83] L. Wan, P. Song, J. Liu, D. Chen, R. Xiao, Y. Zhang, J. Chen, M. Xie, C. Du, *J. Power Sources* **2019**, *438*, 227013.
- [84] T. Liu, F. Zhang, Y. Song, Y. Li, *J. Mater. Chem. A* **2017**, *5*, 17705.
- [85] J. Chen, H. Wei, H. Chen, W. Yao, H. Lin, S. Han, *Electrochim. Acta* **2018**, *271*, 49.
- [86] J. Yi, Y. Qing, C. T. Wu, Y. Zeng, Y. Wu, X. Lu, Y. Tong, *J. Power Sources* **2017**, *351*, 130.
- [87] X. Liu, N. Fechner, M. Antonietti, *Chem. Soc. Rev.* **2013**, *42*, 8237.
- [88] M. Molina-Sabio, F. Rodríguez-Reinoso, *Colloids Surf., A* **2004**, *241*, 15.
- [89] A. Ahmadpour, D. D. Do, *Carbon* **1996**, *34*, 471.
- [90] X. Liu, M. Antonietti, C. Giordano, *Chem. Mater.* **2013**, *25*, 2021.
- [91] P. Kuhn, A. Forget, D. Su, A. Thomas, M. Antonietti, *J. Am. Chem. Soc.* **2008**, *130*, 13333.
- [92] X. Liu, C. Giordano, M. Antonietti, *Small* **2014**, *10*, 193.
- [93] X. Liu, N. Fechner, M. Antonietti, M. G. Willinger, R. Schlögl, *Mater. Horiz.* **2016**, *3*, 214.
- [94] X. Liu, M. Antonietti, *Adv. Mater.* **2013**, *25*, 6284.
- [95] X. Liu, M. Antonietti, *Carbon* **2014**, *69*, 460.
- [96] C. M. Yang, H. Noguchi, K. Murata, M. Yudasaka, A. Hashimoto, S. Iijima, K. Kaneko, *Adv. Mater.* **2005**, *17*, 866.
- [97] H. Hwang, C. H. Kim, J. H. Wee, J. H. Han, C. M. Yang, *Appl. Surf. Sci.* **2019**, *489*, 708.
- [98] T. Lin, W. Chen, F. Liu, C. Yang, H. Bi, F. Xu, F. Huang, *Science* **2015**, *350*, 1508.
- [99] G. Wang, H. Wang, X. Lu, Y. Ling, M. Yu, T. Zhai, Y. Tong, Y. Li, *Adv. Mater.* **2014**, *26*, 2676.
- [100] D. Qiu, N. Guo, A. Gao, L. Zheng, W. Xu, M. Li, F. Wang, R. Yang, *Electrochim. Acta* **2019**, *294*, 398.
- [101] Y. Li, Y. Liang, H. Hu, H. Dong, M. Zheng, Y. Xiao, Y. Liu, *Carbon* **2019**, *152*, 120.
- [102] D. Wang, J. Nai, L. Xu, T. Sun, *J. Energy Storage* **2019**, *24*, 100764.
- [103] W. Yang, W. Yang, L. Kong, A. Song, X. Qin, G. Shao, *Carbon* **2018**, *127*, 557.
- [104] T. Wei, X. Wei, L. Yang, H. Xiao, Y. Gao, H. Li, *J. Power Sources* **2016**, *331*, 373.
- [105] L. Tang, Y. Liu, J. Wang, G. Zeng, Y. Deng, H. Dong, H. Feng, J. Wang, B. Peng, *Appl. Catal., B* **2018**, *231*, 1.
- [106] H. W. Liang, W. Wei, Z. S. Wu, X. Feng, K. Müllen, *J. Am. Chem. Soc.* **2013**, *135*, 16002.
- [107] P. Schmidt-Winkel, J. W. W. Lukens, D. Zhao, P. Yang, B. F. Chmelka, G. D. Stucky, *J. Am. Chem. Soc.* **1999**, *121*, 254.
- [108] S. Schacht, Q. Huo, I. G. Voigt-Martin, G. D. Stucky, F. Schüth, *Science* **1996**, *273*, 768.
- [109] K. Xie, X. Qin, X. Wang, Y. Wang, H. Tao, Q. Wu, L. Yang, Z. Hu, *Adv. Mater.* **2012**, *24*, 347.
- [110] Z. Fan, Y. Liu, J. Yan, G. Ning, Q. Wang, T. Wei, L. Zhi, F. Wei, *Adv. Energy Mater.* **2012**, *2*, 419.
- [111] C. Zhu, M. Takata, Y. Aoki, H. Habazaki, *Chem. Eng. J.* **2018**, *350*, 278.
- [112] M. Mecklenburg, A. Schuchardt, Y. K. Mishra, S. Kaps, R. Adelung, A. Lotnyk, L. Kienle, K. Schulte, *Adv. Mater.* **2012**, *24*, 3486.
- [113] C. Wang, M. J. O'Connell, C. K. Chan, *ACS Appl. Mater. Interfaces* **2015**, *7*, 8952.
- [114] S. He, C. Zhang, C. Du, C. Cheng, W. Chen, *J. Power Sources* **2019**, *434*, 226701.
- [115] Y. Liang, M. G. Schwab, L. Zhi, E. Mugnaioli, U. Kolb, X. Feng, K. Müllen, *J. Am. Chem. Soc.* **2010**, *132*, 15030.
- [116] Y. Fang, Y. Lv, R. Che, H. Wu, X. Zhang, D. Gu, G. Zheng, D. Zhao, *J. Am. Chem. Soc.* **2013**, *135*, 1524.
- [117] C. deA. Filho, A. J. G. Zarbin, *Carbon* **2006**, *44*, 2869.
- [118] T. Kyotani, T. Nagai, S. Inoue, A. Tomita, *Chem. Mater.* **1997**, *9*, 609.
- [119] T. Kyotani, Z. Ma, A. Tomita, *Carbon* **2003**, *41*, 1451.
- [120] C. Liang, Z. Li, S. Dai, *Angew. Chem., Int. Ed.* **2008**, *47*, 3696.
- [121] Y. Xie, D. Kocaefe, C. Chen, Y. Kocaefe, *J. Nanomater.* **2016**, *2016*, 2302595.
- [122] W. Chen, Z. Hu, Y. Yang, X. Wang, Y. He, Y. Xie, C. Zhu, Y. Zhang, L. Lv, *Ionics* **2019**, *25*, 5429.
- [123] Y. K. Kim, J. H. Park, J. W. Lee, *Carbon* **2018**, *126*, 215.
- [124] F. D. Han, Y. J. Bai, R. Liu, B. Yao, Y. X. Qi, N. Lun, J. X. Zhang, *Adv. Energy Mater.* **2011**, *1*, 798.
- [125] X. F. Jiang, R. Li, M. Hu, Z. Hu, D. Golberg, Y. Bando, X. Bin Wang, *Adv. Mater.* **2019**, *31*, 1901186.
- [126] J. Liu, Y. Zhang, L. Zhang, F. Xie, A. Vasileff, S. Z. Qiao, *Adv. Mater.* **2019**, *31*, 1901261.
- [127] Z. Xing, B. Wang, W. Gao, C. Pan, J. K. Halsted, E. S. Chong, J. Lu, X. Wang, W. Luo, C. H. Chang, Y. Wen, S. Ma, K. Amine, X. Ji, *Nano Energy* **2015**, *11*, 600.
- [128] Y. Gogotsi, A. Nikitin, H. Ye, W. Zhou, J. E. Fischer, B. Yi, H. C. Foley, M. W. Barsoum, *Nat. Mater.* **2003**, *2*, 591.
- [129] P. Simon, Y. Gogotsi, *Nat. Mater.* **2008**, *7*, 845.
- [130] M. Schmirler, T. Knorr, T. Fey, A. Lynen, P. Greil, B. J. M. Etzold, *Carbon* **2011**, *49*, 4359.
- [131] H. J. Liu, J. Wang, C. X. Wang, Y. Y. Xia, *Adv. Energy Mater.* **2011**, *1*, 1101.
- [132] M. Oschatz, S. Boukhalifa, W. Nickel, J. P. Hofmann, C. Fischer, G. Yushin, S. Kaskel, *Carbon* **2017**, *113*, 283.

- [133] M. Rose, Y. Korenblit, E. Kockrick, L. Borchardt, M. Oschatz, S. Kaskel, G. Yushin, *Small* **2011**, *7*, 1108.
- [134] W. Y. Tsai, P. C. Gao, B. Daffos, P. L. Taberna, C. R. Perez, Y. Gogotsi, F. Favier, P. Simon, *Electrochem. Commun.* **2013**, *34*, 109.
- [135] M. Oschatz, L. Borchardt, M. Thommes, K. A. Cychosz, I. Senkowska, N. Klein, R. Frind, M. Leistner, V. Presser, Y. Gogotsi, S. Kaskel, *Angew. Chem., Int. Ed.* **2012**, *51*, 7577.
- [136] L. Chuenchom, R. Kraehnert, B. M. Smarsly, *Soft Matter* **2012**, *8*, 10801.
- [137] W.-C. Chu, B. P. Bastakoti, Y. V. Kaneti, J.-G. Li, H. R. Alamri, Z. A. Allothman, Y. Yamauchi, S.-W. Kuo, *Chem. - Eur. J.* **2017**, *23*, 13734.
- [138] H. Wu, G. Yu, L. Pan, N. Liu, M. T. McDowell, Z. Bao, Y. Cui, *Nat. Commun.* **2013**, *4*, 1943.
- [139] Y. Zhao, L. Jiang, *Adv. Mater.* **2009**, *21*, 3621.
- [140] F. Zhang, Y. Meng, D. Gu, Y. Yan, Z. Chen, B. Tu, D. Zhao, *Chem. Mater.* **2006**, *18*, 5279.
- [141] D. Zhao, Q. Huo, J. Feng, B. F. Chmelka, G. D. Stucky, *J. Am. Chem. Soc.* **1998**, *120*, 6024.
- [142] J. Wei, D. Zhou, Z. Sun, Y. Deng, Y. Xia, D. Zhao, *Adv. Funct. Mater.* **2013**, *23*, 2322.
- [143] I. Moriguchi, A. Ozono, K. Mikuriya, Y. Teraoka, S. Kagawa, M. Kodama, *Chem. Lett.* **1999**, *28*, 1171.
- [144] H. Tian, Z. Lin, F. Xu, J. Zheng, X. Zhuang, Y. Mai, X. Feng, *Small* **2016**, *12*, 3155.
- [145] J. Tang, J. Liu, C. Li, Y. Li, M. O. Tade, S. Dai, Y. Yamauchi, *Angew. Chem., Int. Ed.* **2015**, *54*, 588.
- [146] C. Liang, K. Hong, G. A. Guiochon, J. W. Mays, S. Dai, *Angew. Chem., Int. Ed.* **2004**, *43*, 5785.
- [147] L. Peng, C. Te Hung, S. Wang, X. Zhang, X. Zhu, Z. Zhao, C. Wang, Y. Tang, W. Li, D. Zhao, *J. Am. Chem. Soc.* **2019**, *141*, 7073.
- [148] G. Hasegawa, K. Kanamori, T. Kiyomura, H. Kurata, T. Abe, K. Nakanishi, *Chem. Mater.* **2016**, *28*, 3944.
- [149] J. G. Wang, H. Liu, H. Sun, W. Hua, H. Wang, X. Liu, B. Wei, *Carbon* **2018**, *127*, 85.
- [150] Y. Meng, D. Gu, F. Zhang, Y. Shi, L. Cheng, D. Feng, Z. Wu, Z. Chen, Y. Wan, A. Stein, D. Zhao, *Chem. Mater.* **2006**, *18*, 4447.
- [151] X. Zhou, L. Yu, X. W. D. Lou, *Nanoscale* **2016**, *8*, 8384.
- [152] Y. Liang, R. Fu, D. Wu, *ACS Nano* **2013**, *7*, 1748.
- [153] L. Zhou, C. Yang, J. Wen, P. Fu, Y. Zhang, J. Sun, H. Wang, Y. Yuan, *J. Mater. Chem. A* **2017**, *5*, 19343.
- [154] H. Peng, B. Yao, X. Wei, T. Liu, T. Kou, P. Xiao, Y. Zhang, Y. Li, *Adv. Energy Mater.* **2019**, *9*, 1803665.
- [155] S. H. Park, K. H. Kim, K. C. Roh, K. B. Kim, *J. Porous Mater.* **2013**, *20*, 1289.
- [156] L. Estevez, V. Prabhakaran, A. L. Garcia, Y. Shin, J. Tao, A. M. Schwarz, J. Darsell, P. Bhattacharya, V. Shutthanandan, J. G. Zhang, *ACS Nano* **2017**, *11*, 11047.
- [157] A. D. Roberts, X. Li, H. Zhang, *Carbon* **2015**, *95*, 268.
- [158] J. Wang, J. Tang, B. Ding, V. Malgras, Z. Chang, X. Hao, Y. Wang, H. Dou, X. Zhang, Y. Yamauchi, *Nat. Commun.* **2017**, *8*, 15717.
- [159] R. B. Rakhi, B. Ahmed, M. N. Hedhili, D. H. Anjum, H. N. Alshareef, *Chem. Mater.* **2015**, *27*, 5314.
- [160] D. Hulicova, J. Yamashita, Y. Soneda, H. Hatori, M. Kodama, *Chem. Mater.* **2005**, *17*, 1241.
- [161] X. He, H. Yu, L. Fan, M. Yu, M. Zheng, *Mater. Lett.* **2017**, *195*, 31.
- [162] M. Li, J. Xue, *J. Phys. Chem. C* **2014**, *118*, 2507.
- [163] A. D. Roberts, X. Li, H. Zhang, *Chem. Soc. Rev.* **2014**, *43*, 4341.
- [164] P. Hao, Z. Zhao, J. Tian, H. Li, Y. Sang, G. Yu, H. Cai, H. Liu, C. P. Wong, A. Umar, *Nanoscale* **2014**, *6*, 12120.
- [165] B. Anasori, M. R. Lukatskaya, Y. Gogotsi, *Nat. Rev. Mater.* **2017**, *2*, 16098.
- [166] L. Jiang, J. Wang, X. Mao, X. Xu, B. Zhang, J. Yang, Y. Wang, J. Zhu, S. Hou, *Carbon* **2017**, *111*, 207.
- [167] D. Xue, D. Zhu, W. Xiong, T. Cao, Z. Wang, Y. Lv, L. Li, M. Liu, L. Gan, *ACS Sustainable Chem. Eng.* **2019**, *7*, 7024.
- [168] N. Zhang, H. Qiu, Y. Si, W. Wang, J. Gao, *Carbon* **2011**, *49*, 827.
- [169] L. Yu, H. Bin Wu, X. W. (D) Lou, *Acc. Chem. Res.* **2017**, *50*, 293.
- [170] Y. He, X. Zhuang, C. Lei, L. Lei, Y. Hou, Y. Mai, X. Feng, *Nano Today* **2019**, *24*, 103.
- [171] B. Yang, J. Chen, L. Liu, P. Ma, B. Liu, J. Lang, Y. Tang, X. Yan, *Energy Storage Mater.* **2019**, *23*, 522.
- [172] B. Xu, H. Duan, M. Chu, G. Cao, Y. Yang, *J. Mater. Chem. A* **2013**, *1*, 4565.
- [173] W. Li, F. Zhang, Y. Dou, Z. Wu, H. Liu, X. Qian, D. Gu, Y. Xia, B. Tu, D. Zhao, *Adv. Energy Mater.* **2011**, *1*, 382.
- [174] P. Pachfule, D. Shinde, M. Majumder, Q. Xu, *Nat. Chem.* **2016**, *8*, 718.
- [175] Z. Liang, C. Qu, W. Guo, R. Zou, Q. Xu, *Adv. Mater.* **2018**, *30*, 1702891.
- [176] A. M. Abioye, F. N. Ani, *Renewable Sustainable Energy Rev.* **2015**, *52*, 1282.
- [177] J. Lee, Y. A. Lee, C. Y. Yoo, J. J. Yoo, R. Gwak, W. K. Cho, B. Kim, H. Yoon, *Microporous Mesoporous Mater.* **2018**, *261*, 119.
- [178] G. A. Ferrero, A. B. Fuertes, M. Sevilla, M. M. Titirici, *Carbon* **2016**, *106*, 179.
- [179] W. Yang, W. Yang, F. Ding, L. Sang, Z. Ma, G. Shao, *Carbon* **2017**, *111*, 419.
- [180] A. B. Fuertes, M. Sevilla, *ACS Appl. Mater. Interfaces* **2015**, *7*, 4344.
- [181] S. Yu, N. Sun, L. Hu, L. Wang, Q. Zhu, Y. Guan, B. Xu, *J. Power Sources* **2018**, *405*, 132.
- [182] M. Sevilla, A. B. Fuertes, *ACS Nano* **2014**, *8*, 5069.
- [183] Y. Jiang, J. Yan, X. Wu, D. Shan, Q. Zhou, L. Jiang, D. Yang, Z. Fan, *J. Power Sources* **2016**, *307*, 190.
- [184] B. Yang, J. Chen, S. Lei, R. Guo, H. Li, S. Shi, X. Yan, *Adv. Energy Mater.* **2018**, *8*, 1702409.
- [185] J. Meng, C. Niu, L. Xu, J. Li, X. Liu, X. Wang, Y. Wu, X. Xu, W. Chen, Q. Li, Z. Zhu, D. Zhao, L. Mai, *J. Am. Chem. Soc.* **2017**, *139*, 8212.
- [186] L. F. Chen, Y. Lu, L. Yu, X. W. Lou, *Energy Environ. Sci.* **2017**, *10*, 1777.
- [187] K. Jayaramulu, D. P. Dubal, B. Nagar, V. Ranc, O. Tomanec, M. Petr, K. K. R. Datta, R. Zboril, P. Gómez-Romero, R. A. Fischer, *Adv. Mater.* **2018**, *30*, 1705789.
- [188] L. Wang, T. Wei, L. Sheng, L. Jiang, X. Wu, Q. Zhou, B. Yuan, J. Yue, Z. Liu, Z. Fan, *Nano Energy* **2016**, *30*, 84.
- [189] Z. Li, H. Mi, L. Liu, Z. Bai, J. Zhang, Q. Zhang, J. Qiu, *Carbon* **2018**, *136*, 176.
- [190] R. R. Salunkhe, J. Tang, Y. Kamachi, T. Nakato, J. H. Kim, Y. Yamauchi, *ACS Nano* **2015**, *9*, 6288.
- [191] H. Jin, J. Li, Y. Yuan, J. Wang, J. Lu, S. Wang, *Adv. Energy Mater.* **2018**, *8*, 1801007.
- [192] F. Lai, Y. E. Miao, L. Zuo, H. Lu, Y. Huang, T. Liu, *Small* **2016**, *12*, 3235.
- [193] W. Zhang, N. Lin, D. Liu, J. Xu, J. Sha, J. Yin, X. Tan, H. Yang, H. Lu, H. Lin, *Energy* **2017**, *128*, 618.
- [194] W. L. Zhang, J. H. Xu, D. X. Hou, J. Yin, D. B. Liu, Y. P. He, H. B. Lin, *J. Colloid Interface Sci.* **2018**, *530*, 338.
- [195] T. Zhu, J. Zhou, Z. Li, S. Li, W. Si, S. Zhuo, *J. Mater. Chem. A* **2014**, *2*, 12545.
- [196] F. Xu, Y. Lai, R. Fu, D. Wu, *J. Mater. Chem. A* **2013**, *1*, 5001.
- [197] F. Xu, Z. Tang, S. Huang, L. Chen, Y. Liang, W. Mai, H. Zhong, R. Fu, D. Wu, *Nat. Commun.* **2015**, *6*, 7221.
- [198] J. G. Wang, H. Liu, X. Zhang, X. Li, X. Liu, F. Kang, *Small* **2018**, *14*, 1703950.
- [199] M. Kim, P. Puthiaraj, Y. Qian, Y. Kim, S. Jang, S. Hwang, E. Na, W. S. Ahn, S. E. Shim, *Electrochim. Acta* **2018**, *284*, 98.
- [200] L. Shao, Y. Li, J. Huang, Y. N. Liu, *Ind. Eng. Chem. Res.* **2018**, *57*, 2856.

- [201] Z. Xu, X. Zhuang, C. Yang, J. Cao, Z. Yao, Y. Tang, J. Jiang, D. Wu, X. Feng, *Adv. Mater.* **2016**, *28*, 1981.
- [202] J. Gu, Z. Du, C. Zhang, S. Yang, *Adv. Energy Mater.* **2016**, *6*, 1600917.
- [203] H. Li, J. Li, A. Thomas, Y. Liao, *Adv. Funct. Mater.* **2019**, *29*, 1904785.
- [204] P. Puthiaraj, Y. R. Lee, W. S. Ahn, *Chem. Eng. J.* **2017**, *319*, 65.
- [205] J. Serrano, T. Liu, A. U. Khan, B. Botset, B. J. Stovall, Z. Xu, D. Guo, K. Cao, G. Liu, *Chem. Mater.* **2019**, *31*, 8898.
- [206] T. Liu, Z. Zhou, Y. Guo, D. Guo, G. Liu, *Nat. Commun.* **2019**, *10*, 675.
- [207] Z. Li, D. Wu, X. Huang, J. Ma, H. Liu, Y. Liang, R. Fu, K. Matyjaszewski, *Energy Environ. Sci.* **2014**, *7*, 3006.
- [208] R. Yuan, H. Wang, M. Sun, K. Damodaran, E. Gottlieb, M. Kopeć, K. Eckhart, S. Li, J. Whitacre, K. Matyjaszewski, T. Kowalewski, *ACS Appl. Nano Mater.* **2019**, *2*, 2467.
- [209] Z. Lin, H. Tian, F. Xu, X. Yang, Y. Mai, X. Feng, *Polym. Chem.* **2016**, *7*, 2092.
- [210] Y. X. Tong, X. M. Li, L. J. Xie, F. Y. Su, J. P. Li, G. H. Sun, Y. D. Gao, N. Zhang, Q. Wei, C. M. Chen, *Energy Storage Mater.* **2016**, *3*, 140.
- [211] L. Miao, H. Duan, M. Liu, W. Lu, D. Zhu, T. Chen, L. Li, L. Gan, *Chem. Eng. J.* **2017**, *317*, 651.
- [212] L. Miao, D. Zhu, M. Liu, H. Duan, Z. Wang, Y. Lv, W. Xiong, Q. Zhu, L. Li, X. Chai, L. Gan, *Electrochim. Acta* **2018**, *274*, 378.
- [213] D. Zhu, K. Cheng, Y. Wang, D. Sun, L. Gan, T. Chen, J. Jiang, M. Liu, *Electrochim. Acta* **2017**, *224*, 17.
- [214] S. Huo, M. Liu, L. Wu, M. Liu, M. Xu, W. Ni, Y. M. Yan, *J. Power Sources* **2018**, *387*, 81.
- [215] H. Wang, S. Min, C. Ma, Z. Liu, W. Zhang, Q. Wang, D. Li, Y. Li, S. Turner, Y. Han, H. Zhu, E. Abou-Hamad, M. N. Hedhili, J. Pan, W. Yu, K. W. Huang, L. J. Li, J. Yuan, M. Antonietti, T. Wu, *Nat. Commun.* **2017**, *8*, 13592.
- [216] W. Zhang, S. Wei, Y. Wu, Y.-L. Wang, M. Zhang, D. Roy, H. Wang, J. Yuan, Q. Zhao, *ACS Nano* **2019**, *13*, 10261.
- [217] Y. Wang, F. Chen, Z. Liu, Z. Tang, Q. Yang, Y. Zhao, S. Du, Q. Chen, C. Zhi, *Angew. Chem., Int. Ed.* **2019**, *58*, 15707.
- [218] Z. Wang, M. Zhu, Z. Pei, Q. Xue, H. Li, Y. Huang, C. Zhi, *Mater. Sci. Eng., R* **2019**, *139*, 100520.
- [219] S. Y. Lu, M. Jin, Y. Zhang, Y. B. Niu, J. C. Gao, C. M. Li, *Adv. Energy Mater.* **2018**, *8*, 1602545.
- [220] C. Bommier, R. Xu, W. Wang, X. Wang, D. Wen, J. Lu, X. Ji, *Nano Energy* **2015**, *13*, 709.
- [221] J. Dai, L. Qin, R. Zhang, A. Xie, Z. Chang, S. Tian, C. Li, Y. Yan, *Powder Technol.* **2018**, *331*, 162.
- [222] Y. Zhao, W. Ran, J. He, Y. Song, C. Zhang, D. B. Xiong, F. Gao, J. Wu, Y. Xia, *ACS Appl. Mater. Interfaces* **2015**, *7*, 1132.
- [223] W. Gao, N. Singh, L. Song, Z. Liu, A. L. M. Reddy, L. Ci, R. Vajtai, Q. Zhang, B. Wei, P. M. Ajayan, *Nat. Nanotechnol.* **2011**, *6*, 496.
- [224] M. F. El-Kady, V. Strong, S. Dubin, R. B. Kaner, *Science* **2012**, *335*, 1326.
- [225] L. Li, J. Zhang, Z. Peng, Y. Li, C. Gao, Y. Ji, R. Ye, N. D. Kim, Q. Zhong, Y. Yang, H. Fei, G. Ruan, J. M. Tour, *Adv. Mater.* **2016**, *28*, 838.
- [226] R. Ye, Y. Chyan, J. Zhang, Y. Li, X. Han, C. Kittrell, J. M. Tour, *Adv. Mater.* **2017**, *29*, 1702211.
- [227] Y. Chyan, R. Ye, Y. Li, S. P. Singh, C. J. Arnsch, J. M. Tour, *ACS Nano* **2018**, *12*, 2176.
- [228] W. Zhang, Y. Lei, F. Ming, Q. Jiang, P. M. F. J. Costa, H. N. Alshareef, *Adv. Energy Mater.* **2018**, *8*, 1801840.
- [229] W. Zhang, Y. Lei, Q. Jiang, F. Ming, P. M. F. J. Costa, H. N. Alshareef, *Small Methods* **2019**, *3*, 1900005.
- [230] W. Zhang, Q. Jiang, Y. Lei, H. N. Alshareef, *ACS Appl. Mater. Interfaces* **2019**, *11*, 20905.
- [231] V. Strauss, K. Marsh, M. D. Kowal, M. El-Kady, R. B. Kaner, *Adv. Mater.* **2018**, *30*, 1704449.
- [232] V. Strauss, M. Muni, A. Borenstein, B. Badamdorj, T. Heil, M. D. Kowal, R. Kaner, *Nanoscale* **2019**, *11*, 12712.
- [233] J. Y. Hwang, M. Li, M. F. El-Kady, R. B. Kaner, *Adv. Funct. Mater.* **2017**, *27*, 1605745.
- [234] L. Wang, G. Zhang, B. Han, Y. Chang, H. Li, J. Wang, C. Hu, Z. Chang, Z. Huo, X. Sun, *J. Mater. Chem. A* **2017**, *5*, 6734.
- [235] X. Yang, C. Cheng, Y. Wang, L. Qiu, D. Li, *Science* **2013**, *341*, 534.
- [236] Y. Tao, X. Xie, W. Lv, D. M. Tang, D. Kong, Z. Huang, H. Nishihara, T. Ishii, B. Li, D. Golberg, F. Kang, T. Kyotani, Q. H. Yang, *Sci. Rep.* **2013**, *3*, 2975.

Reprint Order Form

Wiley-VCH Verlag GmbH & Co. KGaA
Small Methods
Boschstr. 12
69469 Weinheim
Germany

Please complete this form and return it via E-Mail to the
Editorial Office at

E-mail: small-methods@wiley-vch.de

Charges for Reprints in Euro (excl. VAT), prices are subject to
change. Minimum order 50 copies; single issues for authors at a
reduced price.

Manuscript No.: _____
Customer No.: (if available) _____
Purchase Order No.: _____
Author: _____
Date: _____

Information regarding VAT: Please note that from German sales tax point of
view, the charge for Reprints, Issues or Posters is considered as supply of
goods and therefore, in general, such delivery is a subject to German sales
tax. However, this regulation has no impact on customers located outside of
the European Union. Deliveries to customers outside the Community are
automatically tax-exempt. Deliveries within the Community to institutional
customers outside of Germany are exempted from the German tax (VAT)
only if the customer provides the supplier with his/her VAT number. The
VAT number (value added tax identification number) is a tax registration
number used in the countries of the European Union to identify corporate
entities doing business there. Starting with a country code (e.g. FR for
France), followed by numbers.

No. of pages	50 copies	100 copies	150 copies	200 copies	300 copies	500 copies
1 4	345,	395,	425,	445,	548,	752,
5 8	490,	573,	608,	636,	784,	1077,
9 12	640,	739,	786,	824,	1016,	1396,
13 16	780,	900,	958,	1004,	1237,	1701,
17 20	930,	1070,	1138,	1196,	1489,	2022,
every additional 4 pages	147,	169,	175,	188,	231,	315,

Please send me and bill me for

no. of reprints airmail (+ 25 Euro)
 surface mail
 Fedex No.: _____

high-resolution PDF file (330 Euro)
E-mail address: _____
 Special Offer: _____

If you order 200 or more reprints you will
get a PDF file for half price.

*Please note: It is not permitted to present the PDF file on
the internet or on company homepages.*

Cover Posters (prices excl. VAT)

Posters of published covers are available in two sizes:

DIN A2 42 x 60 cm / 17 x 24in (one copy: 39 Euro)

DIN A1 60 x 84 cm / 24 x 33in (one copy: 49 Euro)

Postage for shipping posters overseas by airmail:
+ 25 Euro

Postage for shipping posters within Europe by surface
mail: + 15 Euro

Date, Signature

VAT number: _____

Mail reprints / copies of the issue to:

Send bill to:

I will pay by bank transfer

I will pay by credit card

VISA, Mastercard and AMERICAN EXPRESS

For your security please use this link (Credit Card
Token Generator) to create a secure code Credit
Card Token and include this number in the form

							V							
--	--	--	--	--	--	--	---	--	--	--	--	--	--	--

instead of the credit card data. Click here:

https://www.wiley-vch.de/editorial_production/index.php

CREDIT CARD TOKEN NUMBER